Inactive Rhomboid Protease 2 Reduces Liver Fibrosis by Inhibiting Proliferation of Hepatic Stellate Cells

Inaugural dissertation

for the attainment of the title of doctor

in the Faculty of Mathematics and Natural Sciences

at the Heinrich Heine University Düsseldorf presented by

Balamurugan Sundaram

from Thiruvanamalai, India

Dusseldorf, 2020

from the Institute of Molecular Medicine II,

at the Heinrich Heine University Dusseldorf

Published by permission of the Faculty of Mathematics and Natural Sciences
at Heinrich Heine University Düsseldorf

Supervisor: Prof. Dr. Philipp A. Lang
Co-Supervisor: Prof. Dr. Lutz Schmitt

Date of Oral Examination: 27-02-2020

Table of Contents **Page**

Declaration and statement of contribution

I, Balamurugan Sundaram, declare that the content in this dissertation is original. I have cited appropriate texts and figures wherever necessary. No part of this dissertation is submitted somewhere else for consideration of a degree. Part of the dissertation is published in Science Signaling entitled **"*iRhom2 inhibits bile duct obstruction-induced liver fibrosis". Sci. Signal.* 12, eaax1194 (2019).**

I was involved in execution of the experiments, analysis, writing and preparation of the manuscript which consists ≈25% of the published manuscript. I have contributed in the preparation of following figures which are included in the thesis are as follows,

Fig 1A-E; Fig 2A-C, 2G-H; Fig 3A-D; Fig 4C-D; Fig 5A-C; Fig 6B-C; Fig 7E-G; Fig 8A-E; Fig 9A-C, 9E-F; Fig 10B-D; Fig 11C-D; Fig 12A-C; Fig 13A-B; Fig 14A-C; Fig 15A-B; 16 A-C and Graphical Figures 1-7.

Contribution in the other published manuscripts is mentioned in the list of the publications.

Balamurugan Sundaram

Date: 27-02-2020

Place: Dusseldorf, Germany

Publication list and contribution

1. **Sundaram B**, Behnke K, Belancic A, Al-Salihi MA, Thabet Y, Polz R, Pellegrino R, Zhuang Z, Shinde PV, Xu HC, Vasilevska J, Longerich T, Herebian D, Mayatepek E, Bock H, May P, Kordes C, Mak TW, Keitel V, Häussinger D, Scheller J, Pandyra AA, Lang KS, and Lang PA. **iRhom2 inhibits bile duct obstruction induced liver fibrosis.** Sci. Signal. 12, eaax1194 (2019) October 2019. **Contribution to the publication: ≈ 25%**
2. Zhuang Z, Xu HC, Shinde PV, Warfsmann J, Vasilevska J, **Sundaram B,** Behnke K, Huang J, Hoell JI, Borkhardt A, Pfeffer K, Taha MS, Herebian D, Mayatepek E, Brenner D, Ahmadian MR, Keitel V, Wieczorek D, Häussinger D, Pandyra AA, Lang KS, and Lang PA. **Fragile X mental retardation protein protects against tumour necrosis factor-mediated cell death and liver injury**. Gut 2019 gutjnl-2019-318215. **Contribution to the publication: ≈ 2%**
3. Lang E, Pozdeev VI, Shinde PV, Xu HC, **Sundaram B**, Zhuang Y, Poschmann G, Huang J, Stühler K, Pandyra AA, Keitel V, Häussinger D, Lang KS, Lang PA. **Cholestasis induced liver pathology results in dysfunctional immune responses after arenavirus infection.** Sci Rep. 2018 Aug 15;8(1):12179. **Contribution to the publication: ≈ 2%**
4. Behnke K, Zhuang Y, Xu HC, **Sundaram B**, Reich M, Shinde PV, Huang J, Modares NF, Tumanov AV, Polz R, Scheller J, Ware CF, Pfeffer K, Keitel V, Häussinger D, Pandyra AA, Lang KS, Lang PA. **B Cell-Mediated Maintenance of Cluster of Differentiation 169-Positive Cells Is Critical for Liver Regeneration.** Hepatology. 2018 Dec;68(6):2348-2361. **Contribution to the publication: ≈ 2%**
5. Maney SK, McIlwain DR, Polz R, Pandyra AA, **Sundaram B**, Wolff D, Ohishi K, Maretzky T, Brooke MA, Evers A, Vasudevan AA, Aghaeepour N, Scheller J, Münk C, Häussinger D, Mak TW, Nolan GP, Kelsell DP, Blobel CP, Lang KS, Lang PA. Deletions in the cytoplasmic domain of iRhom1 and iRhom2 promote shedding of the TNF receptor by the protease ADAM17. Sci Signal. 2015 Nov 3;8(401):ra109. **Contribution to the publication: ≈ 2%**

Publications apart from PhD studies

1. Nagaraj VA, **Sundaram B**, Varadarajan NM, Subramani PA, Kalappa DM, Ghosh SK, Padmanaban G. Malaria parasite-synthesized heme is essential in the mosquito and liver stages and complements host heme in the blood stages of infection. PLoS Pathog. 2013;9(8): e1003522.
2. Varadarajan NM*, **Sundaram B***, Subramani PA, Kalappa DM, Ghosh SK, Nagaraj VA. Plasmodium berghei glycine cleavage system T-protein is non-essential for parasite survival in vertebrate and invertebrate hosts. Mol Biochem Parasitol. 2014 Oct;197(1-2):50-5. *Equal contribution.
3. **Sundaram B**, Varadarajan NM, Subramani PA, Ghosh SK, Nagaraj VA. Purification of a recombinant histidine-tagged lactate dehydrogenase from the malaria parasite, Plasmodium vivax, and characterization of its properties. Biotechnol Lett. 2014 Dec;36(12):2473-80.
4. Ramos S, Carlos AR*, **Sundaram B***, Jeney V*, Ribeiro A, Gozzelino R, Bank C, Gjini E, Braza F, Martins R, Ademolue TW, Blankenhaus B, Gouveia Z, Faísca P, Trujillo D, Cardoso S, Rebelo S, Del Barrio L, Zarjou A, Bolisetty S, Agarwal A, Soares MP. Renal control of disease tolerance to malaria. Proc Natl Acad Sci U S A. 2019 Mar 19;116(12):5681-5686. *Equal contribution.

List of figures

List of Graphical figures

List of Tables

Abbreviations

ADAM	:	A disintegrin and metalloprotease
ADAM10	:	A disintegrin and metalloprotease 10
ADAM17	:	A disintegrin and metalloprotease domain 17
AH	:	Alcoholic Hepatitis
AIH	:	Autoimmune hepatitis
AKI	:	Acute lung injury
ALD	:	Alcoholic liver disease
ALT	:	Alanine transaminase
AMA	:	Antimitochondrial antibodies
AP-1	:	Activator protein 1
APC	:	Allophycocyanin
AST	:	Aspartate Aminotransferase
BAFFR	:	B-cell activating factor receptor
BCR	:	B-cell receptor
BDL	:	Bile duct ligation
CAFs	:	Cancer-associated fibroblasts
CCL3	:	Chemokine (C-C motif) ligand 3
CCl4	:	Carbon tetrachloride
CCL5	:	Chemokine (C-C motif) ligand 5
CCR1	:	C-C chemokine receptor type 1
CCR2	:	C-C chemokine receptor type 2
CD40	:	Cluster of differentiation 40
CD68	:	Cluster of differentiation 68
CD81	:	Cluster of Differentiation 81
CD95	:	Cluster of Differentiation 95
CDC	:	Centers for Disease Control and Prevention
CFUs	:	Cololy-forming units
Col1A1	:	Collagen, type I, alpha 1
Col3A1	:	Collagen, type III, alpha 1
CTGF	:	Connective tissue growth factor
DAAs	:	Direct-acting Antiviral Agents

DAPI	:	4′,6-diamidino-2-phenylindole
DGCS	:	Diffuse-type gastric cancers
DNA	:	Deoxyribo nucleic Acid
ECM	:	Extracellular matrix
EDTA	:	Ethylenediaminetetraacetic acid
EGF	:	Epidermal growth factor
EGFR	:	Epidermal growth factor receptor
ER	:	Endoplasmic reticulum
GalN	:	D-galactosamine
GFAP	:	Glial fibrillary acid protein
GOT	:	Glutamic oxaloacetic transaminase
GPT	:	Glutamate-pyruvate transaminase
HA	:	Hemophilic arthropathy
HAND2	:	Heart-and neural crest derivatives-expressed protein 2
HB-EGF	:	Heparin binding- epidermal growth factor
HBV	:	Hepatitis B Virus
HCC	:	Hepatocellular carcinoma
HCV	:	Hepatitis C Virus
HSCs	:	Hepatic stellate cells
HSV-1	:	Herpes simplex virus type 1
I/R	:	Intestinal ischemia-reperfusion
IL-1β	:	Interleukin-1beta
IL-6	:	Interleukin-6
IL-8	:	Interleukin-8
IPF	:	Idiopathic pulmanory fibrosis
iRhom1	:	inactive member of rhomboid protease 1
iRhom2	:	inactive member of rhomboid protease 2
IκBα	:	inhibitor of κB α
K16	:	Keratin 16
KCs	:	Kupffer cells
LN	:	Lupus nephritis
LPS	:	Lipopolysaccharide
LRAT	:	Lecithin retinol acyltransferase
LSECs	:	Liver sinusoidal endothelial cells

LTβR	:	Lymphotoxin-β receptor
LY6G	:	Lymphocyte antigen 6 complex locus G6D
NAFLD	:	Non-alcoholic fatty liver disease
NASH	:	Non-alcoholic steatohepatitis
NF	:	Non-cancer fibroblasts
NF-κB	:	Nuclear factor 'kappa light chain enhancer' of activated B cells
PBC	:	Primary biliary cholangitis
PBS	:	Phosphate-buffered saline
PDGF	:	Platelet derived growth factor
PDGFRβ	:	Platelet-derived growth factor receptor-β
PE	:	Phycoerythrin
PRR	:	Pattern recognition receptor
RA	:	Rheumatoid arthritis
RANK	:	Receptor activator of nuclear factor κ B
Rhbdf1	:	Gene encoding iRhom2
Rhbdf2	:	Gene encoding iRhom2
RNA	:	Ribonucleic acid
RQ	:	Relative quantities
SPF	:	Specific pathogen free
SRBI	:	scavenger receptor class B type I
STAT3	:	Signal transducer and activator of transcription 3
STING	:	Stimulator of interferon genes
TACE	:	TNF-α converting enzyme
TCR	:	T-cell receptor
TGEM	:	Thioglycollate-elictied peritoneal macrophages
TGF-α	:	Transforming growth factor-alpha
TGF-β	:	Transforming growth factor-beta
TGN	:	Trans Golgi-network
TIMP3	:	Tissue inhibitor of metalloproteinase 3
TLR4	:	Toll-like receptor 4
TMD	:	Transmembrane domain
TNFR1	:	Tumor Necrosis Factor Receptor 1
TNFR2	:	Tumor Necrosis Factor Receptor 2
TNF-α	:	Tumor Necrosis Factor alpha

TOC	:	Tylosis with oesophageal cancer
TRADD	:	Tumor necrosis factor receptor type 1-associated DEATH domain protein
TRAF2	:	TNF receptor-associated factor 2
TRAPβ	:	Translocon-associated protein β
VEGF	:	Vascular endothelial growth factor
VSV	:	Vesicular stomatitis virus
WHO	:	World Health Organization
WT	:	Wild type
α-SMA	:	Alpha-smooth muscle actin

I dedicate my thesis to GOD and to my family

Acknowledgement

First I would like to thank my supervisor Prof. Dr. Philipp A Lang who gave me the opportunity to join his group. Last five years I got very good support and supervision from my supervisor. He spends lot of time discussing the projects at any time. He spent lot of time for his PhD students to finish the project and publish before we get degree, which is really great. In that way, my project also finished in time and we published before end of my PhD, this would help me to pursue further career in research. He also made me to involve in multiple projects which made me to learn more and gain scientific knowledge. Thank you philipp for your unconditional support and encouragement for last five years. Second I would like to thank my mentor Prof. Dr. Lutz Schmitt for his supervision and support for the last five years. Also, I would like to thank you for the fruitful discussions and suggestions you gave me during annual meetings and MOI III symposiums.

Next, I would like to thank my graduate school Molecules of Infection (MOI) III for their immense support. I learned a lot during MOI course works and from the fellow mates during my stay at the university.

I would like thank all our collabrators who helped me to finish iRhom2 liver fibrosis story. Prof. Dr. Karl S. Lang, Dr. Aleksandra A. Pandyra, Prof. Dr. Dieter Häussinger, Prof. Dr. Jürgen Scheller, Prof. Dr. Tak W. Mak, Prof. Dr. Verena Keitel, Prof. Dr. Hans H. Bock, Prof. Dr. Petra May, Dr. Diran Herebian, Prof. Dr. Ertan Mayatepek, Prof. Dr. Nima Aghaeepour and Prof. Dr. Claus Kordes. Without all of your support, it would be impossible for me to finish the project. I would like to thank Prof. Dr. Thomas Longerich and Dr. Rossella Pellegrino for providing us the human cirrhotic and healthy liver samples to check for iRhom2 expression.

Next I want to thank Dr. Yasser Thabet for his unconditional support and guidance throughout my PhD studies. I learned a lot of things from you, one of them is hepatic stellate cells isolation technique, which really helped me to finish the project. We had good scientific discussions during our coffee and lunch time.

I would like to thank Sathish for teaching me all the techniques initially when I joined the lab and I really liked working with you. I want to thank Chris, who gave critical comment on the project and for his good discussion during the meetings. I would like to thank Prashant, Yuan, and Jun for their great support during my stay in lab. We had lot of good times together,

starting from discussing projects, traveling, going out for dinner etc. Student club discussions with all of you along with philipp was really helpful and progressive to address scientific questions. I want to that Elizabeth Lang and Kristina Behnke for teaching me Bile Duct Ligation. This technique is the basic key for the project and without knowing this technique, I wouldn't have finished the project. I want to thank Robin and Andrea for their support and scientific input to finish the project.

I want to thank Mazin for his support and taking care of the projects when I was not available in the lab. I want to thank Julia for her unconditional support in managing so many things in the lab especially animal protocols for various projects. I would like to thank Pawel, Anfei, Rui, Wei, Anna, Cassy, Arshia, and Krutika for all your support and scientific discussions we had in the lab. I wish you all good success and have good time during your PhD studies in the lab.

I want thank my university friends Mathias, Arun, Ruchika, Senthil, Sushma, Kannan, Meenakshi, and Rizwan. Their words had healed me so many times during my stay at the university.

Finally, I would like to thank my parents who accept my career and allow me to go outside of country for doing PhD. I just love and follow my father footsteps who is very hardworking person to take care of his family. I got great support and pressure from my wife Hema during my last year of PhD to finish things in time. I really have to thank Hema for taking care of things at home when I am busy in the lab, without you this wouldn't be possible. I want to thank both of my sisters Param and Jaga who make my life beautiful all the time.

Chapter 1

Introduction

1.1 Liver: Structure and function

The liver is the largest internal organ in the human body which is located in right upper quadrant in the abdominal cavity below the diaphragm which possesses both endocrine and exocrine function. Hormones like Insulin-like growth factors, Angiotensinogen, and Thrombopoietin are secreted through the endocrine system whereas for the exocrine system, bile is the major secretion compound of the liver. In addition to its endocrine and exocrine properties, the liver also participates in various other functions such as glycogen storage, drug detoxification, control of metabolism, regulation of cholesterol synthesis and transport, urea metabolism, and secretion of an extensive array of plasma proteins including Albumin and Apolipoproteins. Because the liver is involved in various essential functions, liver diseases such as hepatic fibrosis and cirrhosis, hepatocellular carcinoma can destroy the architecture of the liver which eventually leads to liver failure and results in high rates of morbidity and mortality. Liver diseases is the fourth leading cause of death among middle-aged adults in the United States (*1*). So, it's very urgent to discover novel drug targets to reduce the mortality rates due to liver diseases. Characterizing the molecular mechanisms of regulators and signalling cascades which drives liver diseases would pave the way to discover a new drug target.

1.1.1 Architecture of the Liver

The basic architectural unit of the liver is the liver lobule. The liver lobule consists of hepatocytes lined by sinusoidal capillaries that radiate towards a central efferent vein. Liver lobules are roughly hexagonal in shape with each of six corners separated by the presence of a portal triad of vessels which consists of a portal vein, bile duct, and hepatic artery (*1, 2*) (Graphical figure 1).

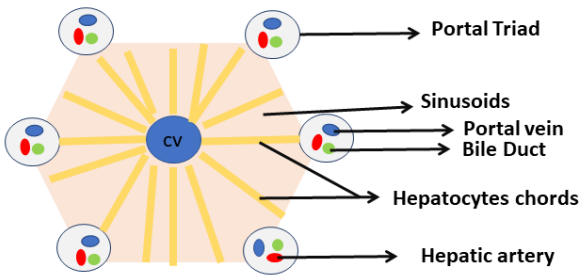

Graphical figure 1: Structure of portion of a liver lobule. Image was adapted from (3).

Both the portal vein and hepatic artery supply blood to the lobule, which flows through a network of sinusoidal capillaries before leaving the lobule through the central vein. Although hepatocytes are the major parenchymal cell type of the liver and account for 78% of the liver volume (*4*), they function together with cholangiocytes (biliary epithelial cells), endothelial cells, sinusoidal endothelial cells, Kupffer cells (resident liver macrophages), pit cells (natural killer cells), and hepatic stellate cells (*1*).

1.1.2 Liver cellular anatomy

The liver is composed of parenchymal cells namely hepatocytes, which are the largest proportion of liver cells with approximately 78% of total liver cells. Non-parenchymal cells include cholangiocytes, hepatic stellate cells, Kupffer cells and liver sinusoidal endothelial cells with approximately 20-40 % of total liver. Each of these cell types possesses unique functions which cooperatively regulate hepatic functions at multiple levels (Graphical figure 2).

Hepatocytes are the major proportion of hepatic cell populations in the liver. They are polyhedral in shape, arranged in single-cell cords or plates. Hepatocytes are linked together via intercellular adhesion complexes and tight junctions (*5*). Hepatocytes are responsible for most of the liver functions such as metabolism, detoxification, synthesis, and storage of nutrients such as carbohydrates, fats, and vitamins. Hepatocyte is involved in endocrine and exocrine functions along with other hepatic cells. These functions are performed by different hepatocytes residing in different zones of hepatic lobules. This zonation has been correlated with the direction blood flow and help in carrying metabolites (*6*). Most of the hepatic toxins cause necrosis and damage, which varies with different zonal of hepatic lobules (*7*).

Cholangiocytes are heterogeneous, highly dynamic population of epithelial cells that line the intra- and extrahepatic ducts of the biliary tree. The bililary tree runs along the portal tracts adjacent to a branch of the portal vein and hepatic artery (*8*), this forms a hallmark anatomical arrangement called portal triad (*9*). In response to injury, cholangiocytes become reactive and acquire a neuroendocrine-like phenotype with the secretion of a number of peptides. These molecules act in an autocrine/paracrine fashion to modulate cholangiocyte biology and determine the evolution of biliary damage. The failure of such mechanisms is believed to influence the progression of cholangiopathies, a group of diseases that selectively target biliary cells (*10*). In normal conditions, one of the most important and well-studied

functions of cholangiocytes is secretin-induced release of bicarbonate into bile. One of the major function of bile is to emulsify dietary fats and facilitate their intestinal absorption (*11*).

Hepatic stellate cells (HSCs) represent a dynamic cell population that can exist in a quiescent or activated state and it is located in the space of Disse. In the quiescent state, HSCs store vitamin A in lipid droplets; however, other functions in this quiescent state remain unclear. Damage to the liver leads to activation of HSCs. Upon activation, HSCs proliferate and progressively lose vitamin A stores. HSCs are also responsible for deposition and organization of collagen in the injured liver. This process contributes to scarring of the liver, which can progress to cirrhosis, a critical pathology contributing to end stage liver disease (*12*).

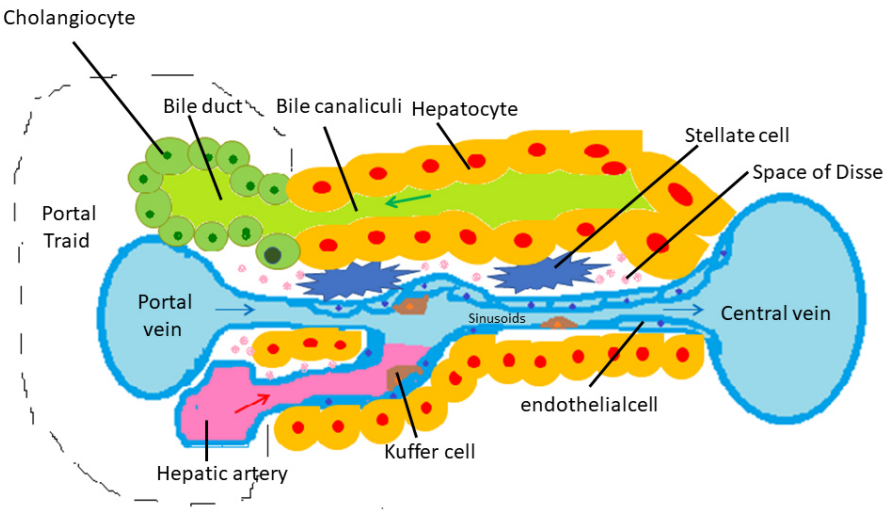

Graphical figure 2: Picture shows different cellular population of the liver. Image was adapted from (3).

Kupffer cells (KCs) are the resident macrophage population of the liver. As shown in Graphical Figure 2, KCs are attached to the lumen of sinusoidal endothelial cells. KCs are scavengers that move along the sinusoids and phagocytose foreign material present in the blood stream; fusion of the phagosome with a lysosome leads to digestion of the ingested material (*13*). Cytokines such as IL-6 and TNF-α which is produced from hepatic macrophages is essential for liver regeneration (*14*). In a same way, Kupffer cells, and monocytes are recruited and/or activated during liver injury which can induce increased pro-inflammatory cytokines in liver tissue which can contribute to liver fibrosis (*15*). So, the

cytokines released from liver resident KCs or recruited monocytes have both beneficial and adverse effects on the liver during its damage and regeneration.

Liver sinusoidal endothelial cells (LSECs) are the largest group of non-parenchymal cells of the liver and line the intrahepatic circulatory vessels to provide a large surface area for nutrient absorption. LSECs form the wall of the liver sinusoids which represent approximately 15 to 20 % of liver cells but only 3% of the total volume. LSECs are comprised of fenestrations, display high endocytic capacity and play a prominent role in maintaining overall liver homeostasis (*16, 17*).

1.1.3 Liver diseases and its causes:

Liver diseases account for approximately 2 million per year worldwide, 1 million is due to liver cirrhosis and 1 million is due to liver hepatitis and liver carcinoma. Together, liver cirrhosis and liver cancer account for 3.5% of all deaths worldwide (*18*). Since the liver is involved in multiple functions, liver injury or liver damage can cause serious complications to the human body. Importantly, liver function can be compromised in many diseased conditions, some of them are mentioned below which are more prevalent and can cause chronic liver disease:

1.1.3.1 Chronic Viral Hepatitis

1.1.3.2 Alcoholic liver disease (ALD)

1.1.3.3 Non-Alcoholic Fatty Liver Disease (NAFLD)

1.1.3.4 Autoimmune Hepatitis (AIH)

1.1.3.5 Primary biliary cholangitis (PBC)

1.1.3.1 Chronic Viral Hepatitis

Hepatitis B (HBV) and hepatitis C (HCV) virus are the two major viruses which can cause chronic liver inflammation (*19, 20*). HBV is a partially double-stranded DNA virus (*21, 22*). The HBV is most commonly transmitted from the mother to child during birth and delivery, as well as through contact with blood and other body fluids (*23, 24*). HBV infects and replicates in hepatocytes (*25*). Chronic HBV infections can cause immune mediated liver damage progressing to liver cirrhosis and hepatocellular carcinoma (HCC) (*26*). Two approaches are used to treat HBV patients (i) interferon therapy and (ii) treatment with nucleoside analog inhibitors of HBV reverse transcription (*26*). Interferon therapy aims to induce host anti-viral immune responses to clear the virus permanently (*27*), whereas nucleoside analog therapy aims to block viral DNA synthesis and thereby reduces the number

of infected hepatocytes. Nucleoside analog therapy can also inhibit progression of fibrotic and cirrhotic liver injury (*28, 29*), which can be life threatening.

HCV is a small enveloped virus with a positive-sense, single-stranded RNA genome that encodes a large polyprotein of 3010 aminoacids (*30*). HCV is a bloodborne virus and transmission happens mostly through blood from infected patient to a non-infected healthy person. Like HBV, HCV also infects hepatocytes. HCV infection is rarely diagnosed during the acute phase; therefore, the treatment of acute hepatitis is very limited. The choice of medications and length of treatment depends on the HCV genotype, severity of liver damage and prior treatments. In 2018, World Health Organization recommended a pan-genotypic direct-acting antivirals (DAAs) for the treatment of HCV infected patients. DAAs are molecules that specifically target viral proteins which results in the disruption of viral replication and infection. There are four classes of DAAs, which are defined by their mechanism of action and therapeutic target. The four classes are nonstructural proteins 3/4A (NS3/4A) protease inhibitors (PIs), NS5B nucleoside polymerase inhibitors (NPIs), NS5B non-nucleoside polymerase inhibitors (NNPIs) and NS5A inhibitors (*31*).

Altogether, both HBV and HCV infections can lead to irreversible liver cirrhosis and HCC.

1.1.3.2 Alcoholic liver disease (ALD)

Alcoholic-associated liver diseases is a major cause of liver diseases worldwide (*32*) and it is associated with high morbidity and mortality rates (*33, 34*). ALD comprises different stages of liver diseases ranging from asymptomatic steatosis, alcoholic steatohepatitis, fibrosis, cirrhosis and its related complications. Moreover, patients can develop an acute-on-chronic form of liver failure called alcoholic hepatitis (AH) (*35, 36*). Alcohol abuse can progress to liver fibrosis, liver cirrhosis, which leads to high risk of complications such as hepatic encephalopathy, renal failure and bacterial infections (*37, 38*). In the pathogenesis of AH, several cytokines have been involved, specially TNF-α has emerged as a key factor in the inflammatory process (*39-41*). So, the anti-TNF agents such as infliximab and etanercept were investigated as potential therapies for AH. However, studies did not support this hypothesis, since anti-TNF treatments has lot of adverse side effects such as increased susceptible to infection and mortality (*42*).

1.1.3.3 Non-Alcoholic Fatty Liver Disease (NAFLD)

NAFLD comprises a large spectrum of clinical and pathological liver conditions such as simple steatosis, non-alcoholic steatohepatitis (NASH) and fibrosis (*43, 44*). NASH is characterized by diffused fatty infiltration, lobular inflammation and ballooning degeneration in the liver. Studies have shown that various cytokines play a pivotal role in the process from steatosis to NASH, importantly TNF-α considered as a key inducer of nutrient and obesity-associated NASH (*45, 46*). During the onset of NASH, TNF-α is able to activate hepatic stellate cells, expression and remodeling of the extracellular matrix, which are important drivers for liver fibrosis (*47*). Studies from different groups have demonstrated that anti-TNF treatment could rescue the hepatic inflammation, liver steatosis, fibrosis and insulin signal transduction in the experimental rat model of NASH (*48, 49*).

1.1.3.4 Autoimmune Hepatitis (AIH)

Autoimmune hepatitis is a rare chronic liver disease which affects mainly women and in AIH our own immune system attacks liver cells causing inflammation. AIH is characterized by increased transaminases, hypergammaglobulinaemia, circulating autoantibodies and interface hepatitis at liver histology. If AIH is not treated in an appropriate time period, it often leads to cirrhosis, liver failure and eventually death (*50*). AIH patients display different cytokine expression such as IL-6, IL-8 and TNF-α (*51*). The anti-TNF-α drug, Infliximab may be considered as a treatment in young patients although the therapy may be associated with infections (*52, 53*).

1.1.3.5 Primary biliary cholangitis (PBC)

Primary biliary cholangitis results from a slow progressive destruction of the small bile ducts of the liver which leads to accumulation of bile and causes damage to the liver tissue which eventually triggers liver fibrosis and cirrhosis (*54, 55*). PBC is characterized by serological presence of the antimitochondrial antibodies (AMA) and considered as immunologically mediated diseases where TNF-α plays a prominent pathogenic role (*56*). A study reported a case of a female patient with Rheumatoid arthritis (RA) and concomitant PBC with poor clinical response to conventional treatment. However, the anti-TNF-α drug, Infliximab treatment improved RA and stabilized the liver function (*56*). Importantly, reversible cholestatic liver disease has been observed in few patients receiving Infliximab for various autoimmune disorders (*57*).

Taken together, liver diseases from different aetiology can cause liver fibrosis. Moreover, TNF-α is considered as one of the important factors which triggers liver fibrosis and cirrhosis in many liver diseases.

1.2 Liver fibrosis and hepatic stellate cells

Fibrosis is defined by the excessive accumulation of extracellular matrix (ECM) such as collagen and fibronectin in and around inflamed or damaged tissue, which can lead to permanent scarring, organ malfunction and, ultimately, death, as seen in end stage liver diseases, kidney diseases, idiopathic pulmanory fibrosis (IPF) and heart failure (*58-60*). Fibrosis is also a major pathological feature of many chronic autoimmune diseases such as scleroderma, rheumatoid arthritis, Crohn's diseases, ulcerative colitis, myelofibrosis and systemic lupus erythematosus (*60*). Fibrosis can be induced by a variety of stimulus including persistent infections, autoimmune reactions, allergic responses, chemical insults, radiation, and tissue injury (*61*). Chronic inflammation in the liver leads to liver cirrhosis, which is the 11th leading cause of death, accounting for 41,743 deaths in US, 2017 according to the Centers for Disease Control and Prevention (CDC). The accumulation of ECM proteins in the liver during liver fibrosis can misshape the hepatic architecture by forming a fibrotic scar, and the subsequent development of nodules of regenerating hepatocytes defines cirrhosis (*62*).

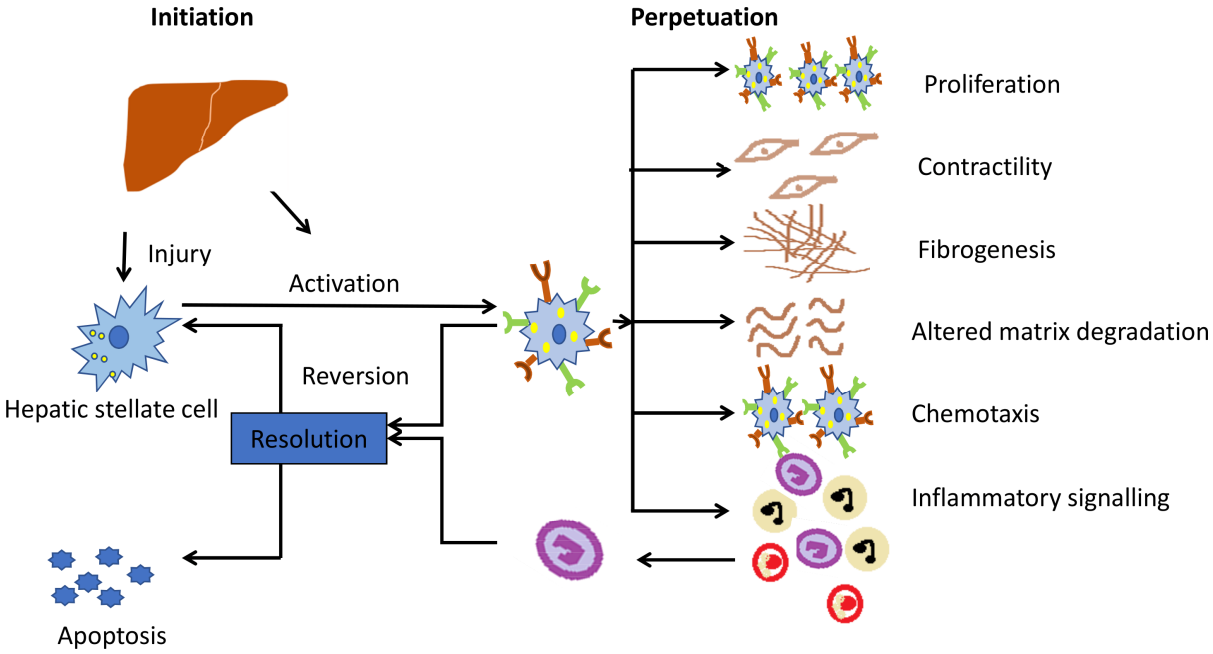

Graphical figure 3: Functions, features and phenotypes of HSCs in normal and diseased liver. Figure was adapted from (63).

Fibrotic changes in liver disease are mediated by increased production of collagens and the transdifferentiation of HSCs into myofibroblasts (*64-66*). HSCs represent approximately 5-8 % of the total liver (*67*). HSCs are progenitor cells that are normally quiescent but proliferate in response to liver injury and contribute to liver regeneration (*68*). Under normal conditions, quiescent HSCs reside in the space of Disse, store Vitamin A, and produce a specific marker called glial fibrillary acid protein (GFAP). Following stimulation with CD95 or other death receptor ligands, HSCs have the paradoxical tendency to proliferate (*69*). In response to liver injury, HSCs undergo a physiological change by reducing their Vitamin A storage, migrate to pericentral areas, and transdifferentiate into collagen type I– and α-smooth muscle actin (α-SMA)–producing myofibroblasts (Graphical figure 3) (*70, 71*).

Over all, activated HSCs are the major driving factor for liver fibrosis during liver injury which can lead to liver cirrhosis and HCC.

1.2.1 Mechanism of HSC activation

Multiple factors can contribute to activation, differentiation and proliferation of HSCs during liver injury. Since, activated HSCs are the major cellular factor which contribute to liver fibrosis, it should be considered as a primary cellular target for anti-fibrotic therapy (*65*). HSCs express specific genes and proteins which help to distinguish them from other liver resident cell types. These markers include: the cell-surface protein platelet-derived growth factor receptor-β (PDGFRβ); the enzyme lecithin retinol acyltransferase (LRAT); the cytoskeletal proteins desmin and glial fibrillary acidic protein (GFAP); and the transcription factor heart-and neural crest derivatives-expressed protein 2 (HAND2) (*65, 72-77*).

The activation of HSCs is mediated by various growth factors such as transforming growth factor-β (TGF-β), platelet derived growth factor (PDGF), vascular endothelial growth factor (VEGF), and connective tissue growth factor (CTGF). These growth factors are generally considered as fibrogenic and proliferative cytokines (*78-83*) in chronic liver diseases. Another important factor is immune cells; hepatic fibrogenesis is induced by multiple resident and recruited immune cells during liver injury. Most importantly, resident Kupffer cells and recruited monocytes can contribute to liver fibrosis by increased production of pro-inflammatory cytokines. Survival of activated HSCs is mainly driven by NF-κB signalling which is activated by macrophage mediated TNF-α and IL-1β production (*15*). Consistently, macrophage depletion results in reduced liver injury and liver fibrosis (*84*) in carbon tetrachloride treated mice. Like cytokines, chemokines also can promote liver fibrosis.

Chemokines such as CCR1 and CCR2 is highly expressed in Ly6G^{hi} infiltrated monocytes which can promote liver fibrosis. Macrophage infiltration and liver fibrogenesis is redcued after BDL and carbon tetrachloride treatment in CCR1 and CCR2 deficient animals (*85, 86*). Chemokine ligands such as CCL3 and CCL5 can also promote HSC activation and immune cell infiltration during liver injury. In absence of CCL3 and CCL5, both HSCs activation and immune cell infiltration is reduced in carbon tetrachloride treated mice (*87, 88*). Hepatic injury is associated with increased bacterial translocation and can activate TLR4, an important pattern recognition receptor (PRR). Bacterial translocation and TLR4 activation can trigger liver fibrosis by inducing chemotaxis of kupffer cells (*89*).

All together, the secretion of growth factors, cytokines and chemokines during liver injury regulates HSC activation, proliferation and transdifferentiation into myofibroblasts which can contribute to liver fibrosis.

1.2.2 Role of TNF-α in HSC activation

TNF-α is a proinflammatory cytokine that can induce liver cell death during liver diseases (*90*). TNF-α is synthesized as a membrane-bound protein that is proteolytically cleaved by the metalloprotease ADAM17, also known as TACE (*91, 92*). TNF-α has diverse biological roles in liver diseases including cytotoxicity, inflammation, growth stimulation and immune modulation (*93*). Increased level of TNF-α were found in patients with PBC (*94*), chronic viral hepatitis (*95*), fulminant hepatic failure (*96*), and alcoholic liver cirrhosis (*97*). Furthermore, TNF-α mediates liver injury in several animal models such as alcohol- or dimethylnitrosamine-induced liver injury (*98, 99*) and by exposure to hepatotoxins such as carbon tetrachloride or amanitin (*100, 101*).

Cholestasis can be induced in animals by BDL, which is used to study chronic liver injury because it duplicates the hepatocyte damage, HSC activation and liver fibrosis similar to what we observe in human liver diseases. Like in other liver disease models, TNF-α is also elevated in BDL animals (*102*). Importantly, liver injury and liver fibrosis is reduced in TNF-α deficient animals by reduced production of ECM (*103, 104*). Previous studies have demonstrated that TNFR1 deficient HSCs showed decreased proliferation upon exposure to PDGF and thereby decreased liver fibrosis in BDL animals, whereas TNFR2 deficient mice didn't show any difference in liver fibrosis compared to WT animals suggesting that TNF-α regulates HSC biology through its binding to TNFR1 (*105*). Consistently, another study

shows that liver fibrosis is reduced in TNFR1 deficient animals in carbon tetrachloride induced liver injury models suggesting that NF-κB, STAT3 and AP1 signals transduced through TNFR1 play important roles in the formation of liver fibrosis (*106*). On the other hand, TNF-α also plays a pivotal role in liver regeneration in partial hepatectomy (*107, 108*) and in carbon tetrachloride induced liver injury model (*109*) showing that TNFR1 is necessary for hepatocyte proliferation through NF-κB and STAT3 signalling pathways.

Taken together, TNF-α acts as a double-edged sword by inducing proliferation of HSCs, which is a hallmark for liver fibrosis in chronic liver diseases and it is also very essential for liver regeneration through the proliferation of hepatocytes during acute liver damage.

1.3 ADAM proteases

ADAM (a disintegrin and metalloprotease) proteins are membrane-anchored metalloproteases that process and shed the ectodomains of membrane-anchored growth factors, cytokines and receptors (*110*). ADAMs are single pass transmembrane metalloproteases which contain well defined domains including an extracellular metalloprotease domain, a disintegrin domain, a cysteine rich domain, a EGF-like domain, a transmembrane domain and a cytoplasmic domain (*110-112*).

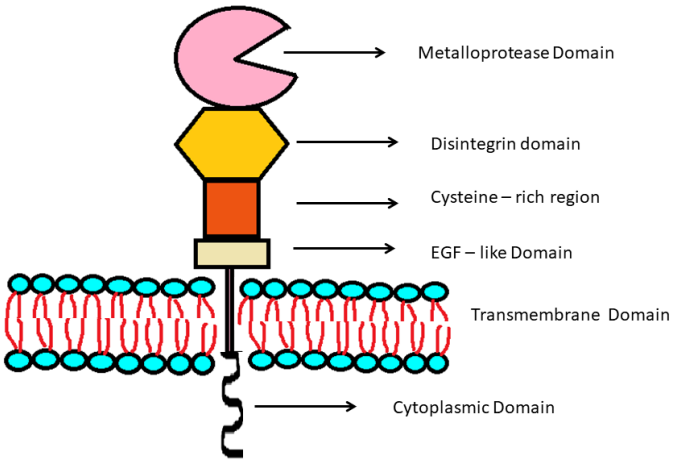

Graphical figure 4: Structure of ADAM domain. Figure was adapted from (110)

The prodomain inhibits the ADAM protease activity and it is cleaved by the protease furin (*113-115*). The ADAM disintegrin-domain can interact with integrins to influence cell adhesion and cell-cell interactions. The disintegrin and EGF-domain are thought to be

involved in substrate recognition (*116*). The catalytically active domain contains a specific sequence: HEXXH in their catalytic site of the metalloprotease domain. ADAMs that do not contain the HEXXH sequence at their conserved metalloprotease domain probably do not possess catalytic activity, and those ADAMs probably can have their biological function mainly by protein-protein interaction (*110, 116*). Among all ADAM proteases, ADAM10 and ADAM17 are well studied ADAMs and they have been shown to be essential in fertilization, angiogenesis, neurogenesis, heart development and cancer (*110*).

1.3.1 ADAM17 / TACE

ADAM17 is a well-defined member of the ADAM family (*110*). ADAM17 was first discovered in 1997 by two research groups showing that the ADAM17 enzyme can release membrane-bound TNF-α into a soluble form (*91, 92*). Importantly, expression of ADAM17 can vary from embryonic development to adult stage and it is widely expressed in different organs such as brain, heart, kidney and skeletal muscle (*91*). ADAM17 is synthesized as inactive protease that requires furin mediated cleavage in the trans Golgi-network (TGN) to become active (*110*). The main function of ADAM17 is to cleave ectodomains of various transmembrane proteins such as Epidermal growth factor receptor (EGFR) ligands, TNF-α and its receptors, adhesion molecules and the amyloid precursor protein (*91, 92, 117-120*). The cleaved ligand can bind either to the same cell (autocrine) or to nearby cells (paracrine) (*121, 122*). Since, ADAM17 is involved in the shedding of 76 membrane-anchored ligands (*123*), its activation has to be tightly regulated. Excess ADAM17 activation can trigger tumor progression by increasing EGFR signalling and also can cause inflammatory related diseases by increased shedding of membrane-bound TNF-α (*124, 125*). On the other hand, low ADAM17 activation can cause defects in development and regeneration (*124*). Mice with specific ADAM17 inactivation in the myeloid cells are protected against endotoxin shock by preventing cleavage of membrane-bound TNF-α (*125*). However, factors regulating ADAM17 activation and maturation is still poorly understood.

1.3.2 Role of ADAM17 in liver diseases

Since ADAM17 is involved in the shedding of various membrane-bound ligands and receptors, it is highly possible that ADAM17 might play a crucial role during liver damage and liver regeneration. Hepatocyte-specific ADAM17 deletion significantly attenuated the induction of TNF-α, TNFR1 and amphiregulin after partial hepatectomy suggesting that

ADAM17 is the primary sheddase during liver regeneration (*126*). Tissue inhibitor of metalloproteinase 3 (TIMP3) is a known inhibitor for ADAM17 activity and it regulates ADAM17 at a posttranslational level (*127*). TIMP3 deficient animals show enhanced activation of ADAM17 by constitutive release of TNF-α and increased activation of TNF signalling in the liver which leads to inappropriate induction of inflammation and TNF-mediated cell death (*128*) suggesting that ADAM17 regulation is very crucial during partial hepatectomy. Conversely, enhanced shedding of ADAM17 ligands such as TNF receptor 1 (TNFR1), TGF-α, amphiregulin and HB-EGF in TIMP3 deficient animals are protected against Fas mediated apoptosis (*129*). Importantly, ADAM17 expression is increased in liver and spleen tissue after partial hepatectomy (*130*) suggesting that ADAM17 activity is indispensable during liver regeneration. ADAM proteases might also regulate liver fibrosis at different levels: (a) release of paracrine-acting cytokines and growth factors, (b) shedding of receptors on HSC membrane, and (c) modulation of ECM (*131*). Studies from different research groups have revealed the expression of several ADAM proteases including ADAM 8, ADAM 9, ADAM 10, ADAM 12, ADAM 17 and ADAM 28 are increased with HSCs activation and their expression was also detectable in fibrotic liver diseases (*132-135*). Recently, two interesting parallel studies demonstrated that the inactive member of rhomboid protease 2 (iRhom2) encoded by *Rhbdf2* is essential for ADAM17 trafficking from endoplasmic reticulum to the cell surface and also for its activation (*136, 137*). Taken together, ADAM17 is a very critical metalloprotease which regulate liver regeneration and liver fibrosis by shedding of membrane-bound growth factors, cytokines and receptors.

1.4 Rhomboid proteases

Rhomboid proteases are well-conserved family of intramembrane serine proteases. The active site of rhomboids is generally buried within the transmembrane domain (TMD), and they cleave substrates in or near transmembrane domains, thereby releasing soluble domains from membrane proteins (*138*). There are four different classes of intramembrane proteases that have been discovered so far such as metalloproteases (*139-141*); aspartyl proteases, of which two classes are gamma secretase and the signal peptide peptidase-like family (*142-144*); and the rhomboid-like family, which are serine proteases (*145, 146*). The first rhomboid was discovered in a Drosophila mutation with an abnormally rhomboid-shaped head skeleton (*147*). Further studies demonstrated that Drosophila rhomboid participated in developmental control by the EGFR pathway (*148, 149*). Eukaryotic rhomboids can be classified into three major groups based on membrane topology, structure and function information: (a) the active

proteases; (b) a tightly clustered group of apparently inactive rhomboid-like proteins (termed iRhoms), which resemble rhomboids in most regards but which lack catalytic residues; and (c) a number of other rhomboid-like proteins that are predicted to be inactive but which do not cluster with themselves or with the iRhoms (*138, 145*) (Graphical figure 5).

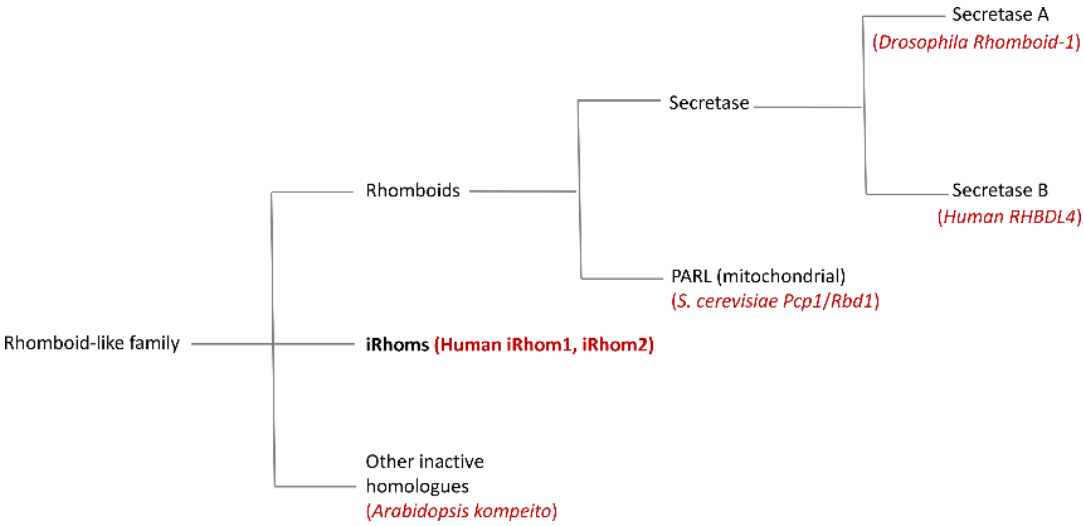

Graphical figure 5: Image shows the rhomboid family. Image was adapted from (138).

1.4.1 iRhom 2 – inactive rhomboid protease 2

iRhom2 is a pseudoprotease which lack the catalytic domain of rhomboid proteases, but they are phylogenetically closely related to ancestral rhomboid family members (*150, 151*). iRhom2 has seven transmembrane domains (TMD) and is predominantly localized in endoplasmic reticulum (ER). iRhoms are conserved in metazoans: Drosophila has one iRhom whereas mammals harbour two iRhoms, namely iRhom1 encoded by *Rhbdf1* and iRhom2 encoded by *Rhbdf2* (*152*). Previous studies demonstrated that iRhom2 expression is particularly restricted to myeloid cells (*136, 137, 153*), high in microglia (brain-resident macrophages) (*154*) and Kupffer cells (liver-resident macrophages) (*155*). iRhom2 knockout mice are viable and didn't show any abnormalities during its development (*136, 137*). iRhom2 has been studied extensively in various infection and inflammatory disease model system using iRhom2 knockout mice. Previous studies had clearly demonstrated that iRhom2 is an essential adaptor for ADAM17 function. ADAM17 interacts with iRhom2 in the endoplasmic reticulum and influences its trafficking to the Golgi where the ADAM17 pro-domain gets cleaved by furin to promote surface expression of ADAM17. ADAM17 failed to

reach plasma membrane in absence of iRhom2 and consistently shedding of ADAM17 ligands was also decreased in iRhom2 deficient animals (*136, 137*) (Graphical figure 6).

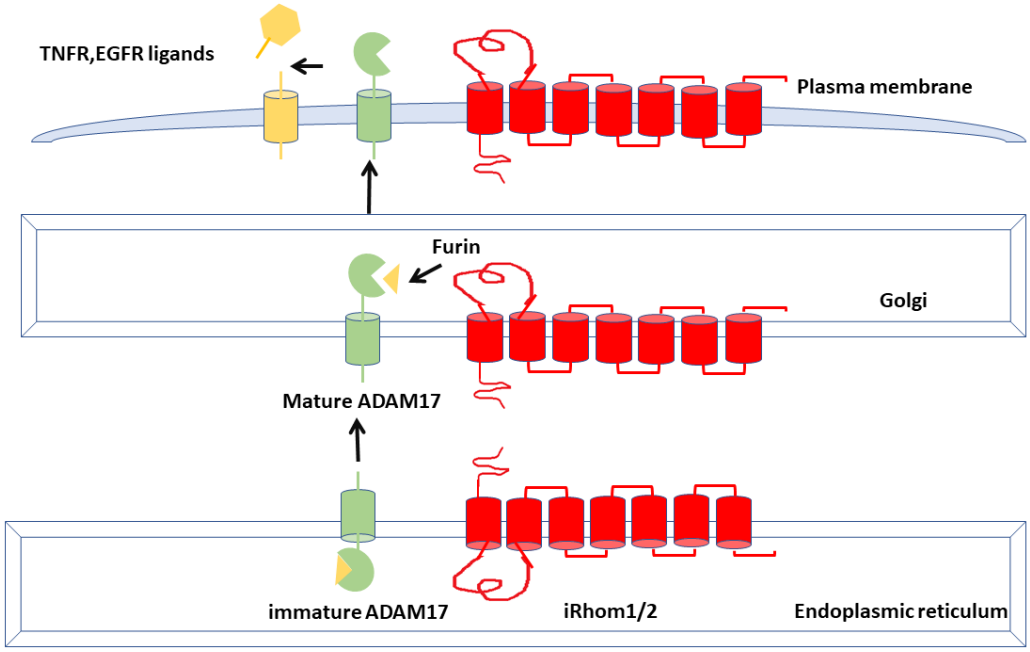

Graphical figure 6: Schematic representation of ADAM17 and iRhom2 trafficking from endoplasmic reticulum to cell surface. Figure was adapted from (152).

As mentioned earlier, membrane bound TNF-α and EGFR ligands can be cleaved by ADAM17 (*91, 92*). Since, TNF-α and EGFR signalling participates in various physiological and pathological conditions, iRhom2 has been studied in various disease model system.

1.4.2 Role of iRhom2 in infectious diseases

In absence of iRhom2, mice are highly susceptible to *Listeria monocytogenes* infection, since TNF-α shedding is abolished in iRhom2 deficient animals to control the infection (*137*). Thioglycollate-elictied peritoneal macrophages (TGEMs) isolated from iRhom2 deficient mice showed reduced shedding of TNF-α upon *Listeria monocytogenes* infection along with increased presence of bacterial titers in spleen, liver, kidney and brain after infection (*137*) highlighting the pivotal role of iRhom2 in pathogen defense. iRhom2 protects stimulator of interferon genes (STING) from its degradation during DNA virus infection. STING is important for the interferon response for virus clearance. Hence, iRhom2 deficient animals are susceptible to lethal herpes simplex virus type 1 (HSV-1) infection (*156*). iRhom2

regulates STING in two different ways: by mediating TRAPβ-dependent translocation and activation of STING and by linking the deubiquitinase EIF3S5 to STING facilitating the deubiquitination and stability of STING (*156*). iRhom2 also protects mitochondrial membrane-located adaptor protein VISA from degradation. VISA is an essential regulator for antiviral genes, iRhom2 deficiency showed reduction in antiviral response to several RNA viruses, including Sendai virus and vesicular stomatitis virus (VSV). iRhom2 deficient mice had higher VSV titers in spleen and liver and these mice are highly susceptible to VSV infection when compared to WT animals (*157*).

1.4.3 Role of iRhom2 in inflammatory diseases

iRhom2 is an important contributor for inflammation as it is tightly connected with ADAM17 / TNF-α signaling. iRhom2 knockout mice showed significant reduction of circulating TNF-α after LPS injection compared to control mice (*137*). Septic shock can be induced *in vivo* by combined injection of D-galactosamine (GalN) and LPS (*158*). iRhom2 deficient animals are protected from TNF-α mediated septic shock and liver damage compared to WT mice. Control mice showed an increased disrupted liver architecture and are highly susceptible to LPS and D-galactosamine (GalN) injection compared to iRhom2 knockout animals (*137*). iRhom2 expression is upregulated in synovial macrophages from rheumatoid arthritis (RA) patients compared to healthy controls. Using K/BxN mouse RA model, this study shows that iRhom2 knockout mice are significantly protected from inflammatory arthritis as shown by less joint swelling, synovial inflammation and cartilage erosion (*159*). iRhom2 deficient animals are protected from kidney inflammatory disease Lupus nephritis (LN) by inhibiting HB-EGF/EGFR and TNF-α signaling in the kidney tissues (*160*). iRhom2 knockout mice are also protected from Hemophilic arthropathy (HA), a degenerative joint disease that is a major manifestation of the bleeding disorder hemophilia A. iRhom2 loss in a mouse model for HA led to a marked reduction in osteopaenia and synovial inflammation (*161*). Airborne particulate matter (PM2.5) induces hepatic steatosis, metabolic syndrome and dyslipidaemia along with an increased expression of iRhom2 and elevated TNF-α in WT mice and these effects are significantly reduced in iRhom2 deficient animals. Knockdown of iRhom2 in Kupffer cells (liver-resident macrophages) leads to decrease in inflammatory cytokines, suggesting a role for iRhom2/ADAM17/TNF-α signaling axis in regulating hepatic inflammation and lipid metabolism in response to PM2.5 (*155*). TNF-α levels are increased in the serum and lungs of wild-type mice when subjected to Intestinal ischemia-reperfusion (I/R) and the effect is significantly reduced in iRhom2 deficient animals suggesting that

iRhom2 can be a novel therapeutic target for acute lung injury (AKI) after Intestinal ischemia-reperfusion (*162*). iRhom2 also participates in mediating pro-inflammatory responses during myocardial infarction, which is driven by TNF-α signalling (*163*). iRhom2 has been suggested as a therapeutic target for LPS-induced cardiac injury by regulating the inflammatory response (*164*). Taken together, iRhom2 is a critical regulator for ADAM17 activity and TNF-α secretion.

1.4.4 Role of iRhom2 in cancer

EGFR and TNF-α signalling are highly implicated in tumour growth and development (*165*). Moreover, iRhom2 has been shown to be involved in the shedding of EGFR ligands and TNF- α together with ADAM17, it is highly possible that iRhom2 could be a major driving factor for tumour progression. Mutations in the iRhom2 gene cause the rare autosomal dominant disease Tylosis with oesophageal cancer (TOC). This is consistent with increased EGFR ligand shedding, proliferation and migration potential observed in tylotic keratinocytes (*166-168*). iRhom2 also regulates thickening of footpad epidermis through its interaction with keratin 16 (K16). iRhom2 interacts with K16 and this interaction is increased in TOC keratinocytes (*169*). iRhom2 is also highly expressed in Cancer-associated fibroblasts (CAFs) which is the major cellular component in the tumour environment which supports tumour growth and development. iRhom2 deletion in CAFS shows reduction in their elongation and motility, whereas overexpression of iRhom2 in non-cancer fibroblasts (NF) showed increased motility in extra cellular matrix in response to TGFB1. iRhom2 has been reported to regulate ADAM17-dependent cleavage of TGFβ receptor (TGFBR1) and contribute to the progression of diffuse-type gastric cancers (DGCs) (*170*).

1.5 TNF-α signalling

TNF-α exists in 2 forms membrane-bound TNF-α (mTNF, 26 KDa) and soluble TNF-α (sTNF, 17 KDa). Membrane-bound TNF-α can be cleaved by ADAM17 together with iRhom2 (*136, 137*). TNF-α signals through 2 transmembrane receptors, TNFR1 and TNFR2 (*171*). Membrane-bound TNF is a potent ligand for TNFR2 that is expressed mostly by immune cells (*171*). On the other hand, TNFR1 is expressed at low levels by most cell types and can respond to both membrane-bound and soluble forms of TNF. Cell death and inflammatory cytokine production in response to TNF signaling is induced primarily by TNFR1 signaling (*172-175*), while the precise role of TNFR2 is relatively unclear (*176, 177*). TNFR2 has been shown to promote TNFR1-mediated cell death signaling (*173, 178, 179*)

and, in other cases, to promote cell survival, proliferation, and tissue homeostasis (*180-184*). TNFR signals nuclear factor-κB (NF-κB) for cell survival by recruiting TRADD and TRAF2, which results in the activation of NF-κB signalling pathway (*185*). NF-κB induces the expression of various pro-inflammatory cytokines and chemokines which plays a critical role in regulating the survival, activation and differentiation of innate immune cells (*186*). NF-κB proteins are normally sequestered in the cytoplasm by an inhibitory protein called inhibitor of κB α (IκBα). There are two different mechanisms by which NF-κB signalling can be activated, the canonical and noncanonical (or alternative) pathways (*187, 188*). The canonical NF-κB pathway responds to diverse stimuli, including ligands of various cytokine receptors, pattern recognition receptors (PRRs), TNFR superfamily members, as well as T-cell receptors (TCR) and B-cell receptors (BCR) (*189*). Upon activation, IKK phosphorylates IκBα and triggers ubiquitin-dependent degradation resulting in rapid and transient nuclear translocation of canonical NF-κB members predominantly p50/RelA and p50/c-Rel dimers (*190-192*). Noncanonical NF-κB pathway responds to a specific group of stimuli, including ligands of a subset of the TNFR superfamily members LTβR, BAFFR, CD40 and RANK (*193, 194*). Noncanonical NF-κB activation does not involve IκBα degradation but relies on processing of the NF-κB2 precursor protein, p100 (*187, 193*). Mostly, canonical NF-κB pathway participates in almost all aspects of immune responses, whereas the noncanonical NF-κB pathway appears to cooperate with canonical NF-κB pathway in the regulation of specific functions of the adaptive immune system (*194*).

Chapter 2

Material and methods

2. Materials and Methods:

Part of the materials and methods have been adapted from a published manuscript,

B. Sundaram, K. Behnke, A. Belancic, M. A. Al-Salihi, Y. Thabet, R. Polz, R. Pellegrino, Y. Zhuang, P. V. Shinde, H. C. Xu, J. Vasilevska, T. Longerich, D. Herebian, E. Mayatepek, H. H. Bock, P. May, C. Kordes, N. Aghaeepour, T. W. Mak, V. Keitel, D. Häussinger, J. Scheller, A. A. Pandyra, K. S. Lang, P. A. Lang, iRhom2 inhibits bile duct obstruction–induced liver fibrosis. *Sci. Signal.* **12**, eaax1194 (2019).

2.1 Animal experiments

All mice were maintained under specific pathogen-free (SPF) conditions at the authorization of the Landesamt für Natur, Umwelt und Verbraucherschutz of North Rhine-Westphalia (LANUV NRW) in accordance with the German laws for animal protection.

Rhbdf2$^{-/-}$ whole-body knockout mice were bred in ZETT - Univeristat Dusseldorf on a C57BL/6 background as previously described, and are available at MMRRC (https://www.mmrrc.org/) (*137*). Experiments were performed in 10 -12 weeks old male mice with littermate controls. All animal experiments were conducted according to the German law for the welfare of animals and were approved by local authorities.

2.1.1 Bile Duct Ligation

Bile Duct Ligation (BDL) is a well-established surgical technique to study liver fibrosis. BDL leads to an acute obstructive jaundice with progressive activation of hepatic stellate cells causing liver fibrosis (*195-197*).

For BDL, Laparotomy was performed predominantly on male mice at 10–14 weeks of age, animals were anaesthetised by isoflurane and placed on a heating pad. The animals were shaved and the skin was disinfected with 70% ethanol and povidone-iodine. A midline incision in the upper abdomen was made and the common bile duct and the gallbladder were identified, isolated, and ligated with silk. Abdomen and peritoneum were closed with a running silk suture. Sham treatment was performed similarly but without ligation of the bile

duct and gallbladder. Animals were monitored during recovery and treated with carprofen (0.05 mg/kg b.w.) after surgical intervention.

2.1.2 Etanercept (Enbrel) treatment

Etanercept (Enbrel, Pfizer) is a well-known inhibitor for TNF-α and previous studies have shown that etanercept treatment helps the host to recover from severe liver damage (*198, 199*). Etanercept was reconstituted in PBS to a final concentration of 10 mg/ml. Mice were subcutaneously injected with 10 mg/kg Etanercept 24h before surgery and every other day after surgery until day 14.

2.2 Analysis of human material

Serum samples from patients suffering from liver disease and healthy volunteers were collected (Table 3, Cohort A). Patients gave informed consent and analysis was approved by the ethics committee of the Faculty of Medicine at the Heinrich-Heine-University of Dusseldorf under the Study-No. 5350. Expression levels of *RHBDF2* were determined in (Table 3, Cohort B) under approval of the ethics committee of the Medical Faculty of University of Heidelberg: Study-No. 206/05.

2.3 Histology

Histological analysis of snap-frozen tissue was performed as previously described (*200*). Briefly, snap-frozen tissue sections were cut to 7 µm sections, air dried and fixed with acetone for 10 min. Sections were blocked with 2% fetal calf serum in PBS for 1h. Sections were stained with primary antibody for 1h, washed with PBS containing 0.05% Tween 20 (Sigma), and incubated with secondary antibody together with DAPI (1:1000) for 1h. Then sections were washed and mounted using fluorescence mounting medium (Dako). Images were taken by the Axio Observer Z1 fluorescence microscope (Zeiss). Analysis of the fluorescence images was performed using ImageJ software. Picro Sirius Red and Masson's Trichrome Staining Kits were purchased from Polysciences, Inc., and staining was performed according to the manufacturer's instructions.

Table 1: List of antibodies used for immunofluorescence (IF)

Primary Antibodies	Company	Dilution
Col1A1	Thermo Scientific	1:100
αSMA	Abcam	1:100
PDGFRβ	Cell Signaling Technology	1:100
Desmin	Cell Signaling Technology	1:100
p65	Santa Cruz Biotechnology	1:100
CD68	Bio-Rad	1:200
F4/80	eBioscience	1:200
LY6G	eBioscience	1:200
Secondary Antibodies	**Company**	**Dilution**
anti-rabbit-Cy	Jackson ImmunoResearch Laboratories, Inc	1:200
anti-rat APC for CD68	Jackson ImmunoResearch Laboratories, Inc	1:200
anti-rat PE for Ki67	Jackson ImmunoResearch Laboratories, Inc	1:200

2.4 RT-PCR analyses

RNA purification was performed according to manufacturer's instructions (Qiagen RNeasy Kit or Trizol). Gene expression of *Rhbdf2, Tnfrsf1a, Tnfrsf1b, Tnf, Hbegf, Areg, Tgfa, Il6r, Il6, Col1a1, Col3a1*, and *Acta2* was performed using FAM/VIC probes (Applied Biosystems) and iTAQ™ One step PCR kit (Bio-Rad). Gene expression of *Il1b, Il10, Cd80, Cd86, Ccl2, Ccl3, Ccl4, Ccl5, Ccl8, Ccl9, Ccl12, Ccl17, Ccl20, Cxcl2, Cxcl9, Cxcl10 Cxcl11,* and *Cxcl13* was performed using SYBR GREEN probes. For analysis, the expression levels of all target genes were normalized to *Gapdh* expression (ΔCt). Gene expression values were then calculated based on the ΔΔCt method, using naive WT mice as a control to which all other samples were compared. Relative quantities (RQ) were determined using the equation: RQ=2^-ΔΔCt.

2.5 Immunoblotting

Briefly, liver tissue was lysed in PBS containing 1% TX-100 (Sigma), EDTA-free protease inhibitor cocktail (Roche), Phospho stop (1 tablet/10mL), and the inhibitors BB-2516 (20μM, Tocris Bioscience) and 1,10-phenanthroline (10mM, Sigma). After lysis, the sample was used for Immunoblotting.

Table 2: List of antibodies used for western blotting

Primary antibodies	Company	Dilution
anti-ADAM17	Abcam	1:2000
anti-p-STAT3	Cell Signaling Technology	1:1000
anti-total-STAT3	Cell Signaling Technology	1:1000
anti-p-ERK1/2	Cell Signaling Technology	1:2000
anti-total-ERK1/2	Cell Signaling Technology	1:2000
anti-total-IκBα	Cell Signaling Technology	1:1000
anti-p-p65	Cell Signaling Technology	1:1000
anti-total-p65	Cell Signaling Technology	1:1000
anti-αSMA	Abcam	1:1000
anti-α-tubulin	Cell Signaling Technology	1:1000
anti-β-actin	Cell Signaling Technology	1:3000

Secondary antibodies	Company	Dilution
Anti-Rabbit HRP	Cell Signaling Technology	1:5000
Anti-Mouse HRP	Cell Signaling Technology	1:5000
IRDye 800CW Anti-Rabbit	LI-COR Biosciences	1:10000
IRDye 680CW Anti-Mouse	LI-COR Biosciences	1:10000

2.6 ELISA

The following ELISA kits were used: TNFR1, TNFR2, IL-6Rα, HB-EGF, and Amphiregulin (R&D Systems); TNF-α (eBioscience); TGF-α (antibodies-online); TGF-β1, IL-6 and IL-1β (Invitrogen). All ELISAs were performed according to the manufacturers' instructions.

2.7 Serum biochemistry

Aspartate aminotransferase (AST, GOT), alanine aminotransferase (ALT, GPT), total bilirubin and LDH were measured using the automated biochemical analyser Spotchem EZ SP-4430 (Arkray, Amstelveen, Netherlands) and the Spotchem EZ Reagent Strips Liver-1.

2.8 Bile acid analysis

Bile acids and their glycine- and taurine derivatives were analyzed by UPLC-MS/MS (*201*). The system consists of an Acquity UPLC-I Class (Waters, UK) coupled to a Waters Xevo-TQS tandem mass spectrometer equipped with an ESI source in the negative ion mode. Data were collected in the multiple reaction monitoring (MRM) mode.

2.9 Bacterial titer estimation

Gut Bacterial translocation have been previously described in bile duct ligated animals (*202, 203*). Briefly, mesenteric lymph nodes were harvested in sterile conditions from *Rhbdf2*$^{+/-}$ *and Rhbdf2*$^{-/-}$ mice after BDL and was homogenized in PBS. The homogenized mesenteric lymph nodes were plated in Blood Agar Plates (containing 5% sheep blood) for total aerobic bacteria. The plates were incubated for 48-72 hrs at 37^{o}C followed by the counting of colony-forming units (CFUs) (*204*).

2.10 HSC isolation

Primary mouse HSCs isolation using sequential pronase-collagense digestion have been previously described (*205*). Briefly, livers were perfused *in situ* with HBSS buffer without Ca^{2+} and Mg^{2+} (Thermo-Fisher Scientific) supplemented with 0.5 mM EGTA for 5 min. Then, liver tissue was perfused with pronase E (0.7 mg/ml, Roche) for 5 min and collagenase P (0.25 mg/ml, Roche) for 6-8 min, respectively, at a flow rate of 5 ml/min in HBSS buffer containing Ca^{2+}. After excision of the liver, the liver was digested *in vitro* for 15 min in HBSS containing 1% DNase I (Roche). HSCs were purified from the remainder of non-parenchymal cells and hepatocyte-derived debris by floatation through 9% (w/v) Optiprep (Axis-Shield PoC AS, Oslo, Norway) in HBSS buffer. The isolated HSCs were cultured in DMEM/F-12 (Thermo Fisher Scientific) supplemented with 10% FCS. For TNF-α treatment, primary HSCs were isolated from *Rhbdf2*$^{+/-}$ and *Rhbdf2*$^{-/-}$and the isolated HSCs were cultured in DMEM/F-12 supplemented with 10% FCS for three days, then the cells were starved in serum free DMEM/F-12 medium for overnight. Next day the cells were treated with and without 50ng/ml TNF-α in DMEM/F-12 supplemented with 10% FCS for 24 hours.

2.11 Hepatocyte and Kupffer cell isolation

Primary mouse hepatocyte and Kupffer cell isolation using collagenase digestion have been previously described (*206, 207*). Briefly, livers were perfused *in situ* with HBSS buffer without Ca^{2+} and Mg^{2+} (Thermo-Fisher Scientific) supplemented with 0.5 mM EGTA for 5 min. Then, liver tissue was perfused with collagenase P (0.25 mg/ml, Roche) for 6-8 min, respectively, at a flow rate of 5 ml/min in HBSS buffer containing Ca^{2+}. After excision of the liver, the liver was digested *in vitro* for 15 min in HBSS containing 1% DNase I (Roche). The digested liver was centrifuged for 3 min at a speed of 30×*g*. The supernatant was used for Kupffer cell isolation while hepatocytes were isolated from the pellet. After the first

centrifugation, the supernatant was slowly layered on the percoll gradient and centrifuged for 30 min at 1200×*g*. The middle interphase was collected and stained for F4/80 and Kupffer cells were sorted (BD FACSAria). Primary hepatocytes isolated from *Rhbdf2*$^{+/-}$ and *Rhbdf2*$^{-/-}$ animals were treated with CHX (10μg/ml) and TNF-α (40ng/ml) for 8 hours in Williams medium.

2.12 Statistical analyses

Data are expressed as mean ± S.E.M. Statistically significant differences between two groups were determined with Mann-Whitney U test. Statistically significant differences between several groups were determined with a one-way analysis of variance (ANOVA). Statistically significant differences between groups in experiments involving more than one time-point were determined using a two-way ANOVA.

Chapter 3

Aim of the study

Aim of the study

Tissue damage and regeneration has to be tightly regulated during infection or injury to maintain the body in homeostatic conditions. If dysregulated it can lead to chronic inflammation or cancer which can cause serious complications to the host. TNF-α is a pleiotropic cytokine mainly produced by macrophages which participates in many critical functions including host defense, cell proliferation and apoptosis. TNF-α has been shown to be essential for innate immune activation to clear pathogens (*208*) and its aberrant production can be associated with the pathogenesis of several diseases, including rheumatoid arthritis, Crohn's disease, atherosclerosis, psoriasis, sepsis, diabetes, and obesity (*209*). So it is clear that the regulation of TNF-α is very crucial for the host survival during infection and injury. Recent studies had shown that the ADAM17 / iRhom2 signaling axis plays a crucial role for TNF-α biology (*136, 137*).

Earlier studies showed TNF-α expression is upregulated in bile duct ligated and carbon tetrachloride treated animals compared to untreated mice (*104, 210*). Since, iRhom2 plays a pivotal role in TNF-α biology, we wanted to uncover the role of iRhom2 in bile duct ligated mice. In this study, we hypothesized that (i) iRhom2 might have pro-inflammatory functions in WT mice compared to iRhom2 deficient animals during bile duct ligation and drive severe complications such as liver fibrosis to the host. ADAM17 not only cleaves TNF-α, but also other ligands such as HB-EGF, TGF-α, amphiregulin (EGF ligands) and IL-6R. Previous studies have shown the importance of these ligands during liver regeneration. Mice lacking EGFR specifically in hepatocytes show decreased hepatocyte proliferation in the initial phase of liver regeneration (*211*). IL-6 trans-signaling can be activated by binding of IL-6 to soluble IL-6R (sIL-6R), and earlier studies have described the importance of IL-6 trans-signaling for the protection of the liver during acute damage to the organ (*212, 213*). Since, ADAM17 / iRhom2 is essential to cleave these ligands, our another hypothesis is that (ii) iRhom2 deficient animals might show decreased liver regeneration and higher susceptibility towards BDL compared to WT animals.

In the context of liver fibrosis, reduced TNF-α shedding from macrophages should alleviate fibrosis, whereas reduced TNFR shedding from other liver cells would have opposite effects. In this study we therefore chose whole body *Rhbdf2*$^{-/-}$ mice to determine which plays a dominant role in liver regeneration and liver fibrosis.

Chapter 4

Results

4. Results

4.1 Increased expression of iRhom2 during liver fibrosis in bile duct ligated mice.

Liver fibrosis can be induced in mice following BDL (*195, 196*) which results in increased production of α-SMA and expression of *Col1a1*, which encodes the α1 chain of collagen type 1, in the liver. To check the activation of liver fibrosis, we did sham and BDL surgery in C57BL/6 WT mice and examined the production of α-SMA and expression of *Col1a1* in the liver tissue harvested on day 14 and 20 post surgery. Consistent with previous studies (*195, 196*), we also identified increased production of α-SMA and expression of *Col1a1* in the BDL liver compared to sham operated animals (Figure 1A-B). Further, we wondered whether the activation of ADAM17 is affected during liver fibrosis in BDL animals. ADAM17 undergoes post-translational modification by removal of the pro-domain in the trans-Golgi network which results in the mature form of the enzyme for its activation (*110*). Interestingly, we detected increased presence of the mature form in the BDL liver when we compared them to sham operated liver (Figure 1C-D). ADAM17 activation can be triggered by iRhom2 which is encoded by *Rhbdf2* (*136, 137*). Notably, hepatic *Rhbdf2* expression increased during liver fibrosis following BDL in mice (Figure 1E).

Taken together, these findings indicate that activation of ADAM17 and expression of iRhom2 is increased during liver fibrosis in the BDL liver compared to sham operated liver leading us to further investigate whether iRhom2 influenced the progression of liver fibrosis.

Figure 1.

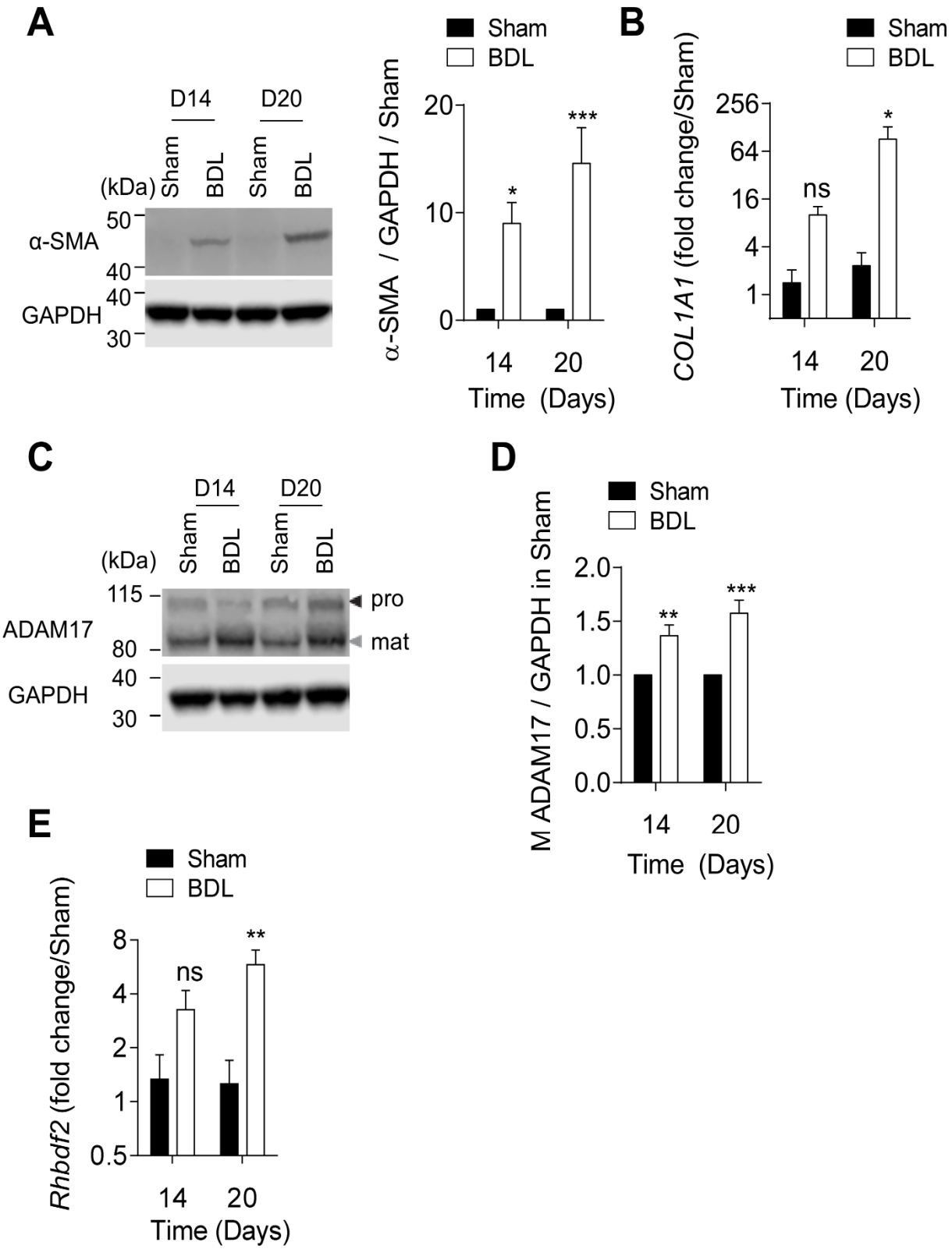
A
D14
D20
Sham
BDL
Sham
BDL
(kDa)
50
α-SMA
40
40
GAPDH
30
Sham
BDL
α-SMA / GAPDH / Sham
20
10
0
*
***
14
20
Time (Days)
B
Sham
BDL
COL1A1 (fold change/Sham)
256
64
16
4
1
ns
*
14
20
Time (Days)
C
D14
D20
Sham
BDL
Sham
BDL
(kDa)
115
pro
ADAM17
80
mat
40
GAPDH
30
D
Sham
BDL
M ADAM17 / GAPDH in Sham
2.0
1.5
1.0
0.5
0.0
**
***
14
20
Time (Days)
E
Sham
BDL
Rhbdf2 (fold change/Sham)
8
4
2
1
0.5
ns
**
14
20
Time (Days)

Figure 1. ADAM17 activity increases during liver fibrosis

(A) *Immunoblotting and quantification of α-SMA in total liver tissue of sham- and BDL-operated WT mice at day 14 (D14) and day 20 (D20) after surgery. Right panel shows the quantification of α-SMA by densitometry. GAPDH is a loading control.* ***(B)*** *Quantification of Col1a1 mRNA in total liver tissue of sham- and BDL-operated mice at day 14 or day 20 after surgery. (**C** to **D**) Immunoblotting and quantification of ADAM17 in total liver tissue of sham-and BDL-operated mice at day 14 (D14) and day 20 (D20) after surgery. Pro and mature (mat) forms of ADAM17 are noted on the immunoblot (C). The mature (M) form of ADAM17 was quantified by densitometry (D). GAPDH is a loading control. (**E**) Quantification of Rhbdf2 mRNA in total liver tissue of sham- and BDL-operated mice at day 14 or day 20 after surgery. ns, not significant. For all experiments, n = 5 mice per condition. Data are shown as means ± SEM. *P < 0.05, **P < 0.01, ***P < 0.001, two-way ANOVA with Bonferroni's multiple comparisons test (A, B, D, and E).*

4.2 Increased presence of circulating TNFRs in BDL mice and in cirrhotic patients

Activation of ADAM17 can trigger increased shedding of its substrates from the cell surface. Previous studies have clearly demonstrated the activation of ADAM17 and expression of iRhom2 can result in increased shedding of TNF-α, L-selectin, heparin-binding epidermal growth factor (HB-EGF), TNFR1, TNFR2, Amphiregulin, Epiregulin, EphB4, KitL2, and Tie2 (*137, 168, 214*). Since, we identified increased mature form of ADAM17 and iRhom2 expression in BDL animals; we speculated that shedding of ADAM17 substrates could also be increased during liver fibrosis in BDL operated animals. As we expected, we determined increased presence of ADAM17 ligands TNFR 1, TNFR 2 and IL-6R (Figure 2A-C) in the sera of BDL mice when compared to sham operated mice. However, other ADAM17 substrates we tested were not detectable or increased in the sera of mice suffering from liver fibrosis (Figure 2D-F). Moreover, we determined TNFRs concentrations in plasma samples from various patients with or without liver cirrhosis and healthy volunteers (table 3, cohort A). The cirrhotic patient group consisted of patients with liver cirrhosis who were infected with hepatitis B virus (HBV), hepatitis C virus (HCV), or the HBV isolate HC-C2. The non-cirrhotic group included healthy volunteers as well as non-cirrhotic patients who were infected with HBV or who were infected with HBV or HCV and also suffered from non-alcoholic steatohepatitis (NASH). We detected increased serum concentrations of TNFRs in cirrhotic patients as compared to non-cirrhotic patients and healthy volunteers (Figure 2G). Furthermore, *RHBDF2* mRNA was increased in human cirrhotic liver tissue compared to non-cirrhotic liver tissue (Figure 2H, table 3, cohort B).

Taken together, these results again proving that the activation of ADAM17 is increased during liver fibrosis in BDL animals compare to sham operated animals. Consistent with our *in vivo* finding, serum from cirrhotic patients also shows increased circulating TNFRs and increased *RHBDF2* mRNA expression in cirrhotic liver tissue compared to non-cirrhotic liver tissue confirming that ADAM17 is activated in cirrhotic patient's liver tissue.

Figure 2.

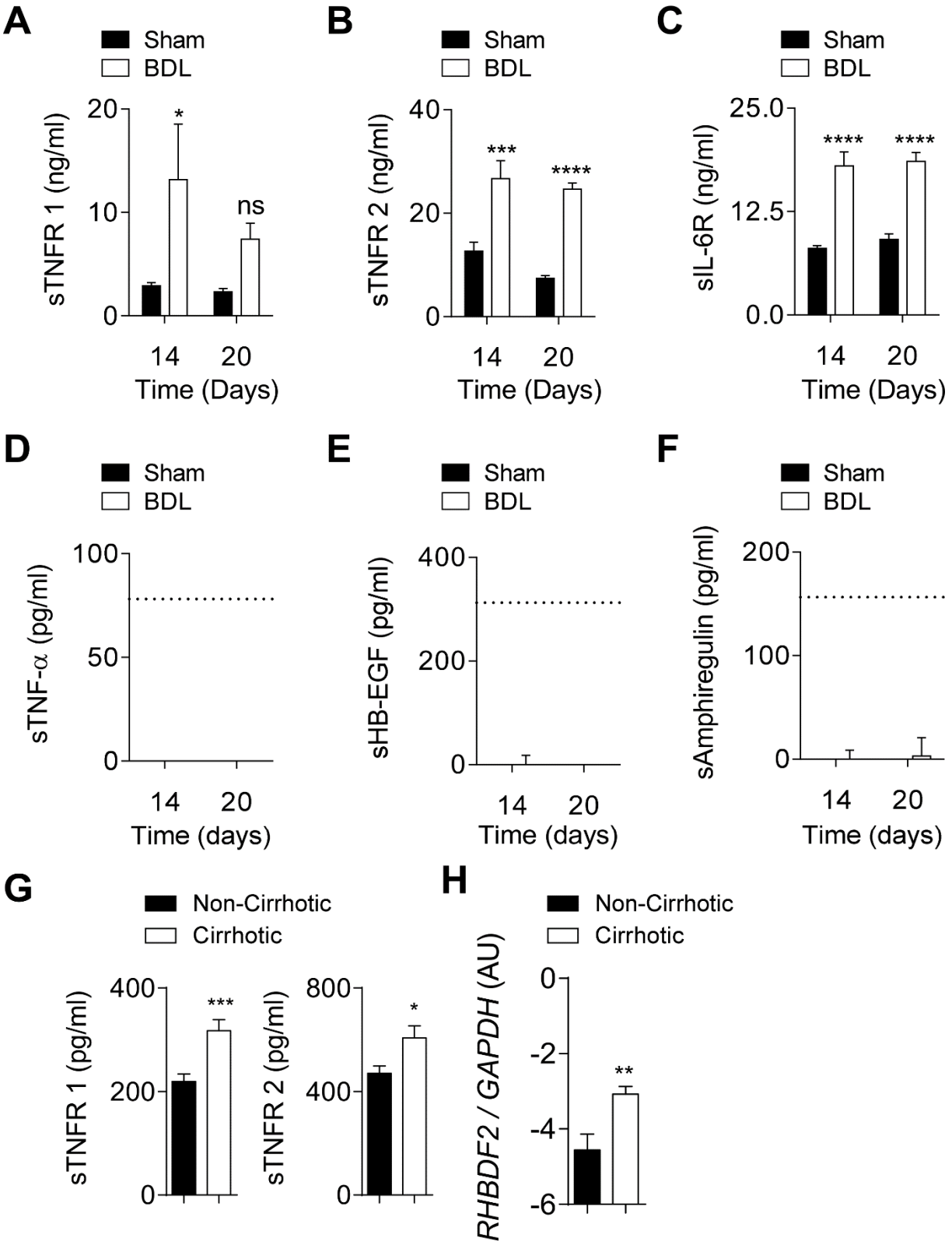
A
Sham
BDL
sTNFR 1 (ng/ml)
20
10
0
*
ns
14
20
Time (Days)
B
Sham
BDL
sTNFR 2 (ng/ml)
40
20
0
***
****
14
20
Time (Days)
C
Sham
BDL
sIL-6R (ng/ml)
25.0
12.5
0.0
****
****
14
20
Time (Days)
D
Sham
BDL
sTNF-α (pg/ml)
100
50
0
14
20
Time (days)
E
Sham
BDL
sHB-EGF (pg/ml)
400
200
0
14
20
Time (days)
F
Sham
BDL
sAmphiregulin (pg/ml)
200
100
0
14
20
Time (days)
G
Non-Cirrhotic
Cirrhotic
sTNFR 1 (pg/ml)
400
200
0
***
sTNFR 2 (pg/ml)
800
400
0
*
H
Non-Cirrhotic
Cirrhotic
RHBDF2 / GAPDH (AU)
0
-2
-4
-6
**

Figure 2. Increased shedding of ADAM17 substrates in BDL animals

(A-C) *Quantification of soluble (s) TNFR1 (A), TNFR2 (B), and IL-6R (C) in serum samples from C57BL/6 mice subjected to sham or BDL operation. Sera were taken at 14 or 20 days after surgery. n = 5 mice per condition* ***(D-F)*** *Quantification of soluble (s) TNF-α (D), HB-EGF (E), and amphiregulin (F) in sera of sham- and BDL-operated C57BL/6 mice 14 or 20 days after surgery. n = 3 mice per condition.* ***(G)*** *Quantification of soluble (s) TNFR1 and TNFR2 in cohorts of patients suffering from liver cirrhosis and in non-cirrhotic patients and healthy volunteers (table 3, Cohort A). n=32-35 patients.* ***(H)*** *Quantification of RHBDF2 mRNA (in arbitrary units, AU) from human cirrhotic liver tissue and non-cirrhotic control tissue (table 3, Cohort B). n=4–17 patients. Data are shown as mean ± SEM. * P<0.05; **P<0.01; ***P<0.001; ****P<0.0001, 2-way ANOVA with Bonferroni's multiple comparisons test (A-C) and Mann-Whitney U test (G-H).*

Table 3. Clinical parameters of cirrhotic and non-cirrhotic patients and healthy volunteers. (A) Mean ± SEM of clinical parameters as well as p-value is presented from cohorts represented in Figure. 2G (cohort A, n=32-35). **(B)** Clinical diagnosis as well as Mean ± SEM of the age and p-value is presented for cohort B shown in Figure. 2H (n=4-17).

(A) Cohort A	**Non-cirrhotic n=35**	**Cirrhotic n=32**	**P value**
Diseases	Healthy volunteer (n=3) HBV (n=21) HBV+NASH (n=9) HCV+NASH (n=2)	HBV+Cirrhosis (n=12) HCV+Cirrhosis (n=14) C2+Cirrhosis (n=6)	
Age (Years)	49.31 ± 1.729	59.19 ± 2.512	P= 0.0016
ALT (U/L)	35.23 ± 3.140	41.75 ± 5.395	P= 0.2900
AST (U/L)	27.94 ± 1.503	40.59 ± 3.820	P= 0.0022
AP (U/L)	79.53 ± 5.692	96.25 ± 5.896	P= 0.0456
Bilirubin (mg/dl)	0.5755 ± 0.05583	0.9591 ± 0.1661	P= 0.0302
(B) Cohort B	**Non-cirrhotic n=4**	**Cirrhotic n=17**	**P value**
Diseases	[Normal liver tissue distant of] Colorectal liver metastasis (n=2) Salivary gland cancer metastasis (n=1) Segmental ischemia (n=1)	HBV+Cirrhosis (n=4) HCV+Cirrhosis (n=2) C2+Cirrhosis (n=3) AIH+Cirrhosis (n=2) Wilson+Cirrhosis (n=3) Kryptogen+Cirrhosis (n=2) PSC+Cirrhosis (n=1)	
Age (Years)	56.50 ± 6.614	44.00 ± 2.980	P=0.0865

4.3 Lack of iRhom2 results in increased liver fibrosis following bile duct ligation

As expected, ADAM17 maturation was decreased in iRhom2-deficient (*Rhbdf2*$^{-/-}$) mice during liver fibrosis following BDL compared to control mice subjected to BDL (Figure 3A), which is consistent with the reduced presence of circulating TNFRs in the sera of *Rhbdf2*$^{-/-}$ mice compared to control animals following BDL (Figure 3B-F). The abundance of soluble IL-6R, which is released by ADAM17-mediated processing of IL-6R, was also decreased in *Rhbdf2*$^{-/-}$ mice compared to control animals following BDL, but EGFR ligands targeted by ADAM17 were not (Figure 3G-H and Figure 4A). The abundance of mRNAs encoding ADAM17 substrates were not significantly different between *Rhbdf2*$^{-/-}$ and control mice 20 days after BDL (Figure 4B). Liver tissue harvested from *Rhbdf2*$^{-/-}$ mice following BDL, however, exhibited significantly increased areas of fibrosis, indicated by increased Picro Sirius red and Masson's Trichrome staining compared to liver tissue harvested from control animals (Figure 4C). Moreover, *Rhbdf2*$^{-/-}$ BDL mice showed increased abundance of hepatic fibrosis markers such as collagen and α-SMA when compared to wild-type BDL controls (Figure 4D).

Taken together, these data indicate that the activity of ADAM17 increases during liver fibrosis and that the absence of iRhom2, despite reducing ADAM17 maturation, exacerbates liver fibrosis compared to control animals.

Figure 3.

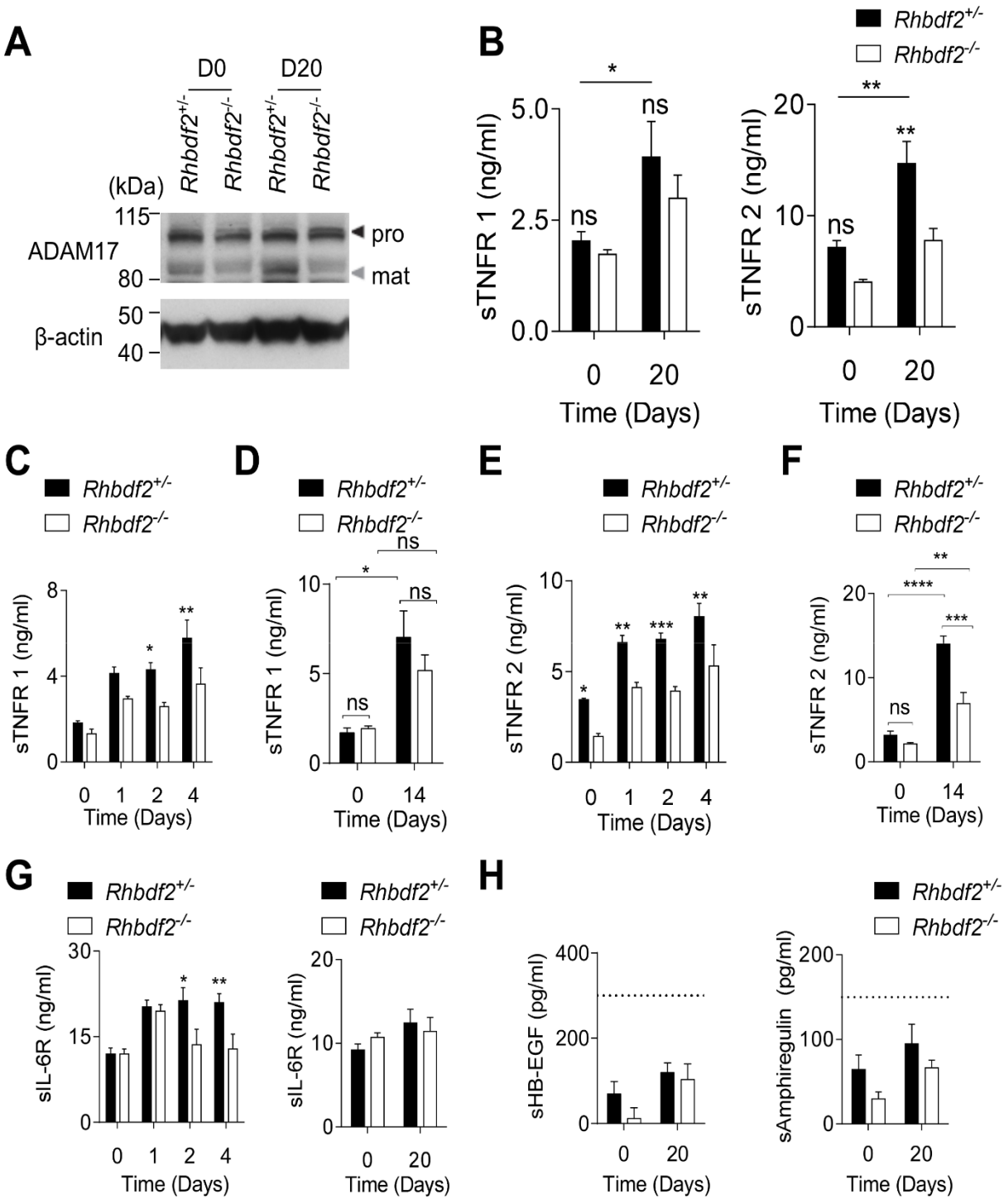
A
D0
D20
Rhbdf2+/-
Rhbdf2-/-
Rhbdf2+/-
Rhbdf2-/-
(kDa)
115
ADAM17
80
pro
mat
50
β-actin
40
B
Rhbdf2+/-
Rhbdf2-/-
sTNFR 1 (ng/ml)
sTNFR 2 (ng/ml)
Time (Days)
Time (Days)
C
D
E
F
sTNFR 1 (ng/ml)
sTNFR 1 (ng/ml)
sTNFR 2 (ng/ml)
sTNFR 2 (ng/ml)
Time (Days)
Time (Days)
Time (Days)
Time (Days)
G
H
sIL-6R (ng/ml)
sIL-6R (ng/ml)
sHB-EGF (pg/ml)
sAmphiregulin (pg/ml)
Time (Days)
Time (Days)
Time (Days)
Time (Days)

Figure 3. iRhom2 deficiency enhances liver fibrosis following BDL.

(A) *Representative immunoblot showing ADAM17 in total liver tissue from Rhbdf2$^{+/-}$ and Rhbdf2$^{-/-}$ mice at day 0 and day 20 after BDL. β-actin is a loading control. n = 6 animals per genotype for each time point.* ***(B)*** *Quantification of soluble (s) TNFR1 and TNFR2 in sera collected from Rhbdf2$^{+/-}$ and Rhbdf2$^{-/-}$ mice at day 0 and day 20 after BDL. n = 5-6 animals per genotype for each time point.* ***(C-G)*** *Quantification of soluble (s) TNFR1 (C, D), TNFR2 (E, F), and IL-6R (G) in sera collected from Rhbdf2$^{+/-}$ and Rhbdf2$^{-/-}$ mice at early and later time points after BDL surgery. n = 4-9 animals per genotype for each time point.* ***(H)*** *Quantification of soluble (s) HB-EGF and amphiregulin in sera collected from Rhbdf2$^{+/-}$ and Rhbdf2$^{-/-}$ mice at later time points after BDL surgery. n = 5 animals per genotype for each time point. Data are shown as mean ± SEM. *P<0.05; **P<0.01; ***P<0.001; ****P<0.0001, 2-way ANOVA with Bonferroni's multiple comparisons test (B-G).*

Figure 4.

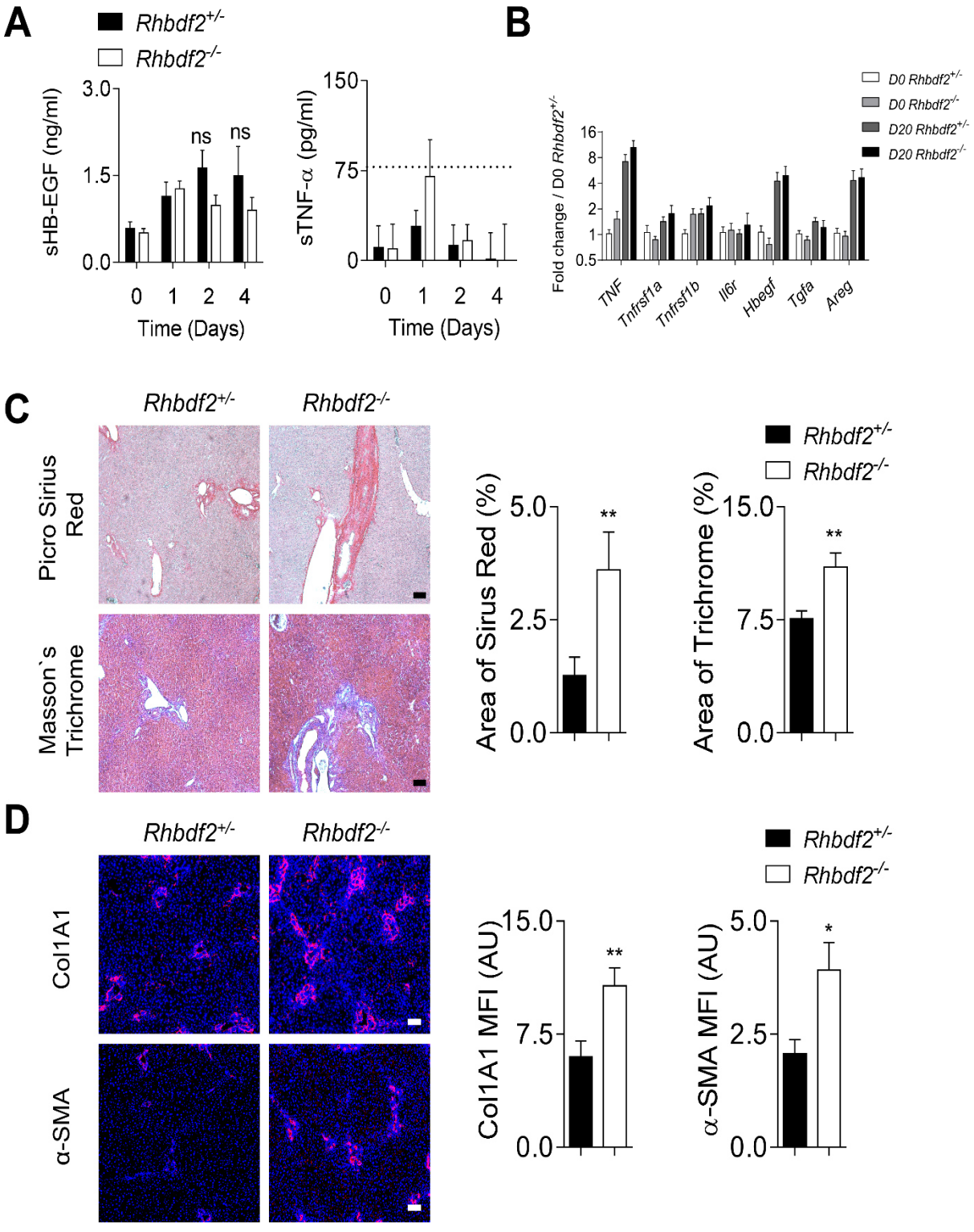
A
Rhbdf2+/-
Rhbdf2-/-
sHB-EGF (ng/ml)
3.0
1.5
0.0
ns
ns
0 1 2 4
Time (Days)
sTNF-α (pg/ml)
150
75
0
0 1 2 4
Time (Days)
B
D0 Rhbdf2+/-
D0 Rhbdf2-/-
D20 Rhbdf2+/-
D20 Rhbdf2-/-
Fold change / D0 Rhbdf2+/-
16
8
4
2
1
0.5
TNF
Tnfrsf1a
Tnfrsf1b
Il6r
Hbegf
Tgfa
Areg
C
Rhbdf2+/-
Rhbdf2-/-
Picro Sirius Red
Masson`s Trichrome
Area of Sirus Red (%)
5.0
2.5
0.0
**
Area of Trichrome (%)
15.0
7.5
0.0
**
D
Rhbdf2+/-
Rhbdf2-/-
Col1A1
α-SMA
Col1A1 MFI (AU)
15.0
7.5
0.0
**
α-SMA MFI (AU)
5.0
2.5
0.0
*

Figure 4. Shedding of ADAM17 substrates in *Rhbdf2*$^{+/-}$ and *Rhbdf2*$^{-/-}$ BDL mice.

(A) *Quantification of soluble (s) HB-EGF and TNF- α in sera collected from Rhbdf2*$^{+/-}$ *and Rhbdf2*$^{-/-}$ *mice at early time points after BDL surgery. n = 6-9 animals per genotype for each time point.* ***(B)*** *Quantification of Tnf, Tnfrsf1a, Tnfrsf1b, Il6r, Hbegf, Tgfa, and Areg mRNA expression in total liver tissue harvested from Rhbdf2*$^{+/-}$ *and Rhbdf2*$^{-/-}$ *mice at day 0 or day 20 after BDL surgery. n = 4-6 mice per genotype for each time point.* ***(C)*** *Imaging and quantification of Picrosirius Red and Masson's Trichrome staining in sections of liver tissue harvested from Rhbdf2*$^{+/-}$*and Rhbdf2*$^{-/-}$ *mice at day 14 after BDL. n = 4-6 mice per genotype. Scale bar, 50μm.* ***(D)*** *Distribution and quantification of Col1A1 and α-SMA in sections of liver tissue harvested from Rhbdf2*$^{+/-}$ *and Rhbdf2*$^{-/-}$ *mice at day 20 after BDL. Nuclei are labelled with DAPI (blue). Scale bar, 100μm. Quantification of Col1A1 and α-SMA by mean fluorescence intensity (MFI) is shown in arbitrary units (AU). n=6 mice per genotype. Data are shown as mean ± SEM. *P<0.05; **P<0.01; Mann-Whitney U test (C and D).*

4.4 *Rhbdf2* expression is induced early in the liver following BDL

In order to determine whether ADAM17 activation occurred after the initiation of liver fibrosis or was an early event prior to the occurrence of fibrosis, we assayed earlier time points after BDL. We observed increased expression of *Rhbdf2* as early as 6 hours after the BDL operation (Figure 5A). Increased *Rhbdf2* expression was observed specifically in liver tissue and not in other organs tested (Figure 5B). Because we observed increased *Rhbdf2* expression, we speculated that ADAM17 activation should also be increased at early time points after the BDL operation. We detected increased expression of mRNAs encoding ADAM17 substrates within 48 hours after BDL in liver tissue compared to sham-operated animals (Figure 5C) and increased abundance of ADAM17 substrates in the circulation, including soluble forms of TNFRs, IL-6R, and HB-EGF (Figure 5D-G). Other ADAM17 substrates were not detected in the sera of BDL or sham-operated mice (Figure 6A). Activation of ADAM17 depended on the presence of iRhom2, because *Rhbdf2*$^{-/-}$ animals showed reduced abundance of mature ADAM17 (Figure 6B-C).

Taken together, these data indicate that early production of iRhom2 following BDL facilitates ADAM17 activation and shedding of its substrates.

Figure 5.

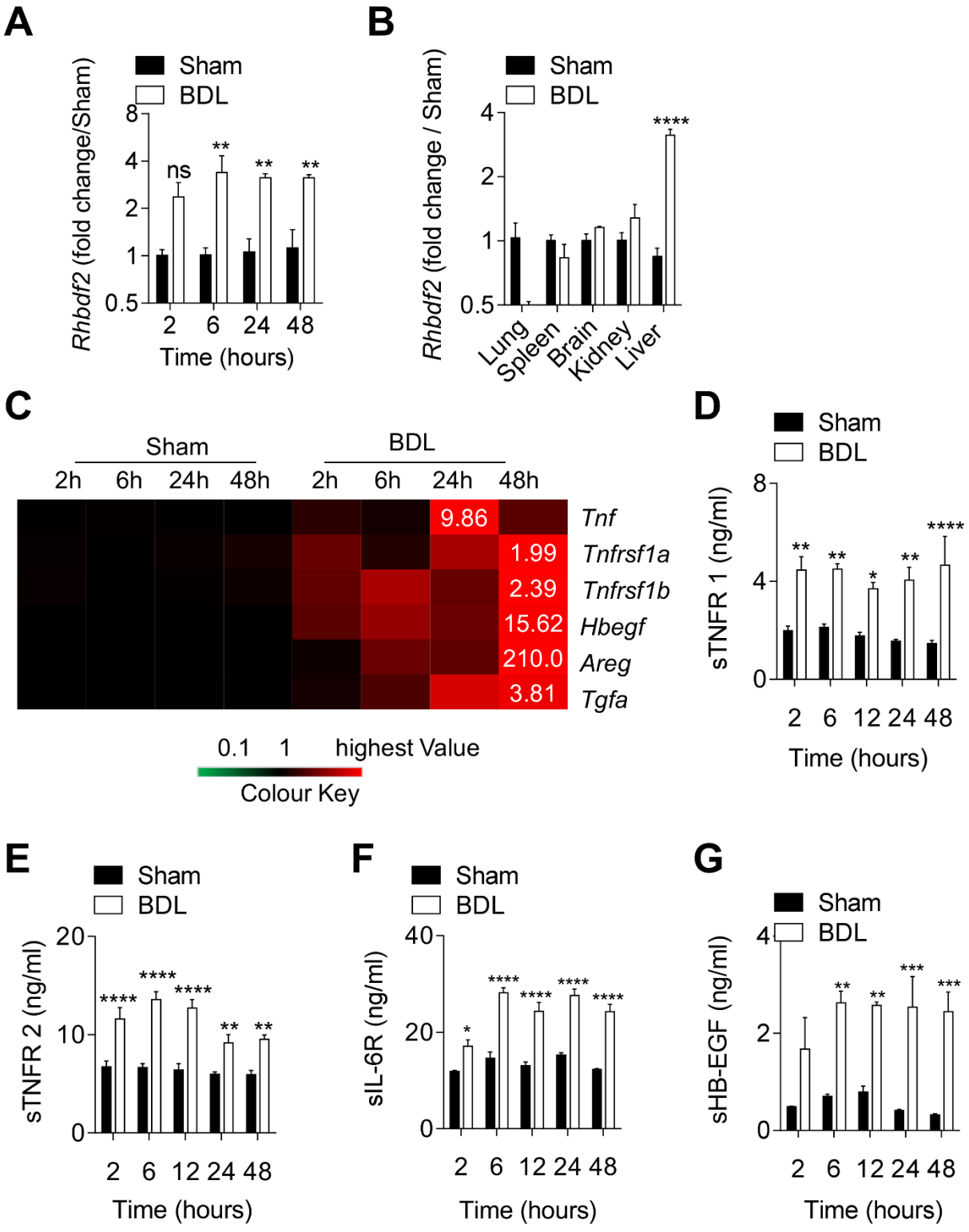
A
Sham
BDL
Rhbdf2 (fold change/Sham)
8
4
2
1
0.5
ns
**
**
**
2
6
24
48
Time (hours)
B
Sham
BDL
Rhbdf2 (fold change / Sham)
4
2
1
0.5
****
Lung
Spleen
Brain
Kidney
Liver
C
Sham
BDL
2h
6h
24h
48h
2h
6h
24h
48h
9.86
1.99
2.39
15.62
210.0
3.81
Tnf
Tnfrsf1a
Tnfrsf1b
Hbegf
Areg
Tgfa
0.1
1
highest Value
Colour Key
D
Sham
BDL
sTNFR 1 (ng/ml)
8
4
0
**
**
*
**
****
2
6
12
24
48
Time (hours)
E
Sham
BDL
sTNFR 2 (ng/ml)
20
10
0
****
****
****
**
**
2
6
12
24
48
Time (hours)
F
Sham
BDL
sIL-6R (ng/ml)
40
20
0
*
****
****
****
****
2
6
12
24
48
Time (hours)
G
Sham
BDL
sHB-EGF (ng/ml)
4
2
0
**
**
***
***
2
6
12
24
48
Time (hours)

Figure 5. *Rhbdf2* expression and shedding of ADAM17 substrates increase early after BDL.

(A) *Quantification of Rhbdf2 mRNA in total liver tissue of sham and BDL wild-type mice at the indicated early time points after surgery. n = 4 animals per condition for each time point.* ***(B)*** *Quantification of Rhbdf2 mRNA in total lung, spleen, brain, kidney, and liver tissue of sham-operated and BDL operated wild-type mice 24 hours after surgery. n = 3-4 mice for each organ.* ***(C)*** *Quantification of Tnf, Tnfrsf1a, Tnfrsf1b, Hbegf, Areg, and Tgfa mRNAs in liver tissue of sham and BDL mice at the indicated time points following surgery was analysed by RT-PCR. The highest value for each transcript, relative to the amount of GAPDH, compared to their expression in sham mice is noted in the heatmap. n=4 animals per condition for each time point.* ***(D-G)*** *Quantification of soluble (s) TNFR1 (D), TNFR2 (E), IL-6R (F), and HB-EGF (G) in serum from sham and BDL mice at the indicated time points following surgery. n=3-6 animals per condition for each time point. Data are shown as mean ± SEM. *P<0.05; **P<0.01; ***P<0.001; ****P<0.0001. 2-way ANOVA with Bonferroni's multiple comparisons test (A-B and D-G).*

Figure 6.

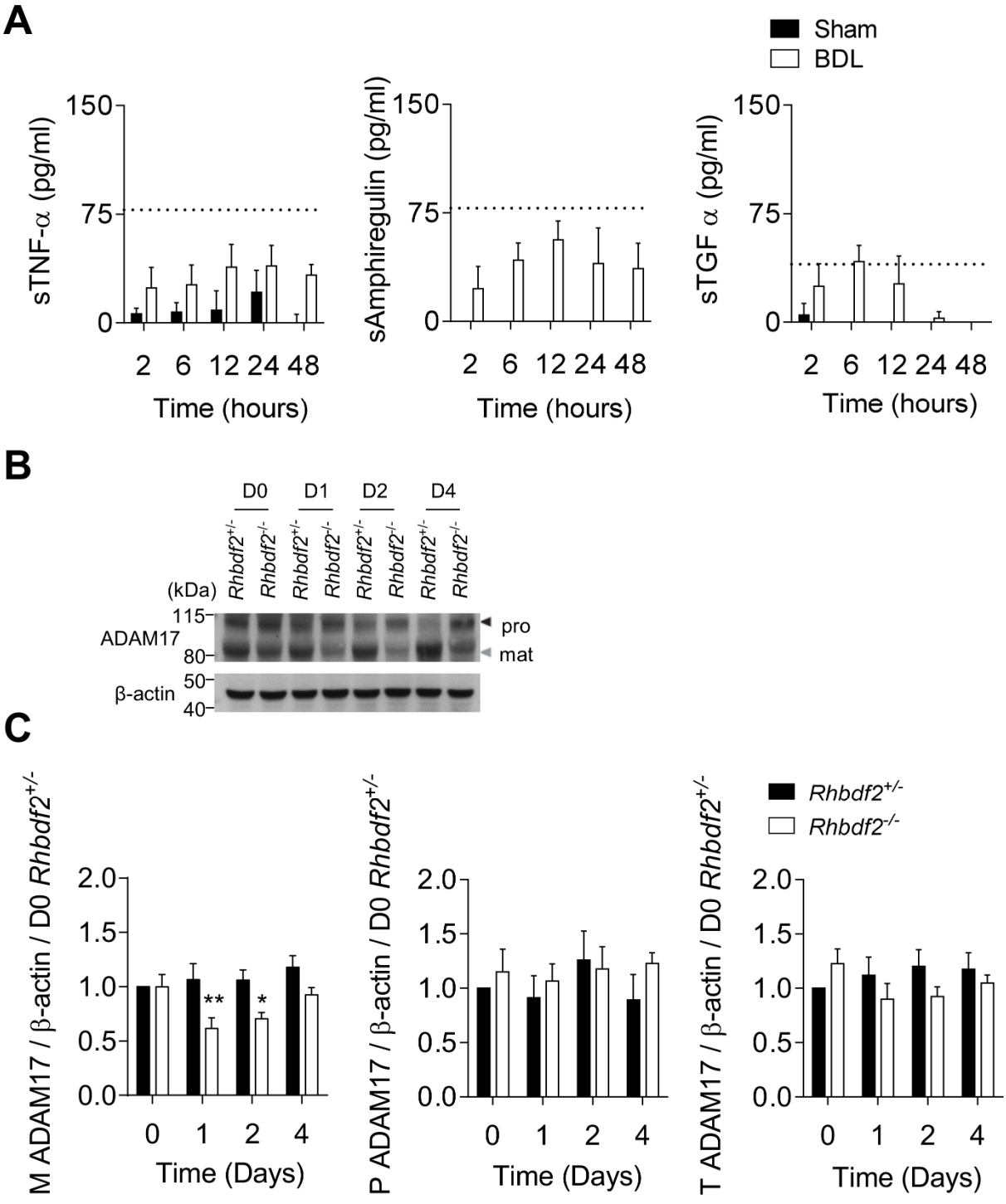
A
Sham
BDL
sTNF-α (pg/ml)
sAmphiregulin (pg/ml)
sTGF α (pg/ml)
150
75
0
2 6 12 24 48
Time (hours)
B
D0
D1
D2
D4
Rhbdf2+/-
Rhbdf2-/-
(kDa)
115
80
ADAM17
pro
mat
50
40
β-actin
C
M ADAM17 / β-actin / D0 Rhbdf2+/-
P ADAM17 / β-actin / D0 Rhbdf2+/-
T ADAM17 / β-actin / D0 Rhbdf2+/-
Rhbdf2+/-
Rhbdf2-/-
2.0
1.5
1.0
0.5
0.0
**
*
0 1 2 4
Time (Days)

Figure 6. ADAM17 maturation is inhibited in the absence of iRhom2 following BDL.
(A) *Quantification of TNF-α, amphiregulin, and TGF-α in sera of sham and BDL wild-type mice at the indicated time points after surgery. n = 5-6 mice per condition for each time point.* ***(B)*** *Representative immunoblot showing ADAM17 in total liver tissue of* $Rhbdf2^{+/-}$ *and* $Rhbdf2^{-/-}$ *mice at early time points following BDL. β-actin is a loading control. n = 6-9 animals per genotype for each time point.* ***(C)*** *Quantification of mature (M), pro (P) and total (T) ADAM17 in total liver tissue of* $Rhbdf2^{+/-}$ *and* $Rhbdf2^{-/-}$ *mice at the indicated time points after BDL surgery. n = 6-9 mice per genotype for each time point. Data are shown as mean ± SEM. *P<0.05; **P<0.01, 2-way ANOVA with Bonferroni's multiple comparisons test (C).*

4.5 Lack of iRhom2 triggers increased presence of activated HSCs after BDL

BDL in mice is accompanied by liver damage, resulting in increased amounts of liver enzymes in the blood. However, when we analyzed hepatic tissue damage by measuring liver enzyme activity following BDL, we did not see significant differences during early or late time points between wild-type and iRhom2-deficient mice (Figure 7A-D). Consistent with this, we did not find a significant difference in the abundance of active caspase 3 between *Rhbdf2*$^{+/-}$ *and Rhbdf2*$^{-/-}$ liver tissue (Figure 7E and 7G). Additionally, when we treated *Rhbdf2*$^{+/-}$ *and Rhbdf2*$^{-/-}$ primary hepatocytes with TNF-α plus Cyclohexamide (CHX), we detected no significant difference in cleaved caspase 8 between the two groups (Figure 7F and 7G). Altogether, this suggests that the phenotypes seen in *Rhbdf2*$^{-/-}$ mice at later time points are not due to defects in hepatocytes but another cell population within the liver. Indeed, we found an increase in areas densely populated with cells, consistent in appearance with fibrotic lesions (*215, 216*), in *Rhbdf2*$^{-/-}$ hematoxylin and eosin–stained liver tissue sections compared to *Rhbdf2*$^{+/-}$ tissue (Figure 8A). Because stellate cells contribute to liver fibrosis by differentiating into myofibroblasts and producing collagens (*195*), we speculated that absence of iRhom2 could induce the proliferation of myofibroblasts derived from HSCs. Activated stellate cells and myofibroblasts can be visualized by staining for platelet-derived growth factor receptor β (PDGFRβ) and the intermediate filament protein Desmin (*217-219*). We found significant increases in PDGFRβ- and Desmin-producing cells in liver tissue harvested from *Rhbdf2*$^{-/-}$ mice compared to control animals after BDL (Figure 8B-C). We also identified decreased abundance of glial fibrillary acidic protein (GFAP), an quiescent HSC marker that is absent in myofibroblasts (*220*) in *Rhbdf2*$^{-/-}$ liver tissue when compared to control liver tissue (Figure 8D-E).

Taken together, these data indicate that early production of iRhom2 following BDL facilitates ADAM17 activation and reduces the presence of activated hepatic stellate cells.

Figure 7.

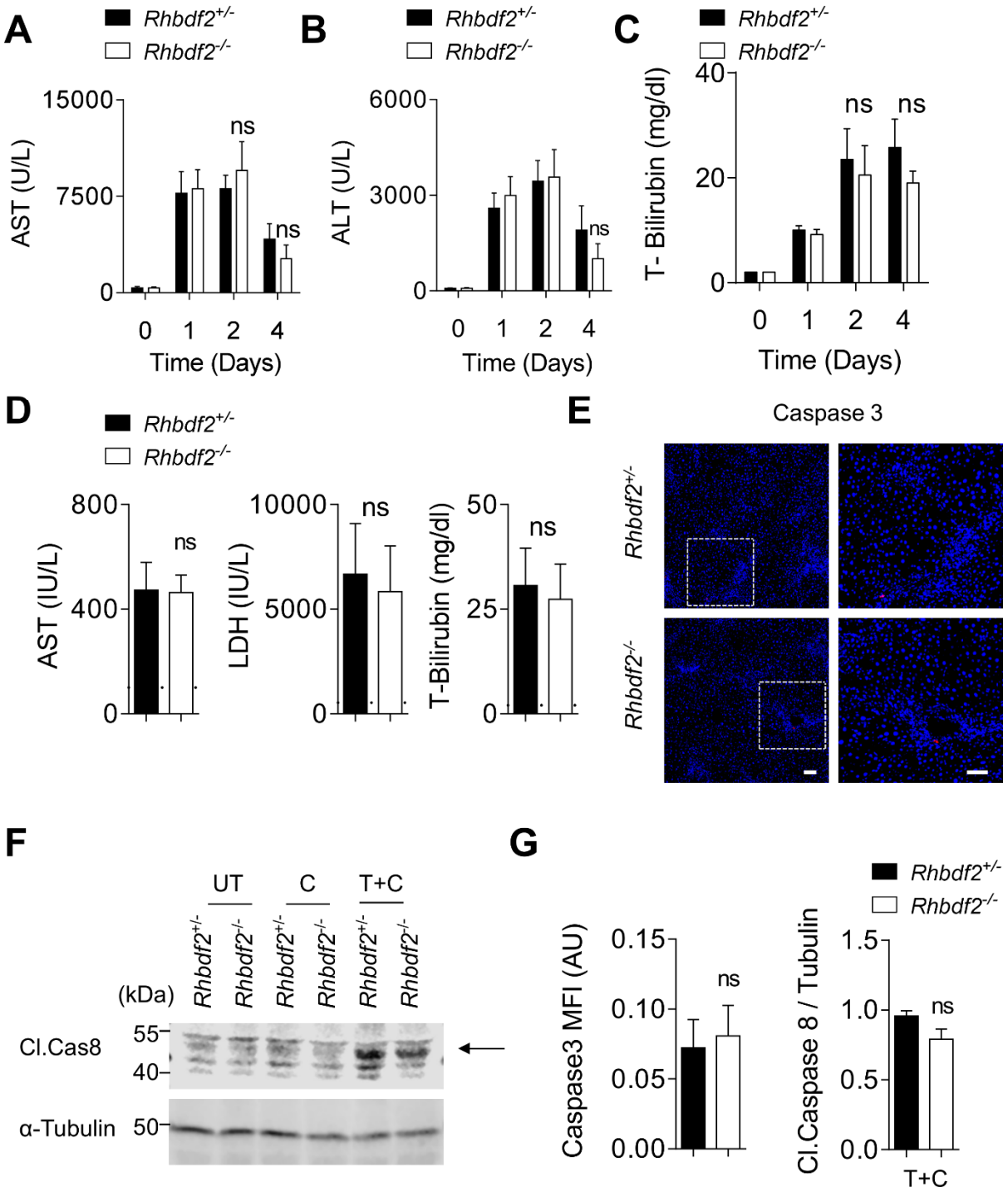
A
Rhbdf2+/-
Rhbdf2-/-
AST (U/L)
15000
7500
0
ns
ns
0 1 2 4
Time (Days)
B
Rhbdf2+/-
Rhbdf2-/-
ALT (U/L)
6000
3000
0
ns
ns
0 1 2 4
Time (Days)
C
Rhbdf2+/-
Rhbdf2-/-
T- Bilirubin (mg/dl)
40
20
0
ns
ns
0 1 2 4
Time (Days)
D
Rhbdf2+/-
Rhbdf2-/-
AST (IU/L)
800
400
0
ns
LDH (IU/L)
10000
5000
0
ns
T-Bilirubin (mg/dl)
50
25
0
ns
E
Caspase 3
Rhbdf2+/-
Rhbdf2-/-
F
UT
C
T+C
Rhbdf2+/-
Rhbdf2-/-
Rhbdf2+/-
Rhbdf2-/-
Rhbdf2+/-
Rhbdf2-/-
(kDa)
Cl.Cas8
55
40
α-Tubulin
50
G
Rhbdf2+/-
Rhbdf2-/-
Caspase3 MFI (AU)
0.15
0.10
0.05
0.00
ns
Cl.Caspase 8 / Tubulin
1.5
1.0
0.5
0.0
ns
T+C

Figure 7. No difference in liver parameters or apoptosis between *Rhbdf2*$^{+/-}$ and *Rhbdf2*$^{-/-}$ mice.

(A-C) *Quantification of liver enzymes AST (A), ALT (B) and T-bilirubin (C) in serum samples from Rhbdf2*$^{+/-}$ *and Rhbdf2*$^{-/-}$ *mice at the indicated time points following BDL. n = 6-9 animals per genotype for each time.* ***(D)*** *Concentration of AST, LDH, and T-bilirubin in sera of Rhbdf2*$^{+/-}$ *and Rhbdf2*$^{-/-}$ *mice 20 days after surgery. n = 6 mice per genotype.* ***(E)*** *Immunostaining and quantification of active caspase 3 in sections of liver tissue harvested from Rhbdf2*$^{+/-}$ *and Rhbdf2*$^{-/-}$ *mice at day 20 after BDL. Nuclei were stained with DAPI (blue). n=6 mice per genotype. Scale bar, 100µm.* ***(F)*** *Representative immunoblot showing cleaved caspase 8 in Rhbdf2*$^{+/-}$ *and Rhbdf2*$^{-/-}$ *primary hepatocytes treated with PBS (untreated, UT), cyclohexamide (C), or both cyclohexamide and TNF-α (T+C). α-tubulin is a loading control. n = 4 mice per genotype for each condition.* ***(G)*** *Quantification of active caspase 3 by mean fluorescence intensity (MFI) is shown in arbitrary units (AU) and cleaved caspase 8 was quantified by densitometry. Data are shown as mean ± SEM.*

Figure 8.

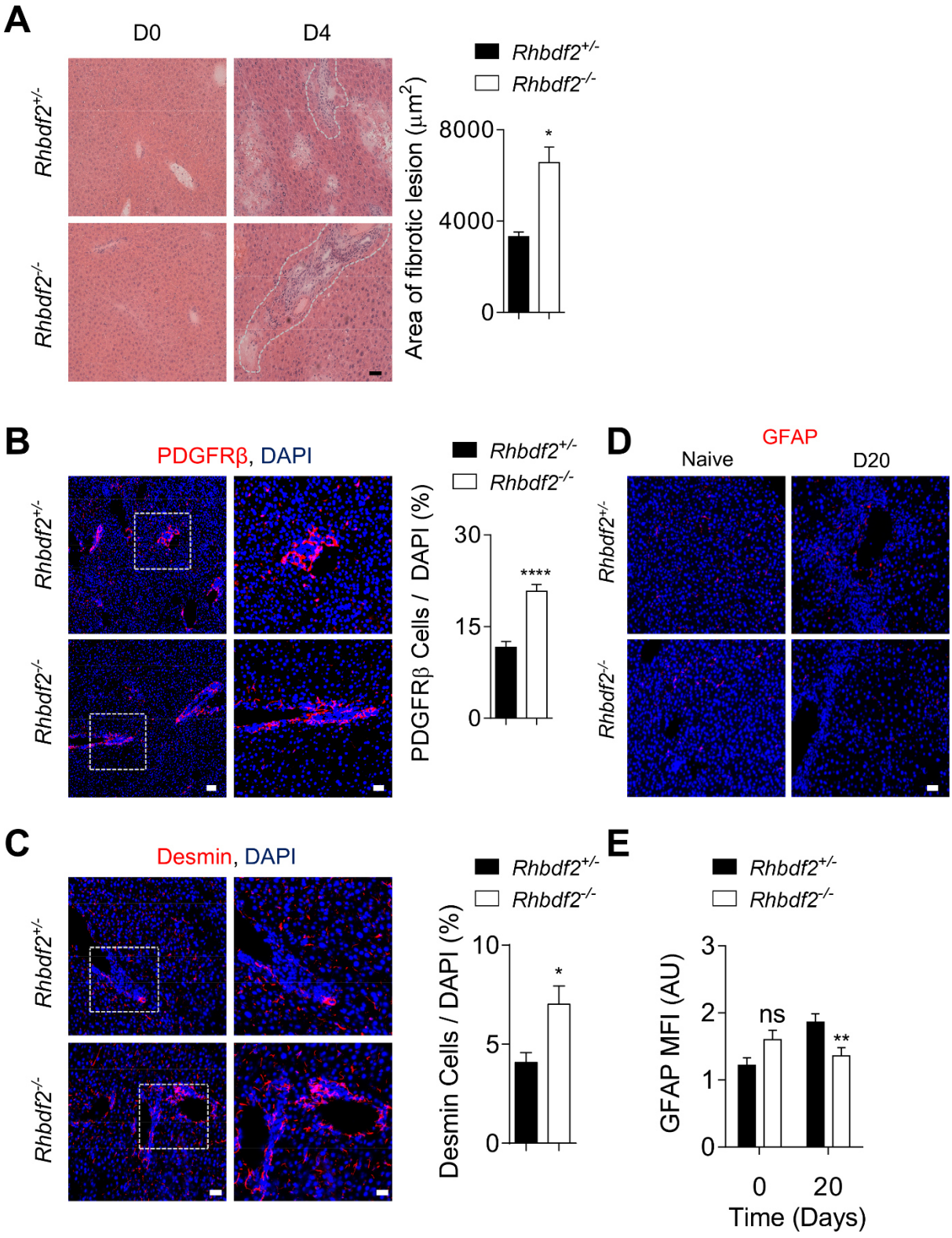
A
D0
D4
Rhbdf2+/-
Rhbdf2-/-
Rhbdf2+/-
Rhbdf2-/-
Area of fibrotic lesion (μm2)
8000
4000
0
*
B
PDGFRβ, DAPI
Rhbdf2+/-
Rhbdf2-/-
PDGFRβ Cells / DAPI (%)
30
15
0
****
D
GFAP
Naive
D20
C
Desmin, DAPI
Desmin Cells / DAPI (%)
10
5
0
*
E
GFAP MFI (AU)
3
2
1
0
ns
**
0
20
Time (Days)

Figure 8. iRhom2 protects against liver fibrosis early after BDL

(A) *Sections of liver tissue harvested from Rhbdf2$^{+/-}$ and Rhbdf2$^{-/-}$ mice at day 0 or day 4 after BDL were stained with Hematoxylin and Eosin. White dashed lines indicate boundaries of fibrotic lesions. The areas of fibrotic lesions were measured and expressed as μm^2. n=6-9 animals per genotype for each time point. Scale bar, 50μm.* ***(B-C)*** *Sections of liver tissue harvested from Rhbdf2$^{+/-}$ and Rhbdf2$^{-/-}$ mice at day 4 after BDL were stained for PDGFRβ (B) or Desmin (C). Boxes indicate the areas magnified in the images on the right. PDGFRβ- or Desmin-positive cells were quantified as a percentage of all cells. n=7-8 animals per genotype. Scale bars, (B): 100μm (left), 50μm (right); (C): 50μm (left), 20μm (right).* ***(D)*** *Immunostaining and quantification of the quiescent hepatic stellate cell marker GFAP in sections of liver tissue harvested from Rhbdf2$^{+/-}$ and Rhbdf2$^{-/-}$ mice at day 0 and day 20 after BDL. Nuclei were stained with DAPI (blue). n=4-6 animals per genotype for each time point. Scale bar, 50μm.* ***(E)*** *Quantification of GFAP by mean fluorescence intensity (MFI) is shown in arbitrary units (AU). Data are shown as mean ± SEM. *P<0.05; **P<0.01; ****P<0.0001, Mann-Whitney U test (A-C), 2-way ANOVA with Bonferroni's multiple comparisons test (E).*

4.6 Lack of iRhom2 leads to decreased TNFR shedding and increased fibrotic markers in stellate cells

Mouse primary HSCs express fibrotic markers when cultured *in vitro* (*221*) (Figure 9A). We confirmed the presence of both pro and mature forms of ADAM17 in primary hepatic stellate cells isolated from C57BL/6 mice (Figure 9B). We observed increased shedding of TNFRs, but not other ADAM17 substrates, in primary HSC cultures (Figure 9C-D). As expected, ADAM17 maturation was significantly reduced in stellate cells from *Rhbdf2*$^{-/-}$ mice compared to those from control animals (Figure 9E-F and Figure 10A). Furthermore, we found increased abundance of mature ADAM17 when we exposed *Rhbdf2*$^{+/-}$ but not *Rhbdf2*$^{-/-}$ stellate cells to TNF-α (Figure 9E-F and Figure 10A). Shedding of TNFR1 in *Rhbdf2*$^{+/-}$ stellate cells was reduced following exposure to TNF-α, whereas shedding of TNFR2 was increased (Figure 10B). Moreover, shedding of both TNFR1 and TNFR2 depended on iRhom2, because *Rhbdf2*$^{-/-}$ stellate cells showed reduced TNFRs in the culture supernatant (Figure 10B). Similar to the data from liver tissue (Figure 4D), we found an increase in fibrotic markers in primary HSCs from *Rhbdf2*$^{-/-}$ animals compared to *Rhbdf2*$^{+/-}$ control cells (Figure 10C-D).

Taken together, these data further demonstrate that shedding of TNFRs depends on iRhom2 and that the absence of iRhom2 can increase the expression of fibrotic markers in primary HSCs.

Figure 9.

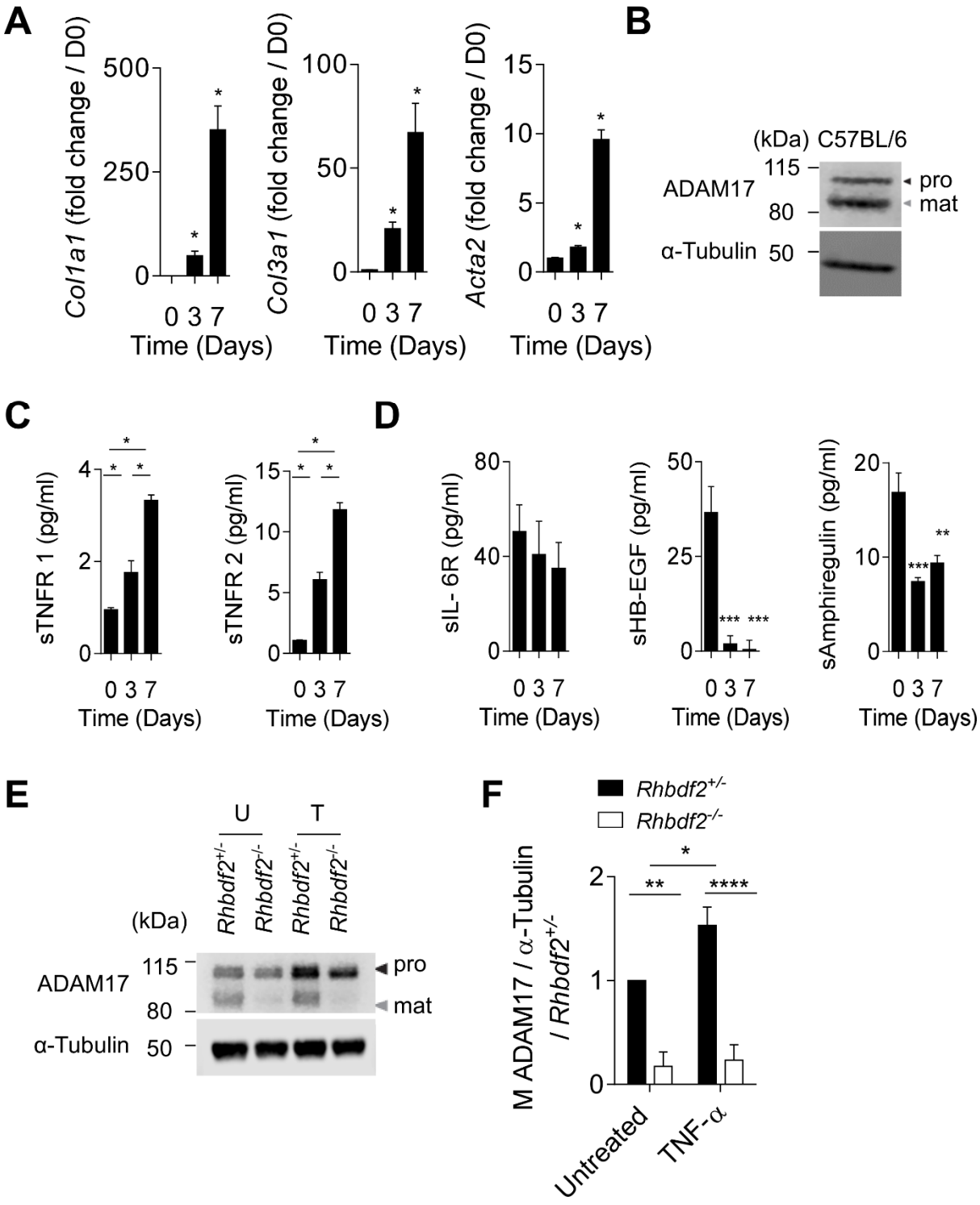
A
Col1a1 (fold change / D0)
500
250
0
0 3 7
Time (Days)
Col3a1 (fold change / D0)
100
50
0
0 3 7
Time (Days)
Acta2 (fold change / D0)
15
10
5
0
0 3 7
Time (Days)
B
(kDa) C57BL/6
ADAM17
115
80
pro
mat
α-Tubulin 50
C
sTNFR 1 (pg/ml)
4
2
0
0 3 7
Time (Days)
sTNFR 2 (pg/ml)
15
10
5
0
0 3 7
Time (Days)
D
sIL- 6R (pg/ml)
80
40
0
0 3 7
Time (Days)
sHB-EGF (pg/ml)
50
25
0
0 3 7
Time (Days)
sAmphiregulin (pg/ml)
20
10
0
0 3 7
Time (Days)
E
U
T
Rhbdf2+/-
Rhbdf2-/-
Rhbdf2+/-
Rhbdf2-/-
(kDa)
ADAM17
115
80
pro
mat
α-Tubulin 50
F
Rhbdf2+/-
Rhbdf2-/-
M ADAM17 / α-Tubulin / Rhbdf2+/-
2
1
0
Untreated
TNF-α

Figure 9. Increased activation of hepatic stellate cells in iRhom2-deficient mice.

(A) *Quantification of Col1a1, Col3a1, and Acta2 mRNAs in HSCs harvested from C57BL/6 mice at the indicated time points. n=4 mice for each time point.* ***(B)*** *Immunblot showing pro and mature (mat) ADAM17 in primary HSCs harvested from C57BL/6 mice. α-tubulin is a loading control. n=4 mice each time point.* ***(C)*** *Quantification of soluble (s) TNFR1 and TNFR2 in supernatants from primary HSCs from C57BL/6 mice at the indicated time points after isolation. n = 4 mice for each time point.* ***(D)*** *Quantification of soluble (s) IL-6R, HB-EGF and amphiregulin in culture supernatants collected from C57BL/6 primary HSCs at the indicated time points. n=8 mice for each time point.* ***(E)*** *Representative immunoblot showing pro- and mature (mat) forms of ADAM17 in primary HSCs isolated from* $Rhbdf2^{+/-}$ *and* $Rhbdf2^{-/-}$ *mice and left untreated (U) or treated with TNF-α (T) for 24 hours. α-tubulin is a loading control. n = 4 mice per genotype for each condition.* ***(F)*** *Densitometric quantification of mature (M) ADAM17 from (E). n = 4 mice per genotype for each condition. Data are shown as mean ± SEM. *P<0.05; **P<0.01; ***P<0.001; ****P<0.0001, Mann-Whitney U test (A and C-D) and 2-way ANOVA with Bonferroni's multiple comparisons test (F).*

Figure 10.

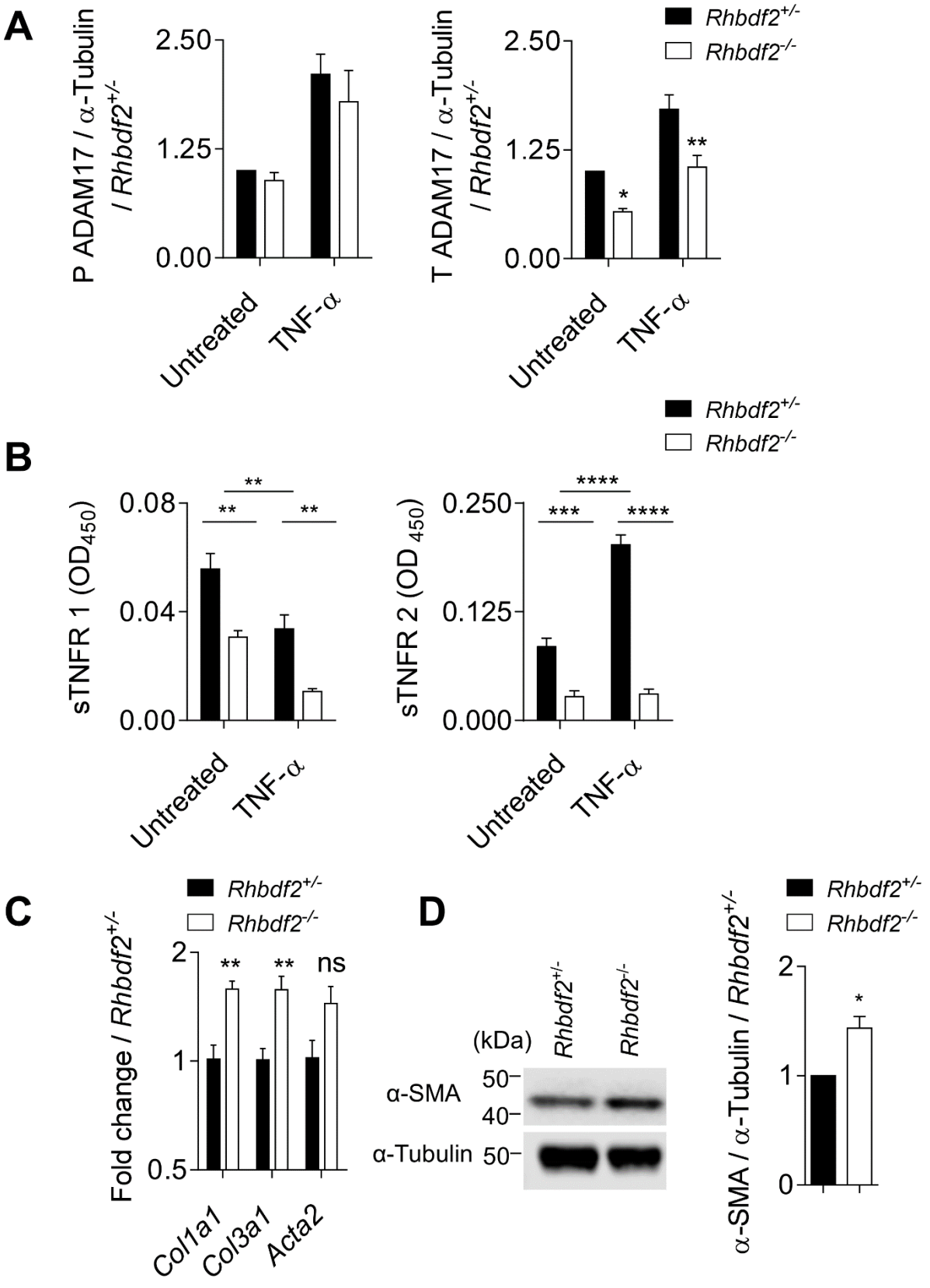
A
P ADAM17 / α-Tubulin / Rhbdf2+/-
2.50
1.25
0.00
Untreated
TNF-α
T ADAM17 / α-Tubulin / Rhbdf2+/-
Rhbdf2+/-
Rhbdf2-/-
*
**
B
sTNFR 1 (OD450)
0.08
0.04
0.00
**
sTNFR 2 (OD450)
0.250
0.125
0.000
***
****
C
Fold change / Rhbdf2+/-
2
1
0.5
ns
Col1a1
Col3a1
Acta2
D
(kDa)
α-SMA
50–
40–
α-Tubulin
α-SMA / α-Tubulin / Rhbdf2+/-

Figure 10. Primary hepatic stellate cells have increased expression of fibrotic markers
(A) *Quantification of Pro (P) and Total (T) ADAM17 in Rhbdf2$^{+/-}$ and Rhbdf2$^{-/-}$ primary hepatic stellate cells, which were treated with or without TNF-α for 24 hours. n=4 mice per genotype for each condition.* ***(B)*** *Quantification of soluble (s) TNFR1 and TNFR2 in supernatants from untreated and TNF-α–treated primary HSCs from Rhbdf2$^{+/-}$ and Rhbdf2$^{-/-}$ mice n = 4 mice per genotype for each condition.* ***(C)*** *Quantification of Col1a1, Col3a1, Acta2 transcripts in 3-day cultures of primary HSCs from Rhbdf2$^{+/-}$ and Rhbdf2$^{-/-}$ mice. n = 4 mice per genotype.* ***(D)*** *Representative immunoblot and quantification of α-SMA in 3-day cultures of primary HSCs from Rhbdf2$^{+/-}$ and Rhbdf2$^{-/-}$ mice. n = 4 mice per genotype. Data are shown as mean ± SEM. *P<0.05; **P<0.01; ***P<0.001; ****P<0.0001, 2-way ANOVA with Bonferroni's multiple comparisons test (A-C) and Mann-Whitney U test (D).*

4.7 Increased TNFR signaling in the absence of iRhom2 triggers stellate cell proliferation and liver fibrosis following BDL

ADAM17 is involved in the shedding of TNF-α and its receptors, epidermal growth factor receptor (EGFR) ligands, and Interleukin-6 receptor (IL-6R). Ligand and receptor shedding affects NF-κB activation, mitogen-activated kinases (MAPKs), extracellular signaling kinase (ERK1/2), and signal transducer and activator of transcription 3 (STAT3) signaling pathways (*110, 168, 222*). Previous studies have clearly demonstrated the importance of these signaling pathways during liver damage and liver regeneration. Mice lacking the p65 (also called RelA) subunit of the transcription factor NF-κB show an embryonic lethal phenotype and massive liver degeneration due to cell death (*223*). Mice lacking EGFR specifically in hepatocytes show decreased hepatocyte proliferation in the initial phase of liver regeneration (*211*). IL-6 trans-signaling can be activated by binding of IL-6 to soluble IL-6R (sIL-6R), and earlier studies have described the importance of IL-6 trans-signaling for the protection of the liver during acute damage to the organ (*212, 213*).

We wanted to uncover which of these hepatic signaling pathways were affected by iRhom2. Although we found increased phosphorylation of ERK1/2 following BDL in both *Rhbdf2*$^{+/-}$ and *Rhbdf2*$^{-/-}$ liver tissue (Figure 11A), we did not observe a significant difference between *Rhbdf2*$^{+/-}$ and *Rhbdf2*$^{-/-}$ mice. This finding was expected in light of the lack of differences in EGFR ligand concentration between the sera of *Rhbdf2*$^{+/-}$ and *Rhbdf2*$^{-/-}$ mice. We detected a significant increase in phosphorylation of the transcription factor STAT3 in liver tissue from naive iRhom2-deficient mice compared to naive *Rhbdf2*$^{+/-}$ animals (Figure 11B). However, following BDL, there was no significant difference in phosphorylated STAT3 between *Rhbdf2*$^{-/-}$ and *Rhbdf2*$^{+/-}$ animals (Figure 11B). The transcription factor NF-κB is a heterodimeric protein that consists of two subunits, p50 and p65; the p65 domain contains the transcriptional activation domain (*224*). Phosphorylation of p65 was increased following BDL in liver tissue harvested from *Rhbdf2*$^{-/-}$ mice when compared to *Rhbdf2*$^{+/-}$ controls (Figure 11C), but we did not observe a difference in the abundance of inhibitor of κB α (IκBα) (Figure 11D). However, we observed increased nuclear p65 in *Rhbdf2*$^{-/-}$ liver tissue compared to controls following BDL at day 20 (Figure 12A). Additionally, we also detected increased expression of the proliferation markers *Ki67* and *Cyclin-A2* in liver tissue harvested from *Rhbdf2*$^{-/-}$ mice compared to *Rhbdf2*$^{+/-}$ controls at early time points after BDL (Figure 12B-C) and more Ki67-positive cells were present in *Rhbdf2*$^{-/-}$ liver tissue compared to control liver tissue at day 20 after BDL (Figure 13A). Furthermore, we observed that most of

the Ki67-positive cells also stained for α-SMA in the absence of iRhom2, which suggests increased proliferation of HSCs in *Rhbdf2*$^{-/-}$ compared to *Rhbdf2*$^{+/-}$ (Figure 13B).

Figure 11.

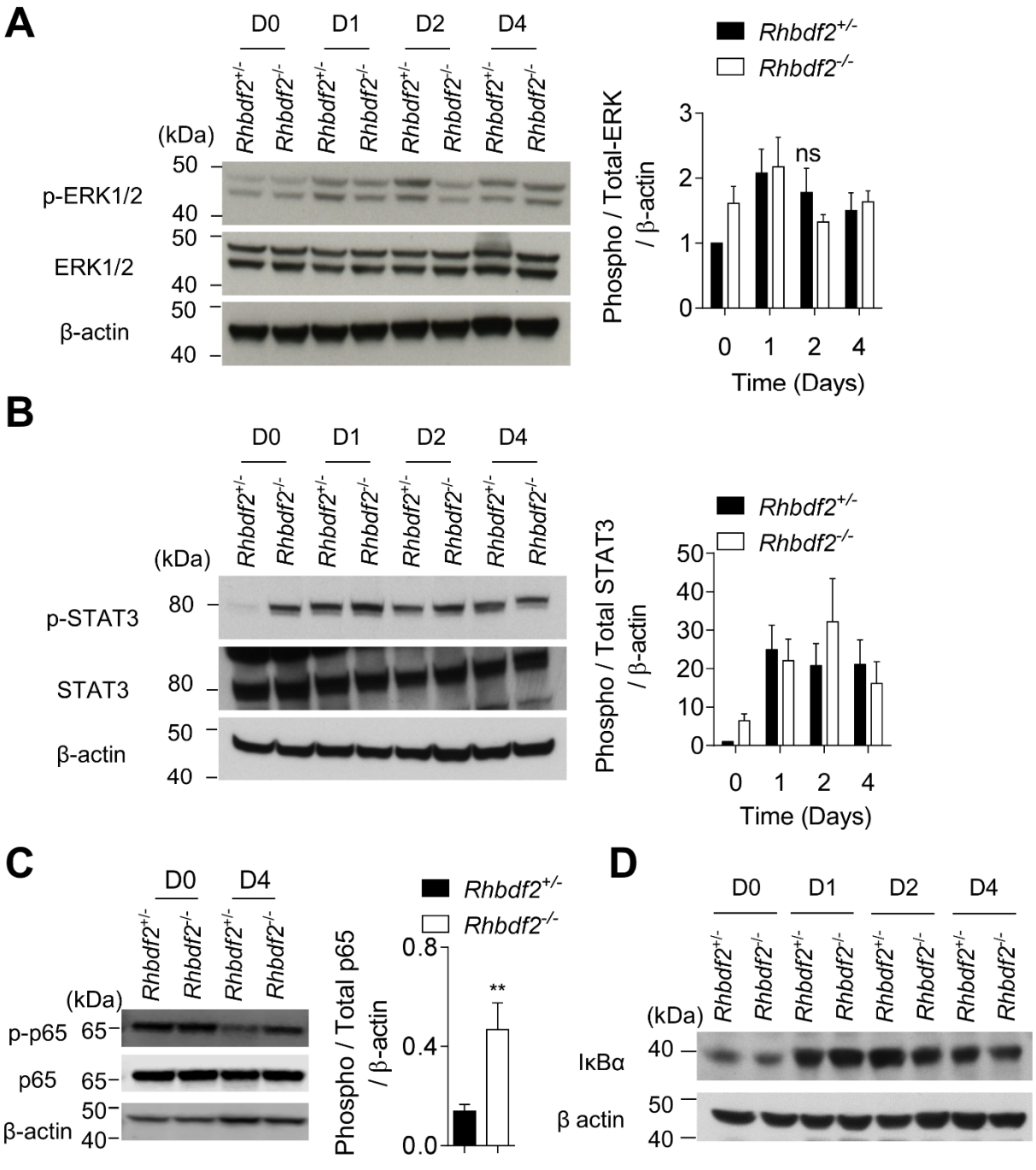
A
D0
D1
D2
D4
Rhbdf2+/-
Rhbdf2-/-
(kDa)
p-ERK1/2
ERK1/2
β-actin
50
40
Phospho / Total-ERK / β-actin
ns
Time (Days)
B
p-STAT3
STAT3
80
Phospho / Total STAT3 / β-actin
C
p-p65
p65
65
Phospho / Total p65 / β-actin
**
D
IκBα

Figure 11. Abundance of phosphoylated ERK1/2, phosphorylated STAT3, phosphorylated p65 and IκBα in *Rhbdf2*$^{+/-}$ and *Rhbdf2*$^{-/-}$ mice following BDL

(A) *Immunoblotting and quantification of phosphorylated ERK1/2 (p-ERK1/2) and total ERK1/2 in total liver tissue harvested from Rhbdf2*$^{+/-}$ *and Rhbdf2*$^{-/-}$ *mice at the indicated time points after BDL surgery. β-actin is a loading control. n=6-9 animals per genotype for each time point.* ***(B)*** *Immunoblotting and quantification of phosphorylated STAT3 (p-STAT3) and total STAT3 in total liver tissue harvested from Rhbdf2*$^{+/-}$ *and Rhbdf2*$^{-/-}$ *mice at the indicated time points after BDL surgery. n = 6-9 animals per genotype for each time point.* ***(C)*** *Immunoblotting and quantification of phosphorylated p65 (p-p65) and total p65 in total liver tissue harvested from Rhbdf2*$^{+/-}$ *and Rhbdf2*$^{-/-}$ *mice at the indicated time points after BDL surgery. n = 6-8 animals per genotype for each time point.* ***(D)*** *Immunoblot showing total IκBα in total liver tissue of Rhbdf2*$^{+/-}$ *and Rhbdf2*$^{-/-}$ *mice at the indicated time points after BDL. n= 6-9 animals per genotype for each time point. Data are shown as mean ± SEM. **P<0.01; Mann-Whitney U test (C).*

Figure 12.

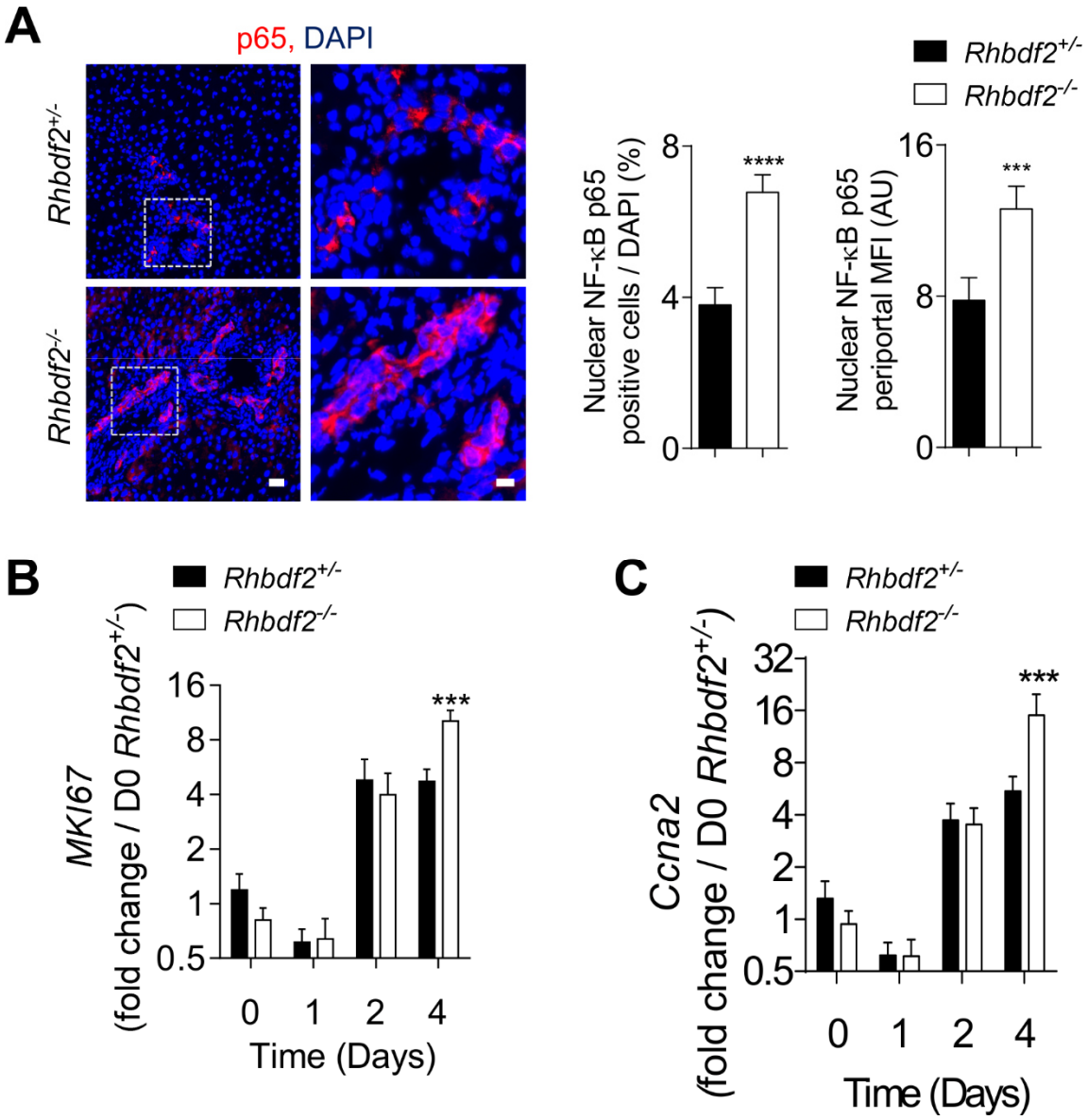

Figure 12. iRhom2 deficiency increases p65 translocation and proliferation markers in the liver. ***(A)*** *Immunostaining and quantification of NF-κB p65 in sections of liver tissue harvested from Rhbdf2$^{+/-}$ and Rhbdf2$^{-/-}$ mice at day 20 after BDL. Nuclei are labelled with DAPI (blue). Boxes indicate the areas magnified in the images on the right. Quantification of p65 is shown as both the percentage of cells that were positive for p65 and the mean fluorescence intensity (MFI) of p65-positive cells. n = 6 mice per genotype. Scale bars, 50µm (left), 20µm (right).* ***(B)*** *Quantification of MKI67 mRNA in total liver tissue harvested from Rhbdf2$^{+/-}$ and Rhbdf2$^{-/-}$ mice at the indicated time points after BDL surgery. n=7-11 animals*

per genotype for each time point. ***(C)*** *Quantification of Ccna2 mRNA in total liver tissue harvested from Rhbdf2$^{+/-}$ and Rhbdf2$^{-/-}$ mice at the indicated time points after BDL surgery. n= 7-11 animals per genotype for each time point.Data are shown as mean ± SEM. ***P<0.001; ****P<0.0001, Mann-Whitney U test (A), 2-way ANOVA with Bonferroni's multiple comparisons test (B and C).*

Figure 13.

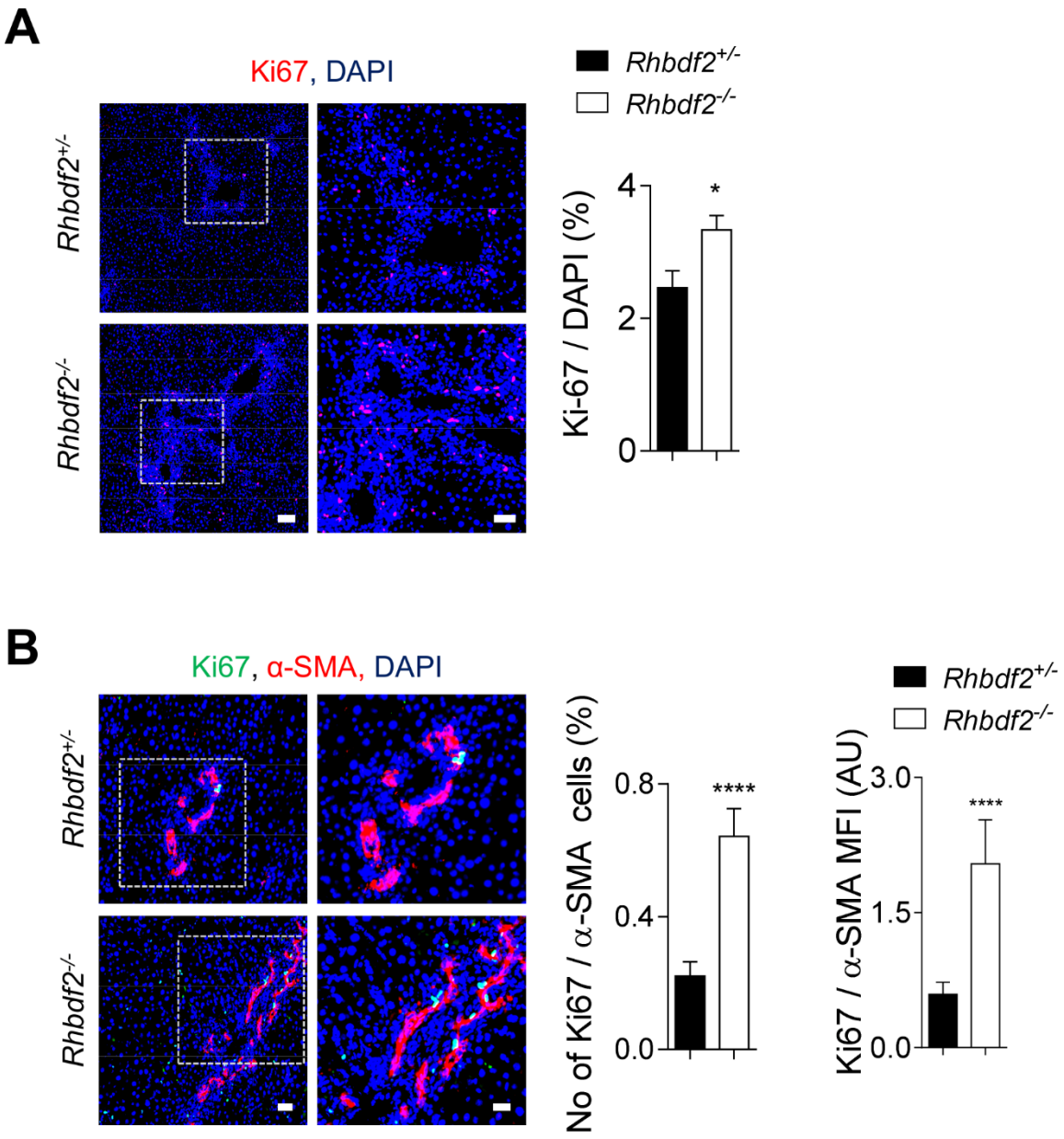

Figure 13. iRhom2 deficiency increases Ki67 staining near to fibrotic area.

(A) *Immunostaining and quantification of the proliferation marker Ki67 in sections of liver tissue harvested from Rhbdf2$^{+/-}$ and Rhbdf2$^{-/-}$ mice at day 20 after BDL. Ki67-positive cells were quantified as a percentage of all cells. n = 6 animals per genotype. Scale bars, 100µm (left), 50µm (right).* ***(B)*** *Immunostaining for Ki67 and α-SMA in sections of liver tissue harvested from Rhbdf2$^{+/-}$ and Rhbdf2$^{-/-}$ mice at day 20 after BDL. α-SMA positive cells that were also Ki67 positive were quantified as percentage and MFI. n=6 animals per genotype.*

*Scale bars, 50µm (left), 20µm (right). Data are shown as mean ± SEM. *P<0.05; **P<0.01; ***P<0.001; ****P<0.0001, Mann-Whitney U test (A and B).*

4.8 Etanercept treatment rescues liver fibrosis in of *Rhbdf2*$^{-/-}$ mice.

It has been previously shown that TNFR2 knockout mice have no major phenotype with regards to BDL-induced fibrosis (*225*). However, in our setting soluble TNFR2 shed from ADAM17-positive cells could play a role in competitively inhibiting soluble TNF-α, which would further explain the differences in BDL-induced fibrosis between *Rhbdf2*$^{+/-}$ and *Rhbdf2*$^{-/-}$ mice. The unshed TNFRs on HSCs from *Rhbdf2*$^{-/-}$ mice as well as the increases in nuclear translocation of p65 and proliferation markers in liver tissue of *Rhbdf2*$^{-/-}$ mice subjected to BDL led us to hypothesize that increased TNFR signaling in HSCs of iRhom2-deficient mice contributes to their increased proliferation and the subsequent progression of liver fibrosis. To test this hypothesis, we inhibited TNFR signaling by treating iRhom2-deficient mice with recombinant TNFR2-Fc (Etanercept), which binds to TNF-α and prevents TNF-α–induced signaling (*159*), starting on the day before BDL surgery. We found reduced nuclear p65 translocation in Etanercept-treated *Rhbdf2*$^{-/-}$ mice compared to PBS-treated mice (Figure 14A) as well as reduced proliferation, as determined by Ki67 staining (Figure 14B). Etanercept-treated mice showed a significant reduction in Ki67 staining in areas positive for α-SMA (Figure 14C) suggesting that blocking TNF-α signaling in iRhom2-deficient liver inhibited HSC proliferation within the fibrotic areas. We detected no changes in macrophage infiltration (Figure 15A) or in expression of genes encoding inflammatory cytokines (Figure 15B-C), with the exception of IL-10 , which is induced during inflammation and fibrosis (*226, 227*), but was reduced with Etanercept treatment (Figure 15B). Furthermore, we found increased abundance of GFAP in the livers of Etanercept-treated *Rhbdf2*$^{-/-}$ BDL mice (Figure 16A) compared to PBS-treated BDL mice, indicating the presence of quiescent HSCs rather than myofibroblasts. This is consistent with the observed reduction in liver fibrotic lesions of Etanercept-treated *Rhbdf2*$^{-/-}$ BDL mice (Figure 16B). PDGFRβ-positive cells were also reduced in Etanercept-treated *Rhbdf2*$^{-/-}$ BDL mice compared to PBS-treated controls (Figure 16B). These phenotypes were accompanied by reductions in α-SMA and collagen after Etanercept treatment compared to PBS treatment (Figure 16C).

Taken together, these findings demonstrate that the absence of iRhom2 results in increased liver fibrosis, which can be alleviated through anti-TNF-α therapy.

Figure 14.

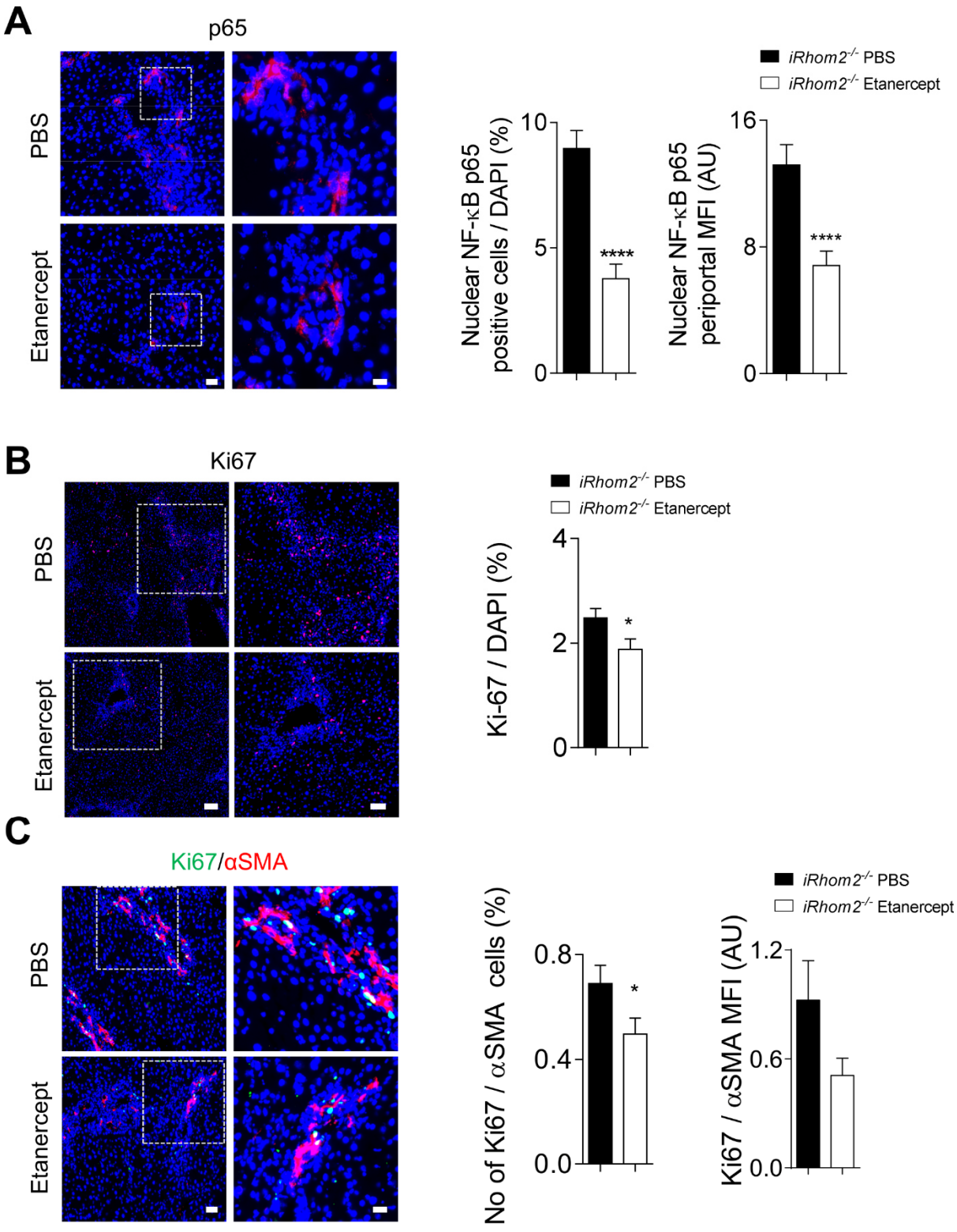
A
p65
PBS
Etanercept
iRhom2-/- PBS
iRhom2-/- Etanercept
Nuclear NF-κB p65 positive cells / DAPI (%)
10
5
0
****
Nuclear NF-κB p65 periportal MFI (AU)
16
8
0
****
B
Ki67
PBS
Etanercept
iRhom2-/- PBS
iRhom2-/- Etanercept
Ki-67 / DAPI (%)
4
2
0
*
C
Ki67/αSMA
PBS
Etanercept
iRhom2-/- PBS
iRhom2-/- Etanercept
No of Ki67 / αSMA cells (%)
0.8
0.4
0.0
*
Ki67 / αSMA MFI (AU)
1.2
0.6
0.0

Figure 14. Etanercept treatment reduces cell proliferation in the livers of *Rhbdf2*$^{-/-}$ mice.

(A) *Immunostaining and quantification of NF-κB p65 in sections of liver harvested from Rhbdf2*$^{-/-}$ *PBS- or Etanercept-treated mice 14 days after BDL. Nuclei are labelled with DAPI (blue). Boxes indicate the areas magnified in the images on the right. Quantification of cells with nuclear p65 is shown as both the percentage of positive cells and the mean fluorescence intensity (MFI). Scale bars, 50μm (left), 10μm (right).* ***(B)*** *Immunostaining and quantification of Ki67 in sections of liver tissue harvested from Rhbdf2*$^{-/-}$ *PBS- or Etanercept-treated mice 14 days after BDL. Ki67-positive cells were quantified as a percentage of all cells. Scale bar, 100μm (left), 50μm (right).* ***(C)*** *Immunostaining and quantification of Ki67 and α-SMA in sections of liver tissue harvested from Rhbdf2*$^{-/-}$ *PBS- or Etanercept-treated mice 14 days after BDL. α-SMA–positive cells that were also Ki67 positive were quantified as % and MFI. Scale bars, 50μm (left), 20μm (right).. For all panels, n = 7 mice for each condition. Data are shown as mean ± SEM. *P<0.05; ****P<0.0001, Mann-Whitney U test (A-C).*

Figure 15.

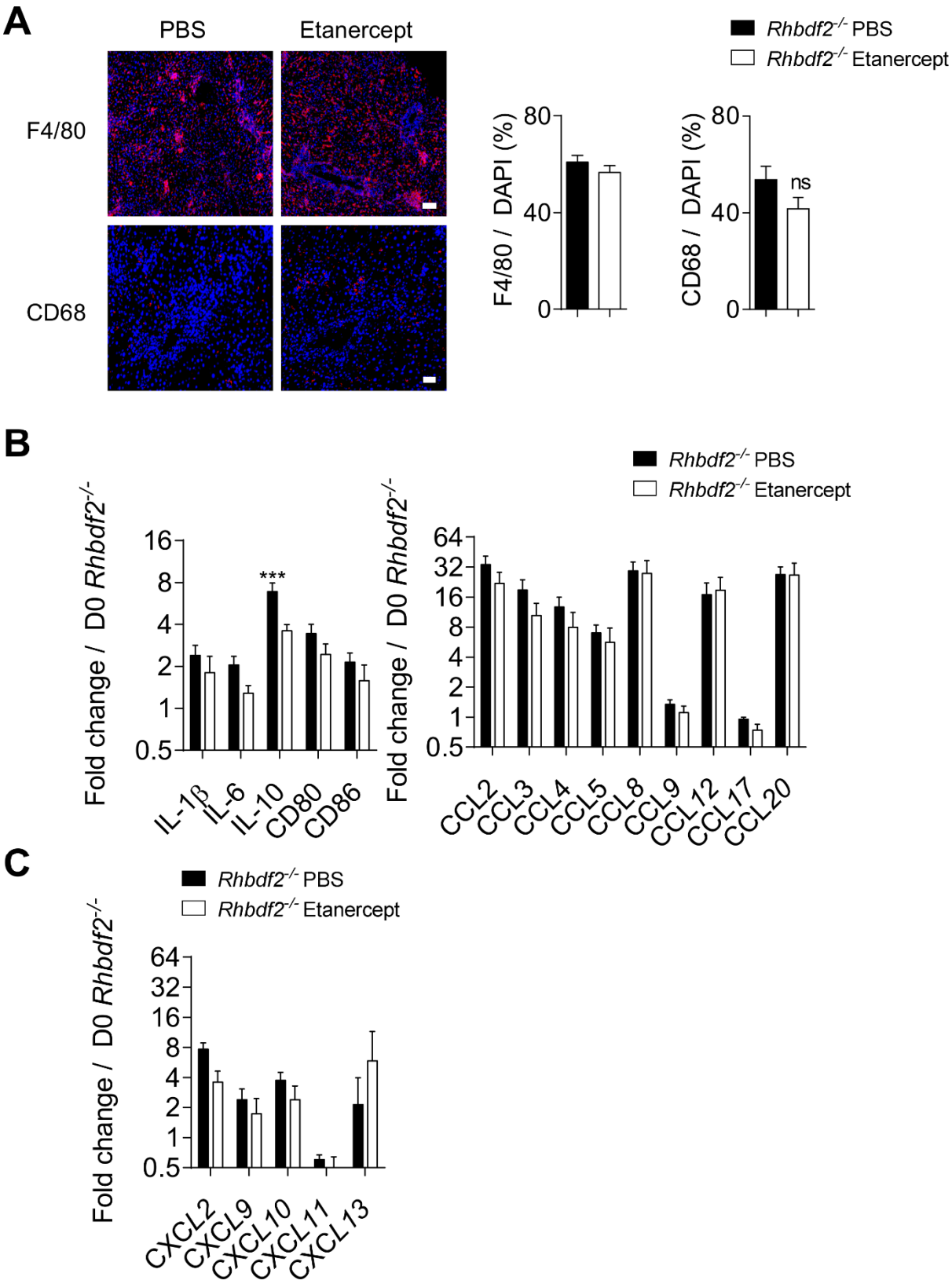
A
PBS
Etanercept
F4/80
CD68
Rhbdf2-/- PBS
Rhbdf2-/- Etanercept
F4/80 / DAPI (%)
CD68 / DAPI (%)
80
40
0
ns
B
Rhbdf2-/- PBS
Rhbdf2-/- Etanercept
Fold change / D0 Rhbdf2-/-
16
8
4
2
1
0.5
***
IL-1β
IL-6
IL-10
CD80
CD86
64
32
16
8
4
2
1
0.5
CCL2
CCL3
CCL4
CCL5
CCL8
CCL9
CCL12
CCL17
CCL20
C
Rhbdf2-/- PBS
Rhbdf2-/- Etanercept
Fold change / D0 Rhbdf2-/-
64
32
16
8
4
2
1
0.5
CXCL2
CXCL9
CXCL10
CXCL11
CXCL13

Figure 15. Expression of Cytokines and chemokines in Etanercept-treated *Rhbdf2*$^{-/-}$ BDL mice.

(A) *Sections of liver tissue harvested from Rhbdf2*$^{-/-}$ *PBS- or Etanercept- treated mice 14 days after BDL were stained for F4/80 or CD68 together with DAPI to label nuclei (blue). Scale bars, 100µm (F4/80), 50 µm (CD68). Right panel shows quantification of F4/80 and CD68 cells as %. n = 7 animals for each condition.* ***(B–C)*** *Quantification of Il1b, IL6, Il10, Cd80, Cd86, Ccl2, Ccl3, Ccl4, Ccl5, Ccl8, Ccl9, Ccl12, Ccl17, Ccl20, Cxcl2, Cxcl9, Cxcl10, Cxcl11, and Cxcl13 mRNAs in total liver tissue harvested from PBS- and Etanercept-treated Rhbdf2*$^{-/-}$ *mice after BDL surgery. n = 7 animals for each condition. Data are shown as mean ± SEM.*

Figure 16.

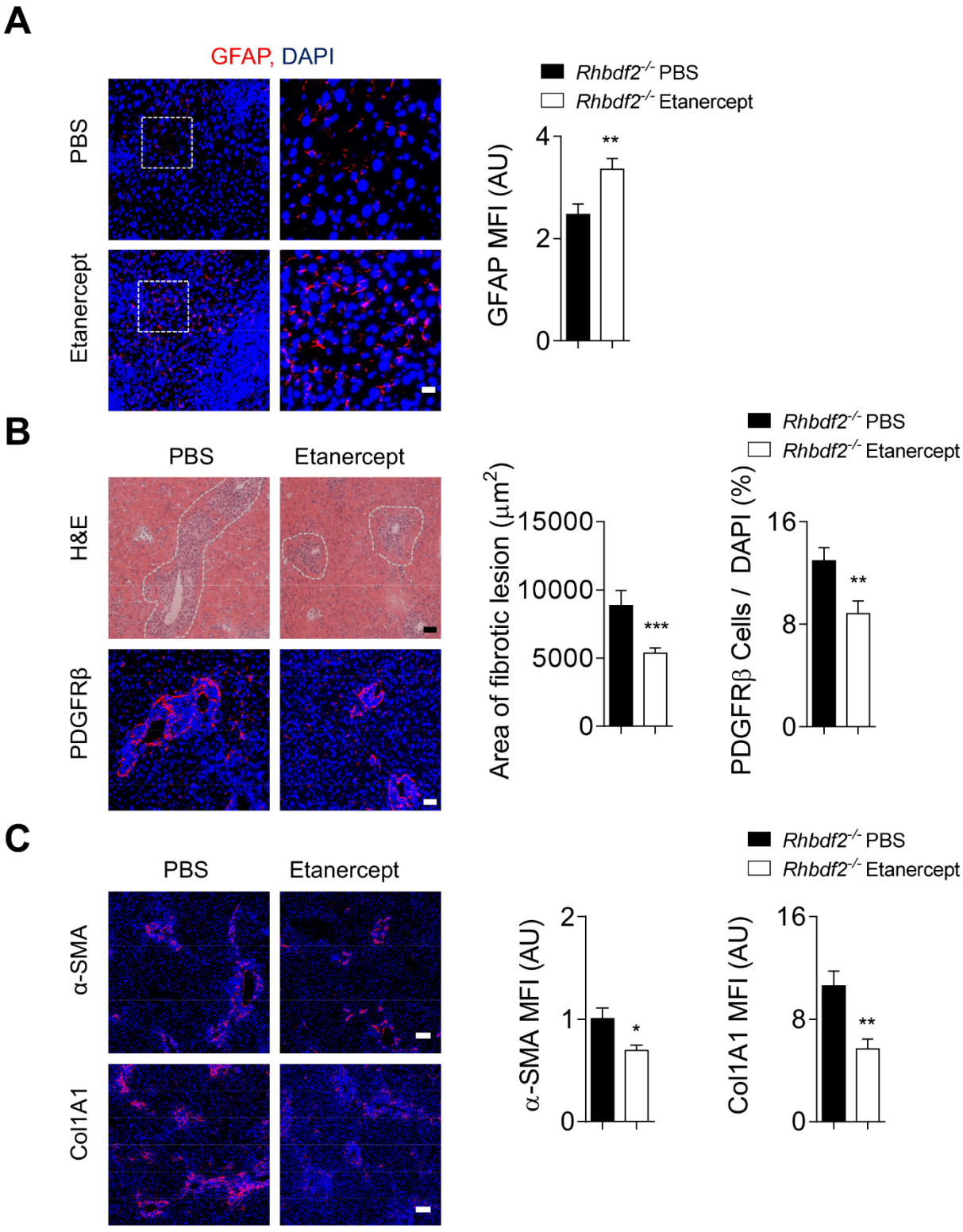
A
GFAP, DAPI
PBS
Etanercept
Rhbdf2-/- PBS
Rhbdf2-/- Etanercept
GFAP MFI (AU)
4
2
0
**
B
PBS
Etanercept
H&E
PDGFRβ
Area of fibrotic lesion (μm2)
15000
10000
5000
0
***
PDGFRβ Cells / DAPI (%)
16
8
0
**
C
α-SMA
Col1A1
α-SMA MFI (AU)
2
1
0
*
Col1A1 MFI (AU)
16
8
0
**

Figure 16. Etanercept treatment rescues liver fibrosis in *Rhbdf2*$^{-/-}$ mice.

(A) *Immunostaining and quantification of GFAP, which marks HSCs that have not transdifferentiated into myofibroblasts, in sections of liver harvested from Rhbdf2*$^{-/-}$ *PBS- or Etanercept-treated mice 14 days after BDL. Nuclei are stained with DAPI (blue). Boxes indicate the areas magnified in the images on the right. GFAP was quantified as mean fluorescence intensity (MFI). Scale bars, 50µm (left), 20µm (right).* ***(B)*** *Sections of liver tissue harvested from Rhbdf2*$^{-/-}$ *PBS- or Etanercept-treated mice 14 days after BDL were stained with Hematoxylin and Eosin or with antibodies recognizing PDGFRβ. White dashed lines indicate the boundaries of fibrotic lesions boundaries. The sizes of fibrotic lesions were quantified in* μm^2*, and PDGFRβ-positive cells were quantified as a percentage of all cells in each section. Scale bar, 50µm.* ***(C)*** *Immunostaining and quantification of α-SMA and Col1A1 in sections of liver tissue harvested from Rhbdf2*$^{-/-}$ *PBS- or Etanercept-treated mice 14 days after BDL. Cells positive for α-SMA or Col1A1 were quantified as MFI. Scale bar, 100µm. For all panels, n = 7 mice for each condition. Data are shown as mean ± SEM. *P<0.05; **P<0.01; ***P<0.001, Mann-Whitney U test was used (A-C).*

Chapter 5
Discussion

In this study we found that iRhom2 protected against liver fibrosis following BDL by promoting ADAM17 maturation, leading to increased shedding of TNFRs, and therefore less TNF-α signaling, in HSCs. The absence of iRhom2 caused an increase in the number of activated stellate cells along with increased expression of fibrotic markers after BDL, both of which were alleviated by anti-TNF-α therapy.

The release of TNF-α into the circulation is triggered by ADAM17-mediated cleavage of membrane-bound TNF-α from the cell surface (*91, 92*). Because iRhom2 stimulates ADAM17 maturation, it consequently promotes shedding of soluble TNF-α (*136, 137*). Thus, iRhom2-deficient mice are protected against LPS-induced septic shock but susceptible to bacterial infection (*137*). Importantly, earlier studies have documented that cytokines such as TNF-α and IL-1β from Kupffer cells can contribute to the survival of hepatic stellate cells during liver damage (*15*). Similarly, other studies show that the sustained activation of hepatic NF-κB in macrophages could contribute to liver inflammation and fibrosis (*99, 228*) whereas depletion of hepatic macrophages significantly reduced NF-κB activity, inflammation and fibrosis in liver (*229*) . Interestingly, iRhom2 also has been shown to be expressed in myeloid cellular compartments such as macrophages (*137, 159*). From these observations, and considering that iRhom2 is produced in Kupffer cells, it might be logical to speculate that the absence of iRhom2 would alleviate liver fibrosis induced by BDL. However, our data indicate that the absence of iRhom2 aggravated liver fibrosis, leading us to speculate that iRhom2 negatively regulates liver fibrosis in bile duct ligated mice.

ADAM17 cleaves not only membrane-bound TNF-α (*91, 92*), but also TNFR1 and TNFR2 (*117*). Indeed, compared to iRhom2-deficient animals, we found increased circulating TNFRs in wild-type mice after BDL, suggesting that there were more unshed TNFRs on the surface of liver cells in the mutant mice. Consistent with our finding, a study with ADAM17 hypomorphic mice (*230*) which has decreased or low residual ADAM17 activity show that atherosclerotic lesions are significantly increased in ADAM17 hypomorphic mice compared to WT controls (*231*). This study identified that ADAM17 hypomorphic mice had more macrophages and vascular smooth muscle cells compared to wild-type controls. Mechanically, the study shows that reduced ADAM17-mediated shedding led to significantly increased presence of membrane bound TNF-α and TNFR2, resulting in a constitutive activation of TNFR2 signaling (*231*). This study lead us to hypothesize that the phenotype we observed in iRhom2 deficient mice could be because of increased presence of unshed TNFRs

on the surface of liver cells which would result in a corresponding increase in TNF-α–induced signaling, which would eventually drive to liver fibrosis.

Although iRhom2 triggers ADAM17 maturation, its absence does not completely abolish ADAM17 maturation or activity, and thus may not block all shedding of TNF-α after BDL (*102*). Additionally, unshed membrane-bound TNF-α can also bind to and activate both TNFR1 and 2, albeit with different efficiencies (*232, 233*), suggesting a potential iRhom2-independent mechanism for initiating profibrotic TNF-α signaling after BDL. We expect if the latter is the case it would be more likely to occur in HSCs than in hepatocytes given that our data show differences in NF-κB signaling, which is downstream of TNF-α, and subsequent proliferation in HSCs with no difference in TNF-α–induced apoptosis in primary hepatocytes. Consistent with this, we did not find a significant difference in circulating liver enzymes and cleaved caspase 3 between *Rhbdf2*$^{+/-}$ and *Rhbdf2*$^{-/-}$ mice after BDL, which led us to speculate that TNF-α–TNFR signaling in hepatocytes of *Rhbdf2*$^{+/-}$ and *Rhbdf2*$^{-/-}$ mice is comparable during BDL. Notably, our experiments were performed in a whole-body iRhom2-deficient mouse model and although we analyzed the overall effects of iRhom2 deficiency during BDL, we cannot make definitive conclusions regarding the function of iRhom2 in specific cell types. We can only conclude that iRhom2 reduces the numbers of stellate cells and alleviates liver fibrosis following BDL, but this phenotype might not be uniquely linked to a specific iRhom2-producing cell type and could result from the actions of iRhom2 in multiple cell types. HSC specific deletion of iRhom2 or ADAM17 would clarify the question that the protective effect of iRhom2 is mediated by its action in HSCs or whether other relevant cell types that also produce iRhom2 (such as hepatocytes, Kupffer cells, or monocyte-derived macrophages) are involved. However, our *in vitro* experiments with primary HSCs clearly showed that ADAM17 maturation and TNFR shedding is significantly abolished in absence of iRhom2 along with increased expression of fibrotic markers suggesting that iRhom2 can affect HSC activation.

Interestingly, during liver fibrosis we measured increased circulating TNFR2 in WT mice compared to iRhom2 deficient animals. To mimic the *in vivo* setting, we also isolated and stimulated primary HSCs from both *Rhbdf2*$^{+/-}$ and *Rhbdf2*$^{-/-}$ mice with TNF-α. We measured increased shedding of TNFR2 in WT HSCs upon TNF-α treatment whereas TNFR1 was decreased, while shedding of both receptors was abolished in iRhom2 deficient HSCs. Earlier studies have described that membrane TNF-α is a strong ligand for TNFR2 (*171*). Vascular smooth muscle cells also can contribute to cardiac fibrosis (*234-236*). Moreover ADAM17

hypomorphic mice showed more vascular smooth muscle cells through membrane bound TNF-α and membrane TNFR2 signaling (*231*) probably through NF-κB signalling which is consistent with our finding. Etanercept (Enbrel) is a recombinant TNFR2-Fc, which binds to TNF-α and prevents TNF-α–induced signalling (*237-239*). Moreover, Anti-TNF-α antibody have been used for various liver diseases such as Alcoholic Hepatitis (AH), Non-Alcoholic Fatty Liver Disease (NAFLD), Autoimmune Hepatitis (AIH), and Primary Biliary Cholangitis (PBC) to reduce liver inflammation and liver fibrosis by blocking TNF-α signaling (*48, 49, 52, 57, 240, 241*). Because we hypothesize that iRhom2 deficient liver tissue has enhanced TNF-α signalling, we treated iRhom2 deficient mice with Etanercept and checked for liver fibrosis. Consistent with previous studies, we also observed decreased liver fibrosis in Etanercept treated iRhom2 deficient mice which again supports our hypothesis that unshed TNFRs on HSCs from *Rhbdf2*$^{-/-}$ mice could trigger increased TNF-TNFR signaling which eventually contributes to their increased proliferation and the subsequent progression of liver fibrosis.

Sequence alterations in the cytoplasmic tail of iRhom2 can increase ADAM17 activity and consequently increase TNFR shedding (*166, 168, 242*). It is possible that posttranslational modifications of iRhom2 might trigger ADAM17 maturation and TNFR shedding following cholestasis and therefore have a protective effect against BDL-induced liver fibrosis. Notably, mutations that affect the cytoplasmic tail of iRhom2 are also associated with the establishment of esophageal cancer (*166*). Future studies could investigate whether inactivating mutations or reduced abundance of iRhom2 correlate with liver fibrosis or hepatocellular carcinoma in patients. iRhom2 has multiple biological functions apart from its role in ADAM17 maturation. Specifically, iRhom2 can bind to STING and prevent its degradation (*156*). Accordingly, iRhom2 promotes interferon regulatory factor 3 (IRF3) phosphorylation and translocation into the nucleus and consequently contributes to IFN-I production during viral infection (*156, 157*). Furthermore, STING and IRF3 are able to promote hepatocyte death and liver fibrosis during carbon tetrachloride treatment, albeit IFN-I is beneficial following BDL (*243-245*). However, our data in iRhom2-deficient animals suggest that iRhom2 is rather beneficial during the establishment of liver fibrosis. Hence we speculate that in our study, the role of iRhom2 in liver fibrosis is independent from its stabilizing effect on STING. Furthermore, iRhom2 can regulate the cytoskeletal scaffolding protein Keratin 16 (*169*). In the liver, keratins protect hepatocytes from apoptosis and necrosis (*246*), and keratins such as K8 and K18 variants and K19 are associated with liver

disease (*246-249*). Accordingly, mice expressing variants of K18 exhibit an increase in Fas-induced liver damage compared to TNF-α–induced liver damage (*250*). Additionally, iRhom2 influences K16 abundance with effects extending to its binding partner K6 (*169*). One could speculate that iRhom2 affects the equilibrium of keratins in liver tissue, thereby affecting the establishment of liver fibrosis. However, when we analyzed tissue damage following BDL in iRhom2-deficient mice and controls, we did not observe any significant differences, making keratins unlikely contributors to liver fibrosis in our model system. We observed an increased presence of cells positive for CD68, a well-established marker for activated macrophages (*163*), in liver tissue from iRhom2-deficient mice, which could contribute to increased TNF-α–TNFR signaling in stellate cells.

Other ADAM17 substrates have also been reported to play roles in liver fibrosis. Ectodomain shedding of EGFR ligands and TNFR1 can critically regulate acute liver damage (*129*), and conditional deletion of HB-EGF results in increased liver injury following acute toxic hepatitis (*251*). Furthermore, overexpression of HB-EGF results in aggravated liver fibrosis following chronic liver injury (*252*), whereas another report has shown that treatment with the EGFR inhibitor erlotimib alleviated establishment of liver fibrosis (*253*). Our findings showed no significant difference in HB-EGF in the sera of control or iRhom2-deficient mice. Moreover, decreased HB-EGF concentrations, which would be expected in the absence of iRhom2, would rather alleviate liver fibrosis. Moreover, we observed no significant differences in EGFR signaling. Hence, we speculate that increased liver fibrosis in the absence of iRhom2 cannot be explained mechanistically by changes in EGFR signaling. The absence of gp130, a critical factor essential for IL-6R signaling, increases liver damage following BDL, which is associated with increased bacterial burden (*254*). It has also been shown that lack of IL-6, gp130, and STAT3 signaling in the liver promotes the establishment of steatohepatitis (*255*). Bacterial translocation following BDL triggers an IFN-I signature resulting in immunosuppression (*203*). In our investigation we also observed reduced soluble IL-6R in the sera of iRhom2-deficient animals after BDL. However, STAT3 phosphorylation following BDL was not affected by iRhom2. Additionally, we did not see any differences in bacterial titers or IFN-I–regulated genes in iRhom2-deficient mice compared to control animals. Although other signaling pathways might be affected by iRhom2 and contribute to the establishment of liver fibrosis, in our model TNF-α blockade reduced the presence of stellate cells in the liver and alleviated fibrosis in iRhom2-deficient mice.

Since we identified more activated hepatic stellate cells and increased expression of extracellular matrix proteins in iRhom2 deficient liver, it would be interesting to study further, whether iRhom2 deficient mice develop hepatocellular carcinoma after BDL by keeping them for long time kinetics. Because most clinical studies describe that liver fibrosis is one key driving factor which can cause liver cirrhosis which eventually leads to hepatocellular carcinoma. Also, to strengthen the study, an anti-fibrotic function of iRhom2 could be characterized in HSC specific iRhom2 knockout mice which would clearly demonstrate that hepatic cells participate in driving liver fibrosis in absence of iRhom2. Moreover, an anti-fibrotic role of iRhom2 can be characterized in other liver fibrosis models such as carbon tetrachloride-induced fibrosis, Thioacetamide-induced fibrosis and Dimethylnitrosamine-induced fibrosis. In summary, we identified iRhom2 to be protective against BDL induced liver fibrosis (Graphical figure 7).

Graphical figure 7: Schematic representation of anti-fibrotic function of iRhom2 in hepatic stellate cells

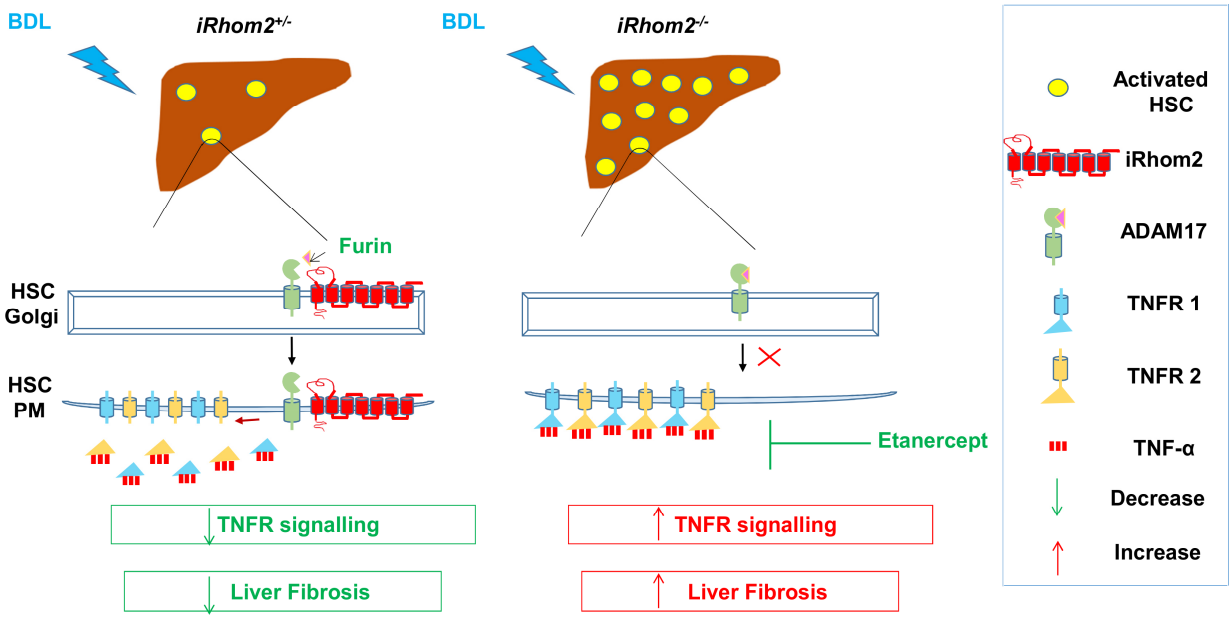

Proposed model illustrating the anti-fibrotic function of iRhom2 in cholestasis induced liver fibrosis.

Liver fibrosis is mainly driven by activation and proliferation of hepatic stellate cells (HSCs) during liver damage. iRhom2 expression activates ADAM17 and triggers increased shedding of TNFRs from the HSC plasma membrane. In the absence of iRhom2, the uncleaved TNFRs remain on the surface of the HSC plasma membrane consisting more TNF mediated activation and increased proliferation via NF-κB signalling (PM – Plasma membrane).

Chapter 6
Bibliography

1. K. Si-Tayeb, F. P. Lemaigre, S. A. Duncan, Organogenesis and development of the liver. *Dev Cell* **18**, 175-189 (2010).
2. S. R. Abdel-Misih, M. Bloomston, Liver anatomy. *Surg Clin North Am* **90**, 643-653 (2010).
3. M. Gordillo, T. Evans, V. Gouon-Evans, Orchestrating liver development. *Development* **142**, 2094-2108 (2015).
4. A. Blouin, R. P. Bolender, E. R. Weibel, Distribution of organelles and membranes between hepatocytes and nonhepatocytes in the rat liver parenchyma. A stereological study. *J Cell Biol* **72**, 441-455 (1977).
5. P. Bioulac-Sage *et al.*, Hepatocellular adenoma subtype classification using molecular markers and immunohistochemistry. *Hepatology* **46**, 740-748 (2007).
6. A. W. Duncan, C. Dorrell, M. Grompe, Stem cells and liver regeneration. *Gastroenterology* **137**, 466-481 (2009).
7. G. K. Michalopoulos, M. C. DeFrances, Liver regeneration. *Science* **276**, 60-66 (1997).
8. M. Strazzabosco, S. Somlo, Polycystic liver diseases: congenital disorders of cholangiocyte signaling. *Gastroenterology* **140**, 1855-1859, 1859 e1851 (2011).
9. J. H. Tabibian, A. I. Masyuk, T. V. Masyuk, S. P. O'Hara, N. F. LaRusso, Physiology of cholangiocytes. *Compr Physiol* **3**, 541-565 (2013).
10. L. Maroni *et al.*, Functional and structural features of cholangiocytes in health and disease. *Cell Mol Gastroenterol Hepatol* **1**, 368-380 (2015).
11. J. L. Boyer, Bile formation and secretion. *Compr Physiol* **3**, 1035-1078 (2013).
12. M. Sato, S. Suzuki, H. Senoo, Hepatic stellate cells: unique characteristics in cell biology and phenotype. *Cell Struct Funct* **28**, 105-112 (2003).
13. P. J. MacPhee, E. E. Schmidt, A. C. Groom, Evidence for Kupffer cell migration along liver sinusoids, from high-resolution in vivo microscopy. *Am J Physiol* **263**, G17-23 (1992).
14. R. Taub, Liver regeneration: from myth to mechanism. *Nat Rev Mol Cell Biol* **5**, 836-847 (2004).
15. J. P. Pradere *et al.*, Hepatic macrophages but not dendritic cells contribute to liver fibrosis by promoting the survival of activated hepatic stellate cells in mice. *Hepatology* **58**, 1461-1473 (2013).
16. J. Poisson *et al.*, Liver sinusoidal endothelial cells: Physiology and role in liver diseases. *J Hepatol* **66**, 212-227 (2017).
17. E. Maslak, A. Gregorius, S. Chlopicki, Liver sinusoidal endothelial cells (LSECs) function and NAFLD; NO-based therapy targeted to the liver. *Pharmacol Rep* **67**, 689-694 (2015).
18. S. K. Asrani, H. Devarbhavi, J. Eaton, P. S. Kamath, Burden of liver diseases in the world. *J Hepatol* **70**, 151-171 (2019).
19. A. S. Lok, B. J. McMahon, A. A. f. t. S. o. L. D. Practice Guidelines Committee, Chronic hepatitis B. *Hepatology* **34**, 1225-1241 (2001).
20. G. M. Lauer, B. D. Walker, Hepatitis C virus infection. *N Engl J Med* **345**, 41-52 (2001).
21. C. T. Bock *et al.*, Structural organization of the hepatitis B virus minichromosome. *J Mol Biol* **307**, 183-196 (2001).
22. J. E. Newbold *et al.*, The covalently closed duplex form of the hepadnavirus genome exists in situ as a heterogeneous population of viral minichromosomes. *J Virol* **69**, 3350-3357 (1995).
23. P. J. Cote *et al.*, Cyclosporin A modulates the course of woodchuck hepatitis virus infection and induces chronicity. *J Immunol* **146**, 3138-3144 (1991).
24. A. R. Jilbert *et al.*, Characterization of age- and dose-related outcomes of duck hepatitis B virus infection. *Virology* **244**, 273-282 (1998).
25. M. Dandri, J. Petersen, Mechanism of Hepatitis B Virus Persistence in Hepatocytes and Its Carcinogenic Potential. *Clin Infect Dis* **62 Suppl 4**, S281-288 (2016).
26. C. Seeger, W. S. Mason, Molecular biology of hepatitis B virus infection. *Virology* **479-480**, 672-686 (2015).

27. J. H. Hoofnagle, Alpha-interferon therapy of chronic hepatitis B. Current status and recommendations. *J Hepatol* **11 Suppl 1**, S100-107 (1990).
28. P. Marcellin *et al.*, Regression of cirrhosis during treatment with tenofovir disoproxil fumarate for chronic hepatitis B: a 5-year open-label follow-up study. *Lancet* **381**, 468-475 (2013).
29. M. M. Tana, J. H. Hoofnagle, Scar undone: long-term therapy of hepatitis B. *Lancet* **381**, 433-434 (2013).
30. U. A. Ashfaq, T. Javed, S. Rehman, Z. Nawaz, S. Riazuddin, An overview of HCV molecular biology, replication and immune responses. *Virol J* **8**, 161 (2011).
31. F. Poordad, D. Dieterich, Treating hepatitis C: current standard of care and emerging direct-acting antiviral agents. *J Viral Hepat* **19**, 449-464 (2012).
32. J. Rehm *et al.*, Global burden of disease and injury and economic cost attributable to alcohol use and alcohol-use disorders. *Lancet* **373**, 2223-2233 (2009).
33. S. M. Cohen, J. Ahn, Review article: the diagnosis and management of alcoholic hepatitis. *Aliment Pharmacol Ther* **30**, 3-13 (2009).
34. W. G. Hardison, F. I. Lee, Prognosis in acute liver disease of the alcoholic patient. *N Engl J Med* **275**, 61-66 (1966).
35. M. R. Lucey, P. Mathurin, T. R. Morgan, Alcoholic hepatitis. *N Engl J Med* **360**, 2758-2769 (2009).
36. P. Mathurin, R. Bataller, Trends in the management and burden of alcoholic liver disease. *J Hepatol* **62**, S38-46 (2015).
37. M. Adachi, D. A. Brenner, Clinical syndromes of alcoholic liver disease. *Dig Dis* **23**, 255-263 (2005).
38. R. Bataller, B. Gao, Liver fibrosis in alcoholic liver disease. *Semin Liver Dis* **35**, 146-156 (2015).
39. H. Tilg, A. M. Diehl, Cytokines in alcoholic and nonalcoholic steatohepatitis. *N Engl J Med* **343**, 1467-1476 (2000).
40. C. J. McClain, S. Barve, I. Deaciuc, M. Kugelmas, D. Hill, Cytokines in alcoholic liver disease. *Semin Liver Dis* **19**, 205-219 (1999).
41. C. J. McClain, Z. Song, S. S. Barve, D. B. Hill, I. Deaciuc, Recent advances in alcoholic liver disease. IV. Dysregulated cytokine metabolism in alcoholic liver disease. *Am J Physiol Gastrointest Liver Physiol* **287**, G497-502 (2004).
42. J. Colmenero *et al.*, Hepatic expression of candidate genes in patients with alcoholic hepatitis: correlation with disease severity. *Gastroenterology* **132**, 687-697 (2007).
43. N. Rafiq, Z. M. Younossi, Nonalcoholic fatty liver disease: a practical approach to evaluation and management. *Clin Liver Dis* **13**, 249-266 (2009).
44. J. D. Browning, J. D. Horton, Molecular mediators of hepatic steatosis and liver injury. *J Clin Invest* **114**, 147-152 (2004).
45. G. Perseghin, K. Petersen, G. I. Shulman, Cellular mechanism of insulin resistance: potential links with inflammation. *Int J Obes Relat Metab Disord* **27 Suppl 3**, S6-11 (2003).
46. S. E. Shoelson, J. Lee, A. B. Goldfine, Inflammation and insulin resistance. *J Clin Invest* **116**, 1793-1801 (2006).
47. K. Tomita *et al.*, Tumour necrosis factor alpha signalling through activation of Kupffer cells plays an essential role in liver fibrosis of non-alcoholic steatohepatitis in mice. *Gut* **55**, 415-424 (2006).
48. S. S. Koca *et al.*, The treatment with antibody of TNF-alpha reduces the inflammation, necrosis and fibrosis in the non-alcoholic steatohepatitis induced by methionine- and choline-deficient diet. *Inflammation* **31**, 91-98 (2008).
49. R. Barbuio, M. Milanski, M. B. Bertolo, M. J. Saad, L. A. Velloso, Infliximab reverses steatosis and improves insulin signal transduction in liver of rats fed a high-fat diet. *J Endocrinol* **194**, 539-550 (2007).

50. L. European Association for the Study of the, EASL Clinical Practice Guidelines: Autoimmune hepatitis. *J Hepatol* **63**, 971-1004 (2015).
51. D. Akberova, A. P. Kiassov, D. Abdulganieva, Serum Cytokine Levels and Their Relation to Clinical Features in Patients with Autoimmune Liver Diseases. *J Immunol Res* **2017**, 9829436 (2017).
52. C. Weiler-Normann *et al.*, Infliximab as a rescue treatment in difficult-to-treat autoimmune hepatitis. *J Hepatol* **58**, 529-534 (2013).
53. J. Rajanayagam, P. J. Lewindon, Infliximab as rescue therapy in paediatric autoimmune hepatitis. *J Hepatol* **59**, 908-909 (2013).
54. R. Poupon, Primary biliary cirrhosis: a 2010 update. *J Hepatol* **52**, 745-758 (2010).
55. G. M. Hirschfield, M. E. Gershwin, The immunobiology and pathophysiology of primary biliary cirrhosis. *Annu Rev Pathol* **8**, 303-330 (2013).
56. D. Dimopoulou, T. Dimitroulas, E. Akriviadis, A. Garyfallos, Infliximab as a treatment option for patients with rheumatoid arthritis and primary biliary cirrhosis. *Rheumatol Int* **35**, 1913-1916 (2015).
57. V. V. Menghini, A. S. Arora, Infliximab-associated reversible cholestatic liver disease. *Mayo Clin Proc* **76**, 84-86 (2001).
58. R. Bataller, D. A. Brenner, Liver fibrosis. *J Clin Invest* **115**, 209-218 (2005).
59. T. A. Wynn, Integrating mechanisms of pulmonary fibrosis. *J Exp Med* **208**, 1339-1350 (2011).
60. T. A. Wynn, T. R. Ramalingam, Mechanisms of fibrosis: therapeutic translation for fibrotic disease. *Nat Med* **18**, 1028-1040 (2012).
61. T. A. Wynn, Cellular and molecular mechanisms of fibrosis. *J Pathol* **214**, 199-210 (2008).
62. P. Gines, A. Cardenas, V. Arroyo, J. Rodes, Management of cirrhosis and ascites. *N Engl J Med* **350**, 1646-1654 (2004).
63. T. Tsuchida, S. L. Friedman, Mechanisms of hepatic stellate cell activation. *Nat Rev Gastroenterol Hepatol* **14**, 397-411 (2017).
64. K. Iwaisako *et al.*, Origin of myofibroblasts in the fibrotic liver in mice. *Proc Natl Acad Sci U S A* **111**, E3297-3305 (2014).
65. I. Mederacke *et al.*, Fate tracing reveals hepatic stellate cells as dominant contributors to liver fibrosis independent of its aetiology. *Nat Commun* **4**, 2823 (2013).
66. S. L. Friedman, Mechanisms of hepatic fibrogenesis. *Gastroenterology* **134**, 1655-1669 (2008).
67. C. Yin, K. J. Evason, K. Asahina, D. Y. Stainier, Hepatic stellate cells in liver development, regeneration, and cancer. *J Clin Invest* **123**, 1902-1910 (2013).
68. C. Kordes, I. Sawitza, S. Gotze, D. Herebian, D. Haussinger, Hepatic stellate cells contribute to progenitor cells and liver regeneration. *J Clin Invest* **124**, 5503-5515 (2014).
69. R. Reinehr, A. Sommerfeld, D. Haussinger, CD95 ligand is a proliferative and antiapoptotic signal in quiescent hepatic stellate cells. *Gastroenterology* **134**, 1494-1506 (2008).
70. T. Nishio *et al.*, Activated hepatic stellate cells and portal fibroblasts contribute to cholestatic liver fibrosis in MDR2 knockout mice. *J Hepatol* **71**, 573-585 (2019).
71. I. Sawitza, C. Kordes, S. Reister, D. Haussinger, The niche of stellate cells within rat liver. *Hepatology* **50**, 1617-1624 (2009).
72. J. Kluwe *et al.*, Absence of hepatic stellate cell retinoid lipid droplets does not enhance hepatic fibrosis but decreases hepatic carcinogenesis. *Gut* **60**, 1260-1268 (2011).
73. N. C. Henderson *et al.*, Targeting of alphav integrin identifies a core molecular pathway that regulates fibrosis in several organs. *Nat Med* **19**, 1617-1624 (2013).
74. C. Yin, K. J. Evason, J. J. Maher, D. Y. Stainier, The basic helix-loop-helix transcription factor, heart and neural crest derivatives expressed transcript 2, marks hepatic stellate cells in zebrafish: analysis of stellate cell entry into the developing liver. *Hepatology* **56**, 1958-1970 (2012).

75. A. Geerts, History, heterogeneity, developmental biology, and functions of quiescent hepatic stellate cells. *Semin Liver Dis* **21**, 311-335 (2001).
76. E. Miyata *et al.*, Hematopoietic origin of hepatic stellate cells in the adult liver. *Blood* **111**, 2427-2435 (2008).
77. D. Y. Zhang *et al.*, A hepatic stellate cell gene expression signature associated with outcomes in hepatitis C cirrhosis and hepatocellular carcinoma after curative resection. *Gut* **65**, 1754-1764 (2016).
78. C. Hellerbrand, B. Stefanovic, F. Giordano, E. R. Burchardt, D. A. Brenner, The role of TGFbeta1 in initiating hepatic stellate cell activation in vivo. *J Hepatol* **30**, 77-87 (1999).
79. L. Wong, G. Yamasaki, R. J. Johnson, S. L. Friedman, Induction of beta-platelet-derived growth factor receptor in rat hepatic lipocytes during cellular activation in vivo and in culture. *J Clin Invest* **94**, 1563-1569 (1994).
80. P. Kocabayoglu *et al.*, beta-PDGF receptor expressed by hepatic stellate cells regulates fibrosis in murine liver injury, but not carcinogenesis. *J Hepatol* **63**, 141-147 (2015).
81. L. Yang *et al.*, Vascular endothelial growth factor promotes fibrosis resolution and repair in mice. *Gastroenterology* **146**, 1339-1350 e1331 (2014).
82. C. Kantari-Mimoun *et al.*, Resolution of liver fibrosis requires myeloid cell-driven sinusoidal angiogenesis. *Hepatology* **61**, 2042-2055 (2015).
83. G. Huang, D. R. Brigstock, Regulation of hepatic stellate cells by connective tissue growth factor. *Front Biosci (Landmark Ed)* **17**, 2495-2507 (2012).
84. J. S. Duffield *et al.*, Selective depletion of macrophages reveals distinct, opposing roles during liver injury and repair. *J Clin Invest* **115**, 56-65 (2005).
85. K. R. Karlmark *et al.*, Hepatic recruitment of the inflammatory Gr1+ monocyte subset upon liver injury promotes hepatic fibrosis. *Hepatology* **50**, 261-274 (2009).
86. E. Seki *et al.*, CCR1 and CCR5 promote hepatic fibrosis in mice. *J Clin Invest* **119**, 1858-1870 (2009).
87. D. Heinrichs *et al.*, The chemokine CCL3 promotes experimental liver fibrosis in mice. *PLoS One* **8**, e66106 (2013).
88. M. L. Berres *et al.*, Antagonism of the chemokine Ccl5 ameliorates experimental liver fibrosis in mice. *J Clin Invest* **120**, 4129-4140 (2010).
89. E. Seki *et al.*, TLR4 enhances TGF-beta signaling and hepatic fibrosis. *Nat Med* **13**, 1324-1332 (2007).
90. T. Luedde, N. Kaplowitz, R. F. Schwabe, Cell Death and Cell Death Responses in Liver Disease: Mechanisms and Clinical Relevance. *Gastroenterology* **147**, 765-U110 (2014).
91. R. A. Black *et al.*, A metalloproteinase disintegrin that releases tumour-necrosis factor-alpha from cells. *Nature* **385**, 729-733 (1997).
92. M. L. Moss *et al.*, Cloning of a disintegrin metalloproteinase that processes precursor tumour-necrosis factor-alpha. *Nature* **385**, 733-736 (1997).
93. C. Reichel *et al.*, Elevated soluble tumour necrosis factor receptor serum concentrations and short-term mortality in liver cirrhosis without acute infections. *Digestion* **62**, 44-51 (2000).
94. M. Neuman *et al.*, Tumor necrosis factor-alpha and transforming growth factor-beta reflect severity of liver damage in primary biliary cirrhosis. *J Gastroenterol Hepatol* **17**, 196-202 (2002).
95. N. Kinnman, U. Andersson, R. Hultcrantz, In situ expression of transforming growth factor-beta1-3, latent transforming growth factor-beta binding protein and tumor necrosis factor-alpha in liver tissue from patients with chronic hepatitis C. *Scand J Gastroenterol* **35**, 1294-1300 (2000).
96. Y. Muto *et al.*, Enhanced tumour necrosis factor and interleukin-1 in fulminant hepatic failure. *Lancet* **2**, 72-74 (1988).
97. S. Naveau *et al.*, Plasma levels of soluble tumor necrosis factor receptors p55 and p75 in patients with alcoholic liver disease of increasing severity. *J Hepatol* **28**, 778-784 (1998).

98. M. Yin *et al.*, Essential role of tumor necrosis factor alpha in alcohol-induced liver injury in mice. *Gastroenterology* **117**, 942-952 (1999).
99. K. Kitamura *et al.*, Pathogenic roles of tumor necrosis factor receptor p55-mediated signals in dimethylnitrosamine-induced murine liver fibrosis. *Lab Invest* **82**, 571-583 (2002).
100. M. J. Czaja, J. Xu, E. Alt, Prevention of carbon tetrachloride-induced rat liver injury by soluble tumor necrosis factor receptor. *Gastroenterology* **108**, 1849-1854 (1995).
101. M. Leist *et al.*, Tumor necrosis factor-induced apoptosis during the poisoning of mice with hepatotoxins. *Gastroenterology* **112**, 923-934 (1997).
102. M. H. Bemelmans, D. J. Gouma, J. W. Greve, W. A. Buurman, Cytokines tumor necrosis factor and interleukin-6 in experimental biliary obstruction in mice. *Hepatology* **15**, 1132-1136 (1992).
103. E. Gabele *et al.*, TNFalpha is required for cholestasis-induced liver fibrosis in the mouse. *Biochem Biophys Res Commun* **378**, 348-353 (2009).
104. Y. Osawa *et al.*, Tumor necrosis factor-alpha promotes cholestasis-induced liver fibrosis in the mouse through tissue inhibitor of metalloproteinase-1 production in hepatic stellate cells. *PLoS One* **8**, e65251 (2013).
105. N. Tarrats *et al.*, Critical role of tumor necrosis factor receptor 1, but not 2, in hepatic stellate cell proliferation, extracellular matrix remodeling, and liver fibrogenesis. *Hepatology* **54**, 319-327 (2011).
106. K. Sudo, Y. Yamada, H. Moriwaki, K. Saito, M. Seishima, Lack of tumor necrosis factor receptor type 1 inhibits liver fibrosis induced by carbon tetrachloride in mice. *Cytokine* **29**, 236-244 (2005).
107. Y. Yamada, I. Kirillova, J. J. Peschon, N. Fausto, Initiation of liver growth by tumor necrosis factor: deficient liver regeneration in mice lacking type I tumor necrosis factor receptor. *Proc Natl Acad Sci U S A* **94**, 1441-1446 (1997).
108. Y. Yamada, E. M. Webber, I. Kirillova, J. J. Peschon, N. Fausto, Analysis of liver regeneration in mice lacking type 1 or type 2 tumor necrosis factor receptor: requirement for type 1 but not type 2 receptor. *Hepatology* **28**, 959-970 (1998).
109. Y. Yamada, N. Fausto, Deficient liver regeneration after carbon tetrachloride injury in mice lacking type 1 but not type 2 tumor necrosis factor receptor. *Am J Pathol* **152**, 1577-1589 (1998).
110. C. P. Blobel, ADAMs: key components in EGFR signalling and development. *Nat Rev Mol Cell Biol* **6**, 32-43 (2005).
111. T. Klein, R. Bischoff, Active metalloproteases of the A Disintegrin and Metalloprotease (ADAM) family: biological function and structure. *J Proteome Res* **10**, 17-33 (2011).
112. D. F. Seals, S. A. Courtneidge, The ADAMs family of metalloproteases: multidomain proteins with multiple functions. *Genes Dev* **17**, 7-30 (2003).
113. P. E. Gonzales *et al.*, Inhibition of the tumor necrosis factor-alpha-converting enzyme by its pro domain. *J Biol Chem* **279**, 31638-31645 (2004).
114. J. D. Leonard, F. Lin, M. E. Milla, Chaperone-like properties of the prodomain of TNFalpha-converting enzyme (TACE) and the functional role of its cysteine switch. *Biochem J* **387**, 797-805 (2005).
115. M. L. Moss *et al.*, The ADAM10 prodomain is a specific inhibitor of ADAM10 proteolytic activity and inhibits cellular shedding events. *J Biol Chem* **282**, 35712-35721 (2007).
116. D. R. Edwards, M. M. Handsley, C. J. Pennington, The ADAM metalloproteinases. *Mol Aspects Med* **29**, 258-289 (2008).
117. J. J. Peschon *et al.*, An essential role for ectodomain shedding in mammalian development. *Science* **282**, 1281-1284 (1998).
118. S. Lammich *et al.*, Constitutive and regulated alpha-secretase cleavage of Alzheimer's amyloid precursor protein by a disintegrin metalloprotease. *Proc Natl Acad Sci U S A* **96**, 3922-3927 (1999).

119. P. Reddy *et al.*, Functional analysis of the domain structure of tumor necrosis factor-alpha converting enzyme. *J Biol Chem* **275**, 14608-14614 (2000).
120. K. J. Garton *et al.*, Stimulated shedding of vascular cell adhesion molecule 1 (VCAM-1) is mediated by tumor necrosis factor-alpha-converting enzyme (ADAM 17). *J Biol Chem* **278**, 37459-37464 (2003).
121. H. S. Wiley *et al.*, Removal of the membrane-anchoring domain of epidermal growth factor leads to intracrine signaling and disruption of mammary epithelial cell organization. *J Cell Biol* **143**, 1317-1328 (1998).
122. M. Borrell-Pages, F. Rojo, J. Albanell, J. Baselga, J. Arribas, TACE is required for the activation of the EGFR by TGF-alpha in tumors. *EMBO J* **22**, 1114-1124 (2003).
123. J. Scheller, A. Chalaris, C. Garbers, S. Rose-John, ADAM17: a molecular switch to control inflammation and tissue regeneration. *Trends Immunol* **32**, 380-387 (2011).
124. I. Lorenzen *et al.*, Control of ADAM17 activity by regulation of its cellular localisation. *Sci Rep* **6**, 35067 (2016).
125. K. Horiuchi *et al.*, Cutting edge: TNF-alpha-converting enzyme (TACE/ADAM17) inactivation in mouse myeloid cells prevents lethality from endotoxin shock. *J Immunol* **179**, 2686-2689 (2007).
126. R. S. McMahan, K. J. Riehle, N. Fausto, J. S. Campbell, A disintegrin and metalloproteinase 17 regulates TNF and TNFR1 levels in inflammation and liver regeneration in mice. *Am J Physiol Gastrointest Liver Physiol* **305**, G25-34 (2013).
127. A. Amour *et al.*, TNF-alpha converting enzyme (TACE) is inhibited by TIMP-3. *FEBS Lett* **435**, 39-44 (1998).
128. F. F. Mohammed *et al.*, Abnormal TNF activity in Timp3-/- mice leads to chronic hepatic inflammation and failure of liver regeneration. *Nat Genet* **36**, 969-977 (2004).
129. A. Murthy *et al.*, Ectodomain shedding of EGFR ligands and TNFR1 dictates hepatocyte apoptosis during fulminant hepatitis in mice. *J Clin Invest* **120**, 2731-2744 (2010).
130. X. M. Lin *et al.*, Expression of tumor necrosis factor-alpha converting enzyme in liver regeneration after partial hepatectomy. *World J Gastroenterol* **14**, 1353-1357 (2008).
131. D. Schmidt-Arras, S. Rose-John, Regulation of Fibrotic Processes in the Liver by ADAM Proteases. *Cells* **8**, (2019).
132. H. Le Pabic *et al.*, ADAM12 in human liver cancers: TGF-beta-regulated expression in stellate cells is associated with matrix remodeling. *Hepatology* **37**, 1056-1066 (2003).
133. K. Bourd-Boittin *et al.*, CX3CL1/fractalkine shedding by human hepatic stellate cells: contribution to chronic inflammation in the liver. *J Cell Mol Med* **13**, 1526-1535 (2009).
134. C. McKee *et al.*, Amphiregulin activates human hepatic stellate cells and is upregulated in non alcoholic steatohepatitis. *Sci Rep* **5**, 8812 (2015).
135. L. Schwettmann *et al.*, Hepatic expression of A disintegrin and metalloproteinase (ADAM) and ADAMs with thrombospondin motives (ADAM-TS) enzymes in patients with chronic liver diseases. *J Hepatol* **49**, 243-250 (2008).
136. C. Adrain, M. Zettl, Y. Christova, N. Taylor, M. Freeman, Tumor necrosis factor signaling requires iRhom2 to promote trafficking and activation of TACE. *Science* **335**, 225-228 (2012).
137. D. R. McIlwain *et al.*, iRhom2 regulation of TACE controls TNF-mediated protection against Listeria and responses to LPS. *Science* **335**, 229-232 (2012).
138. M. Freeman, Rhomboid proteases and their biological functions. *Annu Rev Genet* **42**, 191-210 (2008).
139. Y. Akiyama, K. Kanehara, K. Ito, RseP (YaeL), an Escherichia coli RIP protease, cleaves transmembrane sequences. *EMBO J* **23**, 4434-4442 (2004).
140. E. A. Duncan, U. P. Dave, J. Sakai, J. L. Goldstein, M. S. Brown, Second-site cleavage in sterol regulatory element-binding protein occurs at transmembrane junction as determined by cysteine panning. *J Biol Chem* **273**, 17801-17809 (1998).

141. R. B. Rawson *et al.*, Complementation cloning of S2P, a gene encoding a putative metalloprotease required for intramembrane cleavage of SREBPs. *Mol Cell* **1**, 47-57 (1997).
142. B. De Strooper *et al.*, Deficiency of presenilin-1 inhibits the normal cleavage of amyloid precursor protein. *Nature* **391**, 387-390 (1998).
143. R. Fluhrer *et al.*, A gamma-secretase-like intramembrane cleavage of TNFalpha by the GxGD aspartyl protease SPPL2b. *Nat Cell Biol* **8**, 894-896 (2006).
144. E. Friedmann *et al.*, SPPL2a and SPPL2b promote intramembrane proteolysis of TNFalpha in activated dendritic cells to trigger IL-12 production. *Nat Cell Biol* **8**, 843-848 (2006).
145. M. K. Lemberg, M. Freeman, Functional and evolutionary implications of enhanced genomic analysis of rhomboid intramembrane proteases. *Genome Res* **17**, 1634-1646 (2007).
146. S. Urban, J. R. Lee, M. Freeman, Drosophila rhomboid-1 defines a family of putative intramembrane serine proteases. *Cell* **107**, 173-182 (2001).
147. U. Mayer, C. Nusslein-Volhard, A group of genes required for pattern formation in the ventral ectoderm of the Drosophila embryo. *Genes Dev* **2**, 1496-1511 (1988).
148. M. Freeman, The spitz gene is required for photoreceptor determination in the Drosophila eye where it interacts with the EGF receptor. *Mech Dev* **48**, 25-33 (1994).
149. M. A. Sturtevant, M. Roark, E. Bier, The Drosophila rhomboid gene mediates the localized formation of wing veins and interacts genetically with components of the EGF-R signaling pathway. *Genes Dev* **7**, 961-973 (1993).
150. M. Freeman, The rhomboid-like superfamily: molecular mechanisms and biological roles. *Annu Rev Cell Dev Biol* **30**, 235-254 (2014).
151. C. Adrain, M. Freeman, New lives for old: evolution of pseudoenzyme function illustrated by iRhoms. *Nat Rev Mol Cell Biol* **13**, 489-498 (2012).
152. I. Dulloo, S. Muliyil, M. Freeman, The molecular, cellular and pathophysiological roles of iRhom pseudoproteases. *Open Biol* **9**, 190003 (2019).
153. Y. Christova, C. Adrain, P. Bambrough, A. Ibrahim, M. Freeman, Mammalian iRhoms have distinct physiological functions including an essential role in TACE regulation. *EMBO Rep* **14**, 884-890 (2013).
154. X. Li *et al.*, iRhoms 1 and 2 are essential upstream regulators of ADAM17-dependent EGFR signaling. *Proc Natl Acad Sci U S A* **112**, 6080-6085 (2015).
155. C. X. Ge *et al.*, iRhom2 deficiency relieves TNF-alpha associated hepatic dyslipidemia in long-term PM2.5-exposed mice. *Biochem Biophys Res Commun* **493**, 1402-1409 (2017).
156. W. W. Luo *et al.*, iRhom2 is essential for innate immunity to DNA viruses by mediating trafficking and stability of the adaptor STING. *Nat Immunol* **17**, 1057-1066 (2016).
157. W. W. Luo *et al.*, iRhom2 is essential for innate immunity to RNA virus by antagonizing ER- and mitochondria-associated degradation of VISA. *PLoS Pathog* **13**, e1006693 (2017).
158. K. Pfeffer *et al.*, Mice deficient for the 55 kd tumor necrosis factor receptor are resistant to endotoxic shock, yet succumb to L. monocytogenes infection. *Cell* **73**, 457-467 (1993).
159. P. D. Issuree *et al.*, iRHOM2 is a critical pathogenic mediator of inflammatory arthritis. *J Clin Invest* **123**, 928-932 (2013).
160. X. Qing *et al.*, iRhom2 promotes lupus nephritis through TNF-alpha and EGFR signaling. *J Clin Invest* **128**, 1397-1412 (2018).
161. C. Haxaire *et al.*, Blood-induced bone loss in murine hemophilic arthropathy is prevented by blocking the iRhom2/ADAM17/TNF-alpha pathway. *Blood* **132**, 1064-1074 (2018).
162. J. H. Kim *et al.*, Role of iRhom2 in intestinal ischemia-reperfusion-mediated acute lung injury. *Sci Rep* **8**, 3797 (2018).
163. D. N. Barnette *et al.*, iRhom2-mediated proinflammatory signalling regulates heart repair following myocardial infarction. *JCI Insight* **3**, (2018).
164. X. L. Lu, C. H. Zhao, H. Zhang, X. L. Yao, iRhom2 is involved in lipopolysaccharide-induced cardiac injury in vivo and in vitro through regulating inflammation response. *Biomed Pharmacother* **86**, 645-653 (2017).

165. P. Saftig, K. Reiss, The "A Disintegrin And Metalloproteases" ADAM10 and ADAM17: novel drug targets with therapeutic potential? *Eur J Cell Biol* **90**, 527-535 (2011).
166. D. C. Blaydon *et al.*, RHBDF2 mutations are associated with tylosis, a familial esophageal cancer syndrome. *Am J Hum Genet* **90**, 340-346 (2012).
167. T. Mokoena, J. G. M. Smit, V. O. Karusseit, C. M. Dorfling, E. J. van Rensburg, Tylosis associated with squamous cell carcinoma of the oesophagus (TOC): Report of an African family with a novel RHBDF2 variant. *Clin Genet* **93**, 1114-1116 (2018).
168. S. K. Maney *et al.*, Deletions in the cytoplasmic domain of iRhom1 and iRhom2 promote shedding of the TNF receptor by the protease ADAM17. *Sci Signal* **8**, ra109 (2015).
169. T. Maruthappu *et al.*, Rhomboid family member 2 regulates cytoskeletal stress-associated Keratin 16. *Nat Commun* **8**, 14174 (2017).
170. T. Ishimoto *et al.*, Activation of Transforming Growth Factor Beta 1 Signaling in Gastric Cancer-associated Fibroblasts Increases Their Motility, via Expression of Rhomboid 5 Homolog 2, and Ability to Induce Invasiveness of Gastric Cancer Cells. *Gastroenterology* **153**, 191-204 e116 (2017).
171. M. Grell *et al.*, The transmembrane form of tumor necrosis factor is the prime activating ligand of the 80 kDa tumor necrosis factor receptor. *Cell* **83**, 793-802 (1995).
172. L. A. Tartaglia, T. M. Ayres, G. H. Wong, D. V. Goeddel, A novel domain within the 55 kd TNF receptor signals cell death. *Cell* **74**, 845-853 (1993).
173. M. Grell *et al.*, Induction of cell death by tumour necrosis factor (TNF) receptor 2, CD40 and CD30: a role for TNF-R1 activation by endogenous membrane-anchored TNF. *EMBO J* **18**, 3034-3043 (1999).
174. H. B. Shu, M. Takeuchi, D. V. Goeddel, The tumor necrosis factor receptor 2 signal transducers TRAF2 and c-IAP1 are components of the tumor necrosis factor receptor 1 signaling complex. *Proc Natl Acad Sci U S A* **93**, 13973-13978 (1996).
175. H. Hsu, J. Xiong, D. V. Goeddel, The TNF receptor 1-associated protein TRADD signals cell death and NF-kappa B activation. *Cell* **81**, 495-504 (1995).
176. P. Vandenabeele, W. Declercq, R. Beyaert, W. Fiers, Two tumour necrosis factor receptors: structure and function. *Trends Cell Biol* **5**, 392-399 (1995).
177. M. Rothe, V. Sarma, V. M. Dixit, D. V. Goeddel, TRAF2-mediated activation of NF-kappa B by TNF receptor 2 and CD40. *Science* **269**, 1424-1427 (1995).
178. X. Li, Y. Yang, J. D. Ashwell, TNF-RII and c-IAP1 mediate ubiquitination and degradation of TRAF2. *Nature* **416**, 345-347 (2002).
179. S. L. Erickson *et al.*, Decreased sensitivity to tumour-necrosis factor but normal T-cell development in TNF receptor-2-deficient mice. *Nature* **372**, 560-563 (1994).
180. J. M. Dopp *et al.*, Expression of the p75 TNF receptor is linked to TNF-induced NFkappaB translocation and oxyradical neutralization in glial cells. *Neurochem Res* **27**, 1535-1542 (2002).
181. M. Grell, F. M. Becke, H. Wajant, D. N. Mannel, P. Scheurich, Tumor necrosis factor (TNF) receptor type 2 mediates thymocyte proliferation independently of TNF receptor type 1. *Eur J Immunol* **28**, 257-263 (1998).
182. J. J. Peschon *et al.*, TNF receptor-deficient mice reveal divergent roles for p55 and p75 in several models of inflammation. *J Immunol* **160**, 943-952 (1998).
183. H. A. Arnett *et al.*, TNF alpha promotes proliferation of oligodendrocyte progenitors and remyelination. *Nat Neurosci* **4**, 1116-1122 (2001).
184. L. Marchetti, M. Klein, K. Schlett, K. Pfizenmaier, U. L. Eisel, Tumor necrosis factor (TNF)-mediated neuroprotection against glutamate-induced excitotoxicity is enhanced by N-methyl-D-aspartate receptor activation. Essential role of a TNF receptor 2-mediated phosphatidylinositol 3-kinase-dependent NF-kappa B pathway. *J Biol Chem* **279**, 32869-32881 (2004).

185. T. W. Mak, W. C. Yeh, Signaling for survival and apoptosis in the immune system. *Arthritis Res* **4 Suppl 3**, S243-252 (2002).
186. T. Liu, L. Zhang, D. Joo, S. C. Sun, NF-kappaB signaling in inflammation. *Signal Transduct Target Ther* **2**, (2017).
187. S. C. Sun, Non-canonical NF-kappaB signaling pathway. *Cell Res* **21**, 71-85 (2011).
188. S. Vallabhapurapu, M. Karin, Regulation and function of NF-kappaB transcription factors in the immune system. *Annu Rev Immunol* **27**, 693-733 (2009).
189. H. Zhang, S. C. Sun, NF-kappaB in inflammation and renal diseases. *Cell Biosci* **5**, 63 (2015).
190. S. Beinke, S. C. Ley, Functions of NF-kappaB1 and NF-kappaB2 in immune cell biology. *Biochem J* **382**, 393-409 (2004).
191. M. Karin, M. Delhase, The I kappa B kinase (IKK) and NF-kappa B: key elements of proinflammatory signalling. *Semin Immunol* **12**, 85-98 (2000).
192. M. S. Hayden, S. Ghosh, Shared principles in NF-kappaB signaling. *Cell* **132**, 344-362 (2008).
193. S. C. Sun, The noncanonical NF-kappaB pathway. *Immunol Rev* **246**, 125-140 (2012).
194. S. C. Sun, Z. G. Liu, A special issue on NF-kappaB signaling and function. *Cell Res* **21**, 1-2 (2011).
195. C. G. Tag *et al.*, Bile duct ligation in mice: induction of inflammatory liver injury and fibrosis by obstructive cholestasis. *J Vis Exp*, (2015).
196. C. G. Tag *et al.*, Induction of experimental obstructive cholestasis in mice. *Lab Anim* **49**, 70-80 (2015).
197. V. Mariotti *et al.*, Animal models of cholestasis: An update on inflammatory cholangiopathies. *Biochim Biophys Acta Mol Basis Dis* **1865**, 954-964 (2019).
198. J. M. Sheen *et al.*, Combined Intraperitoneal and Intrathecal Etanercept Reduce Increased Brain Tumor Necrosis Factor-Alpha and Asymmetric Dimethylarginine Levels and Rescues Spatial Deficits in Young Rats after Bile Duct Ligation. *Front Cell Neurosci* **10**, 167 (2016).
199. U. R. Sorg *et al.*, Cooperative role of lymphotoxin beta receptor and tumor necrosis factor receptor p55 in murine liver regeneration. *J Hepatol* **64**, 1108-1117 (2016).
200. N. Honke *et al.*, Enforced viral replication activates adaptive immunity and is essential for the control of a cytopathic virus. *Nat Immunol* **13**, 51-57 (2011).
201. J. C. Garcia-Canaveras, M. T. Donato, J. V. Castell, A. Lahoz, Targeted profiling of circulating and hepatic bile acids in human, mouse, and rat using a UPLC-MRM-MS-validated method. *J Lipid Res* **53**, 2231-2241 (2012).
202. D. E. Fouts, M. Torralba, K. E. Nelson, D. A. Brenner, B. Schnabl, Bacterial translocation and changes in the intestinal microbiome in mouse models of liver disease. *J Hepatol* **56**, 1283-1292 (2012).
203. C. P. Hackstein *et al.*, Gut microbial translocation corrupts myeloid cell function to control bacterial infection during liver cirrhosis. *Gut* **66**, 507-518 (2017).
204. A. W. Yan *et al.*, Enteric dysbiosis associated with a mouse model of alcoholic liver disease. *Hepatology* **53**, 96-105 (2011).
205. I. Mederacke, D. H. Dapito, S. Affo, H. Uchinami, R. F. Schwabe, High-yield and high-purity isolation of hepatic stellate cells from normal and fibrotic mouse livers. *Nat Protoc* **10**, 305-315 (2015).
206. W. C. Li, K. L. Ralphs, D. Tosh, Isolation and culture of adult mouse hepatocytes. *Methods Mol Biol* **633**, 185-196 (2010).
207. P. Z. Li, J. Z. Li, M. Li, J. P. Gong, K. He, An efficient method to isolate and culture mouse Kupffer cells. *Immunol Lett* **158**, 52-56 (2014).
208. P. V. Shinde *et al.*, Tumor Necrosis Factor-Mediated Survival of CD169(+) Cells Promotes Immune Activation during Vesicular Stomatitis Virus Infection. *J Virol* **92**, (2018).
209. N. Parameswaran, S. Patial, Tumor necrosis factor-alpha signaling in macrophages. *Crit Rev Eukaryot Gene Expr* **20**, 87-103 (2010).

210. I. H. Bahcecioglu *et al.*, TNF-alpha and leptin in experimental liver fibrosis models induced by carbon tetrachloride and by common bile duct ligation. *Cell Biochem Funct* **22**, 359-363 (2004).
211. A. Natarajan, B. Wagner, M. Sibilia, The EGF receptor is required for efficient liver regeneration. *Proc Natl Acad Sci U S A* **104**, 17081-17086 (2007).
212. D. Schmidt-Arras, S. Rose-John, IL-6 pathway in the liver: From physiopathology to therapy. *J Hepatol* **64**, 1403-1415 (2016).
213. N. Fazel Modares *et al.*, IL-6 Trans-signaling Controls Liver Regeneration After Partial Hepatectomy. *Hepatology*, (2019).
214. T. Maretzky *et al.*, iRhom2 controls the substrate selectivity of stimulated ADAM17-dependent ectodomain shedding. *Proc Natl Acad Sci U S A* **110**, 11433-11438 (2013).
215. H. M. Flood *et al.*, The Forkhead box F1 transcription factor inhibits collagen deposition and accumulation of myofibroblasts during liver fibrosis. *Biol Open* **8**, (2019).
216. A. Graf *et al.*, Knockout of histidine decarboxylase decreases bile duct ligation-induced biliary hyperplasia via downregulation of the histidine decarboxylase/VEGF axis through PKA-ERK1/2 signaling. *Am J Physiol Gastrointest Liver Physiol* **307**, G813-823 (2014).
217. P. Kocabayoglu *et al.*, β-PDGF receptor expressed by hepatic stellate cells regulates fibrosis in murine liver injury, but not carcinogenesis. *Journal of hepatology* **63**, 141-147 (2015).
218. D. Zhang *et al.*, Desmin- and vimentin-mediated hepatic stellate cell-targeting radiotracer (99m)Tc-GlcNAc-PEI for liver fibrosis imaging with SPECT. *Theranostics* **8**, 1340-1349 (2018).
219. E. Borkham-Kamphorst *et al.*, Dominant-negative soluble PDGF-β receptor inhibits hepatic stellate cell activation and attenuates liver fibrosis. *Laboratory Investigation* **84**, 766-777 (2004).
220. T. Nishio *et al.*, Activated Hepatic Stellate Cells and Portal Fibroblasts contribute to cholestatic liver fibrosis in MDR2 knockout mice. *Journal of Hepatology*.
221. E. C. Schumacher, S. Gotze, C. Kordes, V. Benes, D. Haussinger, Combined Methylome and Transcriptome Analysis During Rat Hepatic Stellate Cell Activation. *Stem Cells Dev* **26**, 1759-1770 (2017).
222. F. Zunke, S. Rose-John, The shedding protease ADAM17: Physiology and pathophysiology. *Biochim Biophys Acta Mol Cell Res* **1864**, 2059-2070 (2017).
223. A. A. Beg, W. C. Sha, R. T. Bronson, S. Ghosh, D. Baltimore, Embryonic lethality and liver degeneration in mice lacking the RelA component of NF-kappa B. *Nature* **376**, 167-170 (1995).
224. A. S. Baldwin, Jr., The NF-kappa B and I kappa B proteins: new discoveries and insights. *Annu Rev Immunol* **14**, 649-683 (1996).
225. N. Tarrats *et al.*, Critical role of tumor necrosis factor receptor 1, but not 2, in hepatic stellate cell proliferation, extracellular matrix remodeling, and liver fibrogenesis. *Hepatology (Baltimore, Md.)* **54**, 319-327 (2011).
226. L. Hammerich, F. Tacke, Interleukins in chronic liver disease: lessons learned from experimental mouse models. *Clinical and experimental gastroenterology* **7**, 297-306 (2014).
227. E. Sziksz *et al.*, Fibrosis Related Inflammatory Mediators: Role of the IL-10 Cytokine Family. *Mediators of inflammation* **2015**, 764641-764641 (2015).
228. Y. Sunami *et al.*, Hepatic activation of IKK/NFkappaB signaling induces liver fibrosis via macrophage-mediated chronic inflammation. *Hepatology* **56**, 1117-1128 (2012).
229. H. Shen *et al.*, Mouse hepatocyte overexpression of NF-kappaB-inducing kinase (NIK) triggers fatal macrophage-dependent liver injury and fibrosis. *Hepatology* **60**, 2065-2076 (2014).
230. E. L. Hassemer *et al.*, The waved with open eyelids (woe) locus is a hypomorphic mouse mutation in Adam17. *Genetics* **185**, 245-255 (2010).
231. A. Nicolaou *et al.*, Adam17 Deficiency Promotes Atherosclerosis by Enhanced TNFR2 Signaling in Mice. *Arterioscler Thromb Vasc Biol* **37**, 247-257 (2017).

232. L. Alexopoulou *et al.*, Transmembrane TNF protects mutant mice against intracellular bacterial infections, chronic inflammation and autoimmunity. *Eur J Immunol* **36**, 2768-2780 (2006).
233. H. Uysal *et al.*, Transmembrane TNF and Partially TNFR1 Regulate TNFR2 Expression and Control Inflammation in Mycobacterial-Induced Pleurisy. *International journal of molecular sciences* **19**, 1959 (2018).
234. C. D. Douillet *et al.*, Mechanisms by which bradykinin promotes fibrosis in vascular smooth muscle cells: role of TGF-beta and MAPK. *Am J Physiol Heart Circ Physiol* **279**, H2829-2837 (2000).
235. E. Lutgens *et al.*, Transforming growth factor-beta mediates balance between inflammation and fibrosis during plaque progression. *Arterioscler Thromb Vasc Biol* **22**, 975-982 (2002).
236. D. M. Ha *et al.*, Transforming growth factor-beta 1 produced by vascular smooth muscle cells predicts fibrosis in the gastrocnemius of patients with peripheral artery disease. *J Transl Med* **14**, 39 (2016).
237. J. Jin, Y. Chang, W. Wei, Clinical application and evaluation of anti-TNF-alpha agents for the treatment of rheumatoid arthritis. *Acta Pharmacol Sin* **31**, 1133-1140 (2010).
238. W. Liu *et al.*, Efficacy and safety of TNF-alpha inhibitors for active ankylosing spondylitis patients: Multiple treatment comparisons in a network meta-analysis. *Sci Rep* **6**, 32768 (2016).
239. J. Pido-Lopez *et al.*, Inhibition of tumour necrosis factor alpha in the R6/2 mouse model of Huntington's disease by etanercept treatment. *Sci Rep* **9**, 7202 (2019).
240. L. R. Lopetuso *et al.*, Harmful Effects and Potential Benefits of Anti-Tumor Necrosis Factor (TNF)-alpha on the Liver. *Int J Mol Sci* **19**, (2018).
241. N. C. Boetticher *et al.*, A randomized, double-blinded, placebo-controlled multicenter trial of etanercept in the treatment of alcoholic hepatitis. *Gastroenterology* **135**, 1953-1960 (2008).
242. M. A. Brooke *et al.*, iRHOM2-dependent regulation of ADAM17 in cutaneous disease and epidermal barrier function. *Hum Mol Genet* **23**, 4064-4076 (2014).
243. A. Iracheta-Vellve *et al.*, Endoplasmic Reticulum Stress-induced Hepatocellular Death Pathways Mediate Liver Injury and Fibrosis via Stimulator of Interferon Genes. *J Biol Chem* **291**, 26794-26805 (2016).
244. P. Muriel, Alpha-interferon prevents liver collagen deposition and damage induced by prolonged bile duct obstruction in the rat. *J Hepatol* **24**, 614-621 (1996).
245. M. R. Bueno, A. Daneri, J. Armendariz-Borunda, Cholestasis-induced fibrosis is reduced by interferon alpha-2a and is associated with elevated liver metalloprotease activity. *J Hepatol* **33**, 915-925 (2000).
246. N. O. Ku, P. Strnad, H. Bantel, M. B. Omary, Keratins: Biomarkers and modulators of apoptotic and necrotic cell death in the liver. *Hepatology* **64**, 966-976 (2016).
247. N. O. Ku *et al.*, Keratin 8 and 18 mutations are risk factors for developing liver disease of multiple etiologies. *Proc Natl Acad Sci U S A* **100**, 6063-6068 (2003).
248. N. O. Ku, R. Gish, T. L. Wright, M. B. Omary, Keratin 8 mutations in patients with cryptogenic liver disease. *N Engl J Med* **344**, 1580-1587 (2001).
249. D. M. Toivola *et al.*, Keratin 8 and 18 hyperphosphorylation is a marker of progression of human liver disease. *Hepatology* **40**, 459-466 (2004).
250. N. O. Ku, R. M. Soetikno, M. B. Omary, Keratin mutation in transgenic mice predisposes to Fas but not TNF-induced apoptosis and massive liver injury. *Hepatology* **37**, 1006-1014 (2003).
251. T. Takemura *et al.*, Conditional knockout of heparin-binding epidermal growth factor-like growth factor in the liver accelerates carbon tetrachloride-induced liver injury in mice. *Hepatol Res* **43**, 384-393 (2013).
252. Y. Guo *et al.*, Overexpression of Heparin-Binding Epidermal Growth Factor-Like Growth Factor Mediates Liver Fibrosis in Transgenic Mice. *Am J Med Sci* **354**, 199-210 (2017).

253. B. C. Fuchs *et al.*, Epidermal growth factor receptor inhibition attenuates liver fibrosis and development of hepatocellular carcinoma. *Hepatology* **59**, 1577-1590 (2014).
254. T. Wuestefeld *et al.*, Lack of gp130 expression results in more bacterial infection and higher mortality during chronic cholestasis in mice. *Hepatology* **42**, 1082-1090 (2005).
255. D. C. Kroy *et al.*, Lack of interleukin-6/glycoprotein 130/signal transducers and activators of transcription-3 signaling in hepatocytes predisposes to liver steatosis and injury in mice. *Hepatology* **51**, 463-473 (2010).